Doctoral Dissertation

Magnetic structure of Wiegand wire analyzed by magnetization process depending on wire-diameter

磁化過程の線径依存により解明する Wiegand ワイヤの磁気的構造

Department of Mathematics, Physics, Electrical Engineering and Computer Science,
Graduate School of Engineering Science,
Yokohama National University

Liang Jiang　蒋 亮

Dissertation advisor: Professor Yasushi Takemura

January, 2023

Abstract

The Internet of Things (IoT) technology acts as a stimulus for the rapid development of the information industry. It renders production and human lifestyle intelligent, integrated, and networked. The emergence of the IoT technology has promoted the development of new technologies and products, specifically sensor technology. A low-power-consumption self-generating sensor is gradually replacing the conventional sensors and becoming a key product among the new sensors.

In this study, a sensor made of a Wiegand wire (also known as the Wiegand sensor) exhibits low power consumption and spontaneous electrical characteristics. It can be used in the field of the IoT and can supply power for other sensors or electronic devices. As a spontaneous electronic device in the field of IoT application, it can solve the problem of power supply for various sensors and electronic devices. Moreover, it can make these sensors independent of the wired power supply. This helps render the application of sensors and electronic devices more mobile. It provides reliable technical support for the IoT to achieve the Internet of Everything.

In the past, the hysteresis loop was used to study the magnetic structure of Wiegand wires. However, a hysteresis loop cannot analyze the states of coercive and interactive fields inside a Wiegand wire. The first-order reversal curve (FORC) diagram method can help obtain detailed information on the coercive field and interactive field distribution of a Wiegand wire. Therefore, herein, the magnetic structure of a Wiegand wire is studied using the FORC diagram method. According to the FORC diagram, the magnetic structure of a Wiegand wire can be divided into three layers: soft layer, middle layer, and hard core. Furthermore, it can help determine the coercive and interactive fields in a Wiegand wire. Overall, the results obtained using the FORC provide strong evidence of the existence of a central core of the wire with higher coercivity and its outer layer with lower coercivity. The relationship between the magnetization direction and partial region of the FORC distribution diagram is clarified. This analysis infers the reason for the negative region in the FORC. After understanding the magnetic structure, hysteresis loops are used to study the magnetic characteristics of Wiegand wires, e.g., coercivity, remanence, and switching field. Moreover, the magnetization state of each layer in the magnetization process can be analyzed. The final results derived based on the FORC analysis can be obtained considering the height of the large Barkhausen jump of Wiegand wires with different diameters (wherein the inner layer is hard and the outer layer is soft). Under an external magnetic field, the variation trend between the output

voltage of the Wiegand sensor and height of the large Barkhausen jump is consistent. In addition, a simple magnetic structure comprising the soft, middle, and hard layers of Wiegand wires is proposed for the first time based on theoretical calculation. Furthermore, the thicknesses of regions with each direction of magnetization are calculated for the first time.

Thus, an analysis of the magnetic structure, magnetization process, and magnetic characteristics of a Wiegand wire based on the FORC and hysteresis loop methods helps us effectively comprehend the magnetic structure and magnetization state of each layer in the magnetization process of a Wiegand wire. This would help researchers understand Wiegand wires in detail, which is of high significance for expanding the application of the Wiegand wires in the field of IoT.

Table of Contents

Chapter 1: Introduction 5

1.1 Background 5

1.2 Research Objective and Main Contribution 9

1.3 Organization of this Dissertation 11

Chapter 2: Theories 13

2.1 Fundamentals of Magnetic Materials 13

2.1.1 Various Types of Magnetic Behavior of Magnetic Materials 13

2.1.2 Demagnetizing Field and Magnetic Anisotropy 17

2.1.3 Magnetic Domain and Magnetization Process 19

2.2 Wiegand Wire 22

2.2.1 Magnetic Wires and Large Barkhausen Jump 22

2.2.2 Wiegand Wire 24

2.2.3 Wiegand Effect and Wiegand Pulse 25

2.2.4 Magnetic Structure of Wiegand Wire 27

2.3 Methods for Evaluating the Magnetic Structure of Wiegand Wires 28

2.3.1 Magnetic Hysteresis Loops 28

2.3.2 First-Order Reversal Curves (FORCs) 30

Chapter 3: Analysis of the Magnetic Structure of a Wiegand Wire Using FORCs 34

3.1 Preparation of Wiegand Wires with Different Diameters 34

3.2 Measurements of FORCs and Hysteresis Loops 36

3.2.1 Major Hysteresis Loops of Wiegand Wires 38

3.2.2 FORCs and FORC Diagrams of Wiegand Wires 39

3.3 FORC Analysis of Wiegand Wires of Different Diameters 41

3.3.1 Relationship Between Coercivity of Major Hysteresis Loop and FORC Distribution 41

3.3.2 Single and Uniform Magnetic Structure 42

3.3.3 Three Layers of the Magnetic Structure 43

3.3.4 Relationship Between Magnetization Reversal Direction of Wiegand Wire and Partial Region of FORC Distribution Diagram 47

3.4 Summary 51

Chapter 4: Analysis of the Magnetization Process of Wiegand Wires with Different Diameters Based on the Hysteresis Loop 52

4.1 Thickness of Each Magnetic Layer of Wiegand Wires with Different Diameters 52
4.2 Theoretical Calculation of the Volume of the Region of Magnetization 56
4.3 Magnetization Process and Magnetic Structure of Wiegand Wires 60
4.3.1 Wiegand Wire with a Diameter of 0.23 mm 60
4.3.2 Wiegand Wire with a Diameter of 0.18 mm 65
4.3.3 Wiegand Wire with a Diameter of 0.14 mm 67
4.3.4 Wiegand Wire with a Diameter of 0.10 mm 69
4.4 Summary 72

Chapter 5: Analysis of the Magnetic Characteristics of Wiegand Wires with Different Diameters Using Hysteresis Loops 73
5.1 Major Hysteresis Loops 73
5.1.1 Normalized Major Hysteresis Loops 73
5.1.2 Major Hysteresis Loops Normalized Using the Wiegand Wire with a Diameter of 0.23 mm 75
5.2 Minor Hysteresis Loops 78
5.2.1 Coercive Force of Minor Hysteresis Loops 80
5.2.2 Remanence of the Minor Hysteresis Loops 82
5.2.3 Maximum Magnetization of Minor Hysteresis Loops 84
5.3 Large Barkhausen Jump and Induced Pulse of the Wiegand Wires 85
5.4 Switching Field of Wiegand Wires with Different Diameters 88
5.5 Summary 89

Chapter 6: Conclusion 90
References 92
Publications 102

Chapter 1: Introduction

1.1 Background

The Internet of Things (IoT) concept was first proposed by the Auto-ID Laboratory of MIT in 1999. It is a network that connects physical objects to the Internet via information-sensing devices, e.g., radio frequency identification (RFID), and achieves intelligent management and identification.[1] The International Telecommunication Union (ITU), Cluster of European Research Projects on Internet of Things (CERP-IoT), and European Technology Platform on Smart Systems Integration (EPoSS) elaborated their understanding of the IoT. Thus, the IoT concept gradually improved.[2-4] In this network, objects are linked to and exchanged via the Internet using information-sensing devices under the agreed communication protocol to achieve intelligent identification, localization, monitoring, and management (Figure 1.1).

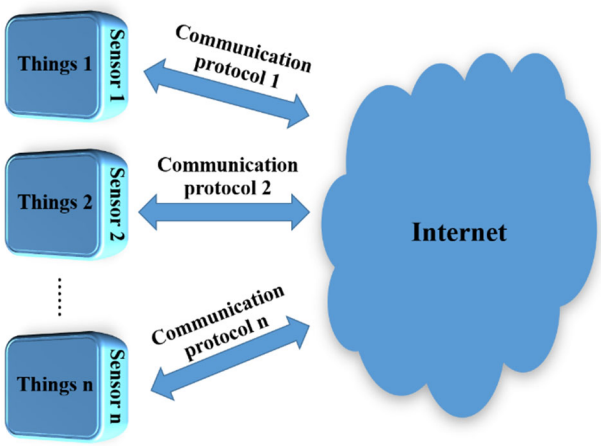

Figure 1.1 Concept of the IoT.

Using the IoT, an individual can query about a specific location and the status of real objects using their data. Using computers and big data, the IoT can enable the centralized control of factory equipment and employees, as well as the remote operation of household equipment and cars. Moreover, the GPS can be used to locate items and prevent them from theft. In addition, roads can be effectively redesigned to reduce car accidents. Moreover, the IoT helps in disaster prediction, crime prevention, and epidemic control. In general, it is essential for the development of intelligent systems related to agriculture, environmental protection, transportation, medicines, industries, finance, and homes (Figure 1.2).[5]

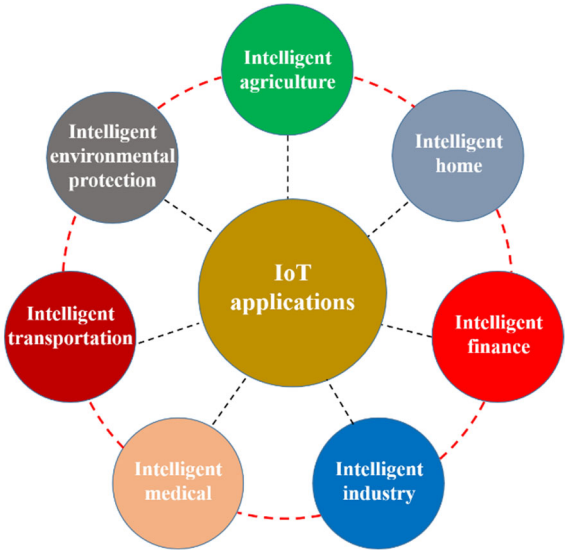

Figure 1.2 IoT applications.

The IoT has attracted considerable attention worldwide. Many countries have promulgated IoT development strategies, e.g., IoT "U Society" (Japan and South Korea), "Sense China Center" (China), "IoT Action Plan" (Europe), and "Smart grid" and "Smart Earth" (the United States) strategies. It is estimated that 80 billion IoT devices would be installed over the next two years.[6] Thus, it is required to develop a self-powered supply system with strong mobility, high-power-supply reliability, and long battery life.

Several sensors can generate pulses, e.g., the Hall sensor, electromagnetic sensor, magnetoresistive sensor, and Wiegand sensor.[7-10] The Wiegand sensor is based on the Wiegand effect. A Wiegand sensor can generate voltage pulses when an alternating magnetic field is applied to it. Therefore, it can supply power to electronic devices.[11-15] The output characteristics of the aforementioned sensors are shown in Figure 1.3. When the excitation frequency, which generates voltage pulses, varies, the pulse width of the output voltage of the Hall and magnetoresistive sensors significantly differ under high- and low-frequency excitations, and power supply is required. Although the pulse width and amplitude of the output voltage of electromagnetic sensors vary under the high- and low-frequency excitations, they do not require a power supply. Consequently, the stability of a self-powered supply comprising the aforementioned three sensors is moderate. At present, the output voltage of Wiegand sensors is unaffected by the excitation frequency. This can help maintain a good voltage-pulse width and amplitude under high- and low-frequency excitations. This can realize the high stability of a self-powered supply without the need of an external power supply.[16-18] Thus, a self-

powered supply comprising a Wiegand sensor solves various power-supply problems of many electronic devices in the field of IoT, including mobility, reliability, and endurance.

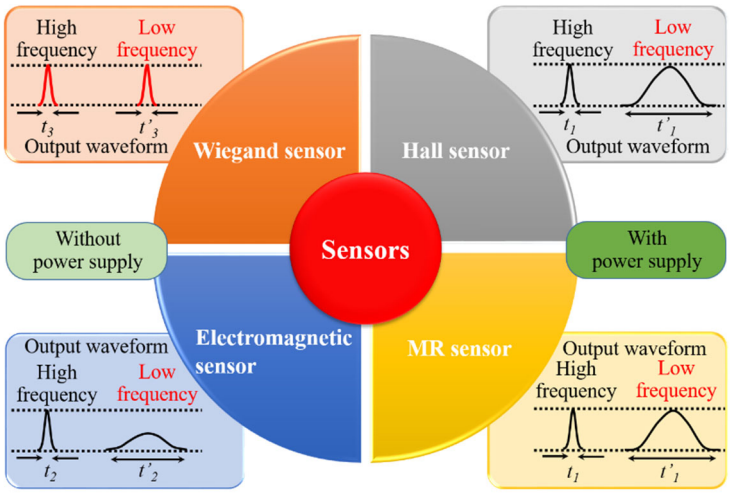

Figure 1.3 Output characteristics of different sensors.

The Wiegand sensor comprises a Wiegand wire and pick-up coil wound around it. Its core component is the Wiegand wire, whose performance directly affects the self-powered performance of the Wiegand sensor (Figure 1.4).[19-22] Therefore, the magnetic structure, magnetic characteristics, and magnetization process of a Wiegand wire are investigated in this study to provide the basis for the better development of its application in the IoT field.

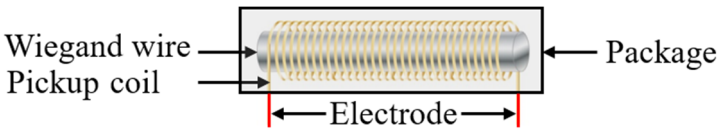

Figure 1.4 Compositions of the Wiegand sensor.

John R. Wiegand developed the first Wiegand wire with an $Ni_{0.48}Fe_{0.52}$ magnetic wire in 1974. It exhibits a magnetic structure with hard outer and soft inner layers.[23-24] In 1981, he observed that vicalloy (composed of $Fe_{0.4}Co_{0.5}V_{0.1}$) can be used to develop a Wiegand wire with better performance.[25] Moreover, he considered a magnetic structure comprising hard outer and soft inner layers. Since then, Wiegand wires have been made of vicalloy. In 1997, Susumu Abe et al. proposed that a Wiegand wire exhibits a magnetic structure with soft outer and hard inner layers.[26] In 2017, Takemura et al.

analyzed the hysteresis loops of Wiegand wires with different diameters after etching. They proposed that the magnetic structure of a Wiegand wire includes soft outer and hard inner layers.[27] However, there was no direct evidence to validate the aforementioned analysis of the magnetic structure of Wiegand wires made of vicalloy. In this study, the FORC diagram method is used to verify that a Wiegand wire includes soft outer and hard inner layers.

1.2 Research Objective and Main Contribution

Since the invention of the Wiegand wire, a few researchers have considered its magnetic structure to be two-layered with hard outer and soft inner layers. Other researchers considered its magnetic structure to be two-layered with soft outer and hard inner layers (Figure 1.5). This study determines the real magnetic structure of a Wiegand wire and demonstrates the distribution of soft and hard layers in the structure. After the magnetic structure of the Wiegand wire is determined, its magnetic characteristics and magnetization process in varying exciting magnetic fields are studied. An understanding of the magnetic structure, magnetization process, and magnetic characteristics would help in the application of Wiegand wires.

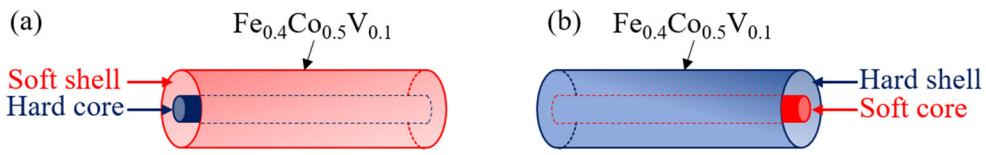

Figure 1.5 Magnetic structure of Wiegand wires: (a) Magnetic structure with the soft shell and hard core; (b) magnetic structure with the hard shell and soft core.

The FORC diagrams and hysteresis loops are used to analyze five types of Wiegand wires with different diameters. An FORC analysis of a Wiegand wire with the smallest diameter reveals that it is a uniform and single magnetic material. Furthermore, its coercivity measured using the major hysteresis loop is ~4.20 mT. This indicates that the inner layer of the Wiegand wire is hard and its outer layer (etched) is soft. The FORC diagram analysis of the other four types of Wiegand wires with different diameters reveals the existence of an interaction layer between their soft and hard layers (also known as the middle layer). Therefore, a three-layered magnetic structure is proposed: a soft outer layer, a hard inner layer, and the middle layer between these. The reason for the generation of a negative region in the FORC diagram is described as well.

Based on the three-layered magnetic structure, the thickness of the soft and middle layers is determined by calculating the ratio of the height of the large Barkhausen jump to the major hysteresis loop and combining the diameter of the hard layer analyzed using the FORC diagram method. A model to calculate the thicknesses of regions with each direction of magnetization of Wiegand wires under applied magnetic field intensities is proposed based on the analysis of minor hysteresis loops. This model

provides a theoretical basis for analyzing the magnetization process of Wiegand wires under different applied magnetic fields.

Magnetic characteristics such as coercivity, remanence, the height of the large Barkhausen jump, and the switching field are analyzed based on the major and minor hysteresis loops of Wiegand wires. The variation trend of the pulse amplitude in the pickup coil and the height of the large Barkhausen jump of the Wiegand wires are compared under different applied magnetic fields. Their variation trends are identical. This indicates that the large Barkhausen jump produces the pulse voltage.

The aforementioned analysis of the magnetic structure, proposed model for calculating the thickness of regions of magnetization and reversed magnetization, magnetization process, and magnetic characteristics of Wiegand wires (Figure 1.6) provide researchers with a better understanding of these wires and a theoretical basis for their application.

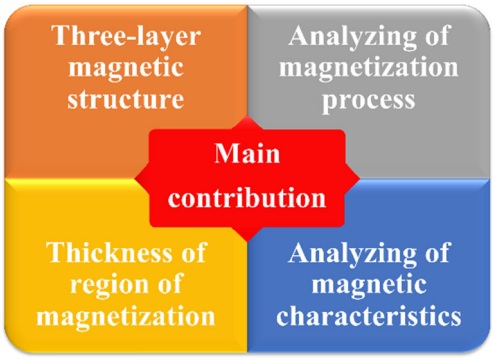

Figure 1.6 Contributions of this study.

1.3 Organization of this Dissertation

In this study, the magnetic structure, magnetic characteristics, and magnetization process of Wiegand wires are analyzed based on FORCs and the hysteresis loop to extend the application of Wiegand sensors in the IoT field.

The background, objective, and contribution of this study are elaborated in the first chapter. Section 1.1 introduces the study background. The development and application of the IoT have significantly facilitated production and human life. The installation of IoT devices continues to grow steadily as many countries are focusing on the IoT development. These IoT devices require stability, long battery life, and self-powered supply. At present, a self-powered supply system made of Wiegand sensors can meet the aforementioned requirements. Hence, studies on the core component (the Wiegand wire) are important. Section 1.2 describes the objective and contribution of this study. The magnetic structure of a Wiegand wire has been a subject of contentious debate since its inception. This study demonstrates the real magnetic structure of Wiegand wires and, thereby, resolves this debate. Then, the contribution of this study is elaborated.

Chapter 2 describes the key theoretical knowledge involved in this study. Section 2.1 elaborates the fundamentals of magnetic materials. The classification of the magnetic behavior of magnetic materials, demagnetizing field, magnetic anisotropy, magnetic domain, and magnetization process are introduced. Section 2.2 details Wiegand wires. First, the magnetic wire and large Barkhausen jump effect are introduced. Then, the Wiegand wire is described (an important magnetic material investigated in this study). Then, the Wiegand effect, Wiegand pulse, and conventional magnetic structure of Wiegand wires are explained. Section 2.3 introduces hysteresis loops and the FORC diagram method.

In Chapter 3, the magnetic structure of Wiegand wires is analyzed based on an FORC diagram. The analysis confirmed that the magnetic structure of a Wiegand wire has three layers: a hard inner layer, a soft outer layer, and the middle layer between them. The reason for the generation of a negative region in the FORC diagram is described as well.

In Chapter 4, the thicknesses of the soft and middle layers of Wiegand wires with different diameters are calculated by combining the height of the large Barkhausen jump. A model for calculating the thicknesses of the regions of magnetization and reversed magnetization is proposed by analyzing the hysteresis loops of Wiegand wires with

different diameters. Moreover, the magnetization process with regard to Wiegand wires with different diameters under different applied magnetic fields is analyzed.

In Chapter 5, the magnetic characteristics of Wiegand wires with different diameters, i.e., coercivity and remanence measured in major and minor hysteresis loops, are analyzed. The variation trends of the pulse voltage in the pick-up coil and height of the large Barkhausen jump are compared. Moreover, variation in the switching field of Wiegand wires under various applied magnetic fields is discussed.

Chapter 6 summarizes the study results. Figure 1.7 shows the organization of this dissertation.

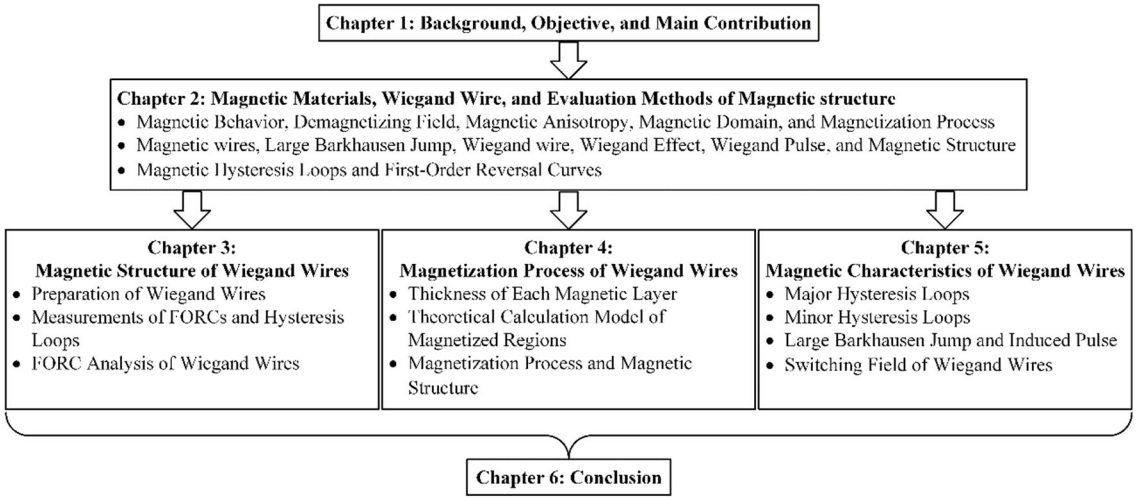

Figure 1.7 Organization of this dissertation.

Chapter 2: Theories

2.1 Fundamentals of Magnetic Materials

2.1.1 Various Types of Magnetic Behavior of Magnetic Materials

An atom possesses a nucleus and electrons. The nucleus exhibits nuclear magnetic moments, and an electron exhibits orbital magnetic and spin magnetic moments. The nuclear magnetic moment is significantly smaller than the other two magnetic moments, and its contribution to the atomic magnetic moment is highly marginal. Thus, the atomic magnetic moment comprises electronic orbital magnetic and spin magnetic moments. The magnetism of a material represents the magnetic moments of atoms that constitute the material. Magnetism exists in all substances. However, a few of these substances are magnetic materials. A material is magnetized when it is subjected to a magnetic field. Its quantity can be expressed by magnetization M, which is the product of magnetic susceptibility χ and the intensity of applied magnetic field H. Certain substances are strongly magnetized, and some are weakly magnetized. According to the magnitude and sign of the susceptibility at magnetization, the magnetism of a substance can be divided into diamagnetism, paramagnetism, ferromagnetism, antiferromagnetism, and ferrimagnetism.[28-29]

The diamagnetism of a material refers to the variation in the electron orbital magnetic moment in atoms under an applied magnetic field. It causes the direction of the magnetic moment to be opposite to that of the applied magnetic field, whereby the magnetic susceptibility of the material is a small negative value. The magnitude of diamagnetism is independent of the temperature and external magnetic field. All substances exhibit diamagnetism under an external magnetic field, thereby generating weak magnetism.[30]

The magnetic moment of each atom in certain substances is denoted as m, and the interaction among the atoms is negligible. At room temperature, in the absence of an applied magnetic field, the thermal energy can randomize the directions of the magnetic moments of these atoms (Figure 2.1). Consequently, the net magnetization is $M = \Sigma m = 0$. The atomic magnetic moments rotate and align along the direction of the magnetic field when an external magnetic field is applied. This results in low positive net magnetic susceptibility. If the strength of the applied magnetic field increases, the total atomic magnetic moment along the direction of the magnetic field linearly increases. At this time, if the strength and direction of the magnetic field are assumed to remain

constant and the temperature increases, M would decrease owing to the enhanced thermal motion. This relationship is known as Curie's law of paramagnetism, wherein magnetization is inversely proportional to temperature.[31] These properties are collectively known as the paramagnetism of substances.

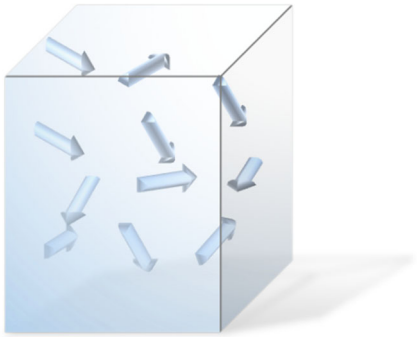

Figure 2.1 Paramagnetism of a material.

The exchange interaction model in quantum mechanics indicates that the exchange interaction between adjacent atoms in a magnetic material aligns the direction of the magnetic moments of adjacent atoms and causes spontaneous magnetization (Figure 2.2). In the absence of an additional magnetic field, small areas of spontaneous magnetization (known as magnetic domain) exist inside the magnetic material. The direction of the atomic magnetic moment in each magnetic domain is consistent. However, the direction between the magnetic domains is arbitrary, whereby the magnetization effects between these domains counteract each other. As a result, the magnetic material does not completely exhibit magnetism. When an external magnetic field is applied, the magnetization of magnetic domains in the magnetic material would be in the direction of the external magnetic field. If the external magnetic field is reversed, the magnetization would not return according to the original magnetization path: there would be a certain lag (i.e., the hysteresis phenomenon). The aforementioned characteristics of the magnetic materials appear below the Curie temperature, i.e., Tc. When the temperature is higher than Tc, the spontaneous magnetization disappears, and the magnetic material exhibits paramagnetism.[32] These properties are collectively known as the ferromagnetism of substances.

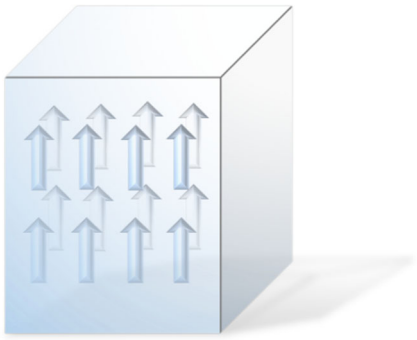

Figure 2.2 Ferromagnetism of a material.

The atoms of antiferromagnetic materials exhibit permanent magnetic moments. The interaction between these magnetic moments is strong but negative. Consequently, the adjacent magnetic moments are in opposite directions. When the total antiparallel magnetic moments are equal and aligned, their magnetization cancels each other out. Therefore, the net magnetization and spontaneous magnetization are zero (Figure 2.3). The magnetic susceptibility of antiferromagnetic materials reaches the maximum level at the Néel temperature, i.e., T_N. The material exhibits paramagnetism when the temperature is higher than T_N and antiferromagnetism when the temperature is less than T_N.[33]

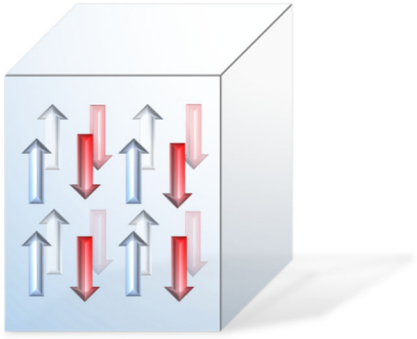

Figure 2.3 Antiferromagnetism of a material.

Ferrimagnetic materials exhibit macroscopic magnetism similar to ferromagnetic materials. Although the distribution of atomic magnetic moments is similar to that of antiferromagnetic materials, these differ. The magnitude of the magnetic moments of antiparallel atoms in the ferrimagnetic material differs when the temperature is less than Tc. This results in non-zero net magnetization and spontaneous magnetization (Figure 2.4).[34]

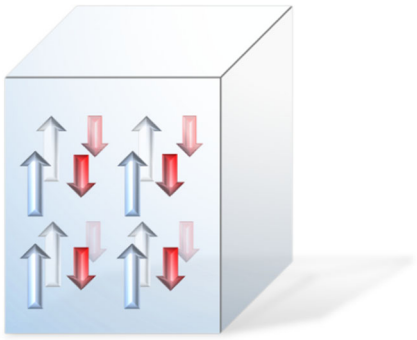

Figure 2.4 Ferrimagnetism of a material.

All substances exhibit magnetism. However, it is not absolute and varies according to the external environment. For example, ferromagnetic substances exhibit ferromagnetism below Tc and paramagnetism above Tc. The magnetism of substances can be classified as weak and strong based on its mechanism. Diamagnetism, paramagnetism, and antiferromagnetism belong to the weak category, and ferromagnetism and ferrimagnetism belong to the strong category. Magnetic materials exhibit high magnetism.[35-36]

Soft and hard magnetic materials can be distinguished according to the degree of demagnetization after magnetization. A soft magnetic material can be magnetized and demagnetized conveniently as its coercivity is low and initial permeability is high. A hard magnetic material becomes difficult to demagnetize as its coercivity is high. It can maintain high magnetism (known as remanence) even when the applied magnetic field is removed after magnetization. The remanence is not affected by the external environment and can be retained for a long time. Therefore, a hard magnetic material can be referred to as a permanent magnetic material.[37-38]

2.1.2 Demagnetizing Field and Magnetic Anisotropy

The magnetization state of a magnetic material is related to its susceptibility and shape. When a sample with a specific size is magnetized, a free magnetic pole would be generated at its ends in the direction opposite to that of the applied magnetic field. The magnetic field generated by the free magnetic pole is the demagnetizing field, i.e., H_d (Figure 2.5 (a)).[39-40] Its amplitude is relevant to the shape and magnetization of the magnetic material, as expressed in Equation (2.1). Here, N denotes the demagnetizing factor. It is affected by the shape of the material.

$$H_{\mathrm{d}} = -NM \tag{2.1}$$

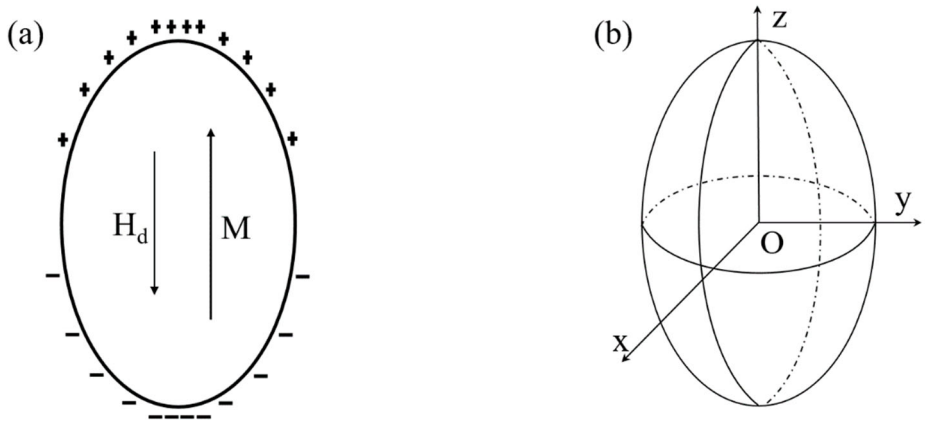

Figure 2.5 (a) Demagnetizing field. (b) Ellipsoidal shape sample.

It becomes difficult to determine the distribution of free magnetic poles on the surface of irregularly shaped magnetic materials, thereby making it difficult to calculate the amplitude of N. Figure 2.5 (b) shows the calculation of the demagnetizing factor of an ellipsoidal sample.[40] The relationship among the demagnetizing factors, i.e., N_x, N_y, and N_z, of the ellipsoidal sample along the x, y, and z directions, respectively, is expressed in Equation (2.2):

$$N_x + N_y + N_z = 1 \tag{2.2}$$

It can be inferred that $N_x = N_y = 1/2$ if the elongated cylinder is magnetized along the long axis (assuming $N_z = 0$).

The magnetic susceptibility or magnetization curve of magnetic materials exhibits different characteristics in different directions under an external magnetic field. This is

known as magnetic anisotropy. A material is directly magnetized along the easy magnetization direction (or easy axis), i.e., the required magnetization energy is minimum for this direction. The material is not directly magnetized along the difficult magnetization direction (or difficult/hard axis), and the required magnetization energy is maximum for this direction.[41]

When the magnetic material of a particular shape is magnetized, magnetization characteristics in different directions vary owing to the demagnetizing field. This is known as shape anisotropy. In the direction of a relatively small size, the demagnetizing field is large, and the magnetic material is not directly magnetized. In the direction of a relatively large size, the demagnetizing field is weak, and the magnetic material is directly magnetized. The Wiegand wire used in this study exhibits the shape of a longitudinal wire, and the shape anisotropy is highly significant. The wire displays uniaxial anisotropy, and its length and radius directions represent the easy and hard axes, respectively.[42-43]

2.1.3 Magnetic Domain and Magnetization Process

In the description of ferromagnetism in Section 2.1.1, magnetic domains have been introduced as small regions of spontaneous magnetization within magnetic materials. Ferromagnetic materials do not exhibit magnetism at the macroscopic scale. These include five types of interaction energy: external magnetic field energy, demagnetizing energy, exchange interaction energy, magnetic anisotropy energy, and magnetic elasticity energy. According to the principle of thermodynamics, the stability of the magnetic state of magnetic materials is determined based on the minimum state of the sum of the aforementioned five types of free energy, i.e., a domain of a magnetic material is generated by the equilibrium distribution of spontaneous magnetization in accordance with the principle of the minimum total free energy.

The stable magnetic state of a magnetic material not subjected to an external magnetic field and stress is determined by the minimum total free energy of exchange interaction, magnetic crystal anisotropy, and demagnetization. The exchange interaction energy can cause spontaneous magnetization, and the magnetic crystal anisotropy energy can magnetize magnetic materials along the easy axis direction. When magnetization attains saturation, these two types of energy are at the lowest state and do not affect the generation of magnetic domains. The free magnetic pole generated by spontaneous magnetization would generate demagnetizing energy. This would increase the total energy of magnetic materials and break the stable state of spontaneous magnetization. Numerous areas of spontaneous magnetization are formed inside the magnetic material to reduce the effect of the demagnetizing energy. Finally, the demagnetizing energy is minimized. These small areas are known as magnetic domains (Figure 2.6).[44] Thus, magnetic domains are formed to minimize the demagnetizing energy.

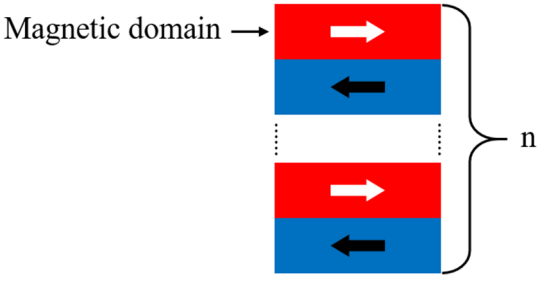

Figure 2.6 Magnetic domain in a uniaxial crystal.

In Figure 2.6, if n = 1, the uniaxial crystal is in the state of uniform magnetization. The demagnetizing energy reaches the maximum level at this instant. If n = 2, two magnetic

domains with alternating opposite magnetization directions are generated in the crystal. This weakens the demagnetizing energy. If the number of magnetic domains with alternating opposite magnetization directions in the crystal is n, the demagnetizing energy would eventually decrease to 1/n of the demagnetizing energy under uniform magnetization.

The magnetization process of the magnetic domain of a magnetic material with uniaxial magnetic crystal anisotropy is shown in Figure 2.7. Point O denotes the ideal demagnetizing state. The direction of the magnetic domain of spontaneous magnetization in the magnetic material is arbitrary. It macroscopically does not exhibit magnetism, i.e., the magnetization intensity is zero. When the magnetic field is applied along the positive direction, the magnetic domain in the direction opposite to the applied magnetic field is deflected toward the opposite direction and achieves the distribution state reaches point B. The intensity of the applied magnetic field continues to increase until the saturation magnetization state at point C. In this state, all the magnetic domains are oriented along the same direction as the applied magnetic field. Then, the applied magnetic field gradually reduces to zero. The direction of the magnetic domain would not return to the distribution state at point O owing to the existence of irreversible magnetization. It rather deflects toward the nearest easy axis along the direction of the applied magnetic field. All the magnetic domains are uniformly distributed in the right hemisphere, as shown at point D. At this instant, residual magnetization exists, and the direction is toward the right side.[40]

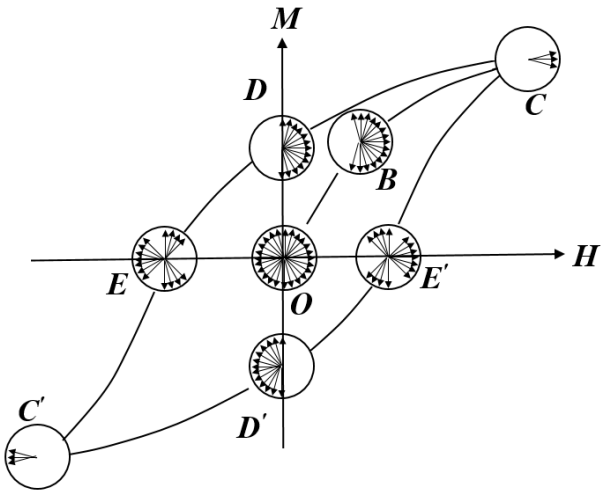

Figure 2.7 Representative magnetization process in a uniaxial polycrystalline material.

Then, the magnetic field is applied along the negative direction. The magnetic domain to the right direction reverses first. Therefore, it attains the distribution state at point E

(also known as the coercive point), where magnetization is zero. However, the distribution state of the magnetic domain differs significantly from that at point O. If the intensity of the applied magnetic field continues to increase along the negative direction, the saturation magnetization state in this direction would reach point C' (which is symmetrical to the state of point C). Then, the intensity of the applied magnetic field is reduced to zero along the positive direction to achieve state D' (which is symmetrical to point D). The states of points E' (which is symmetrical to point E) and C can be obtained if the magnetic field continues to increase along the positive direction. This would complete a cycle of the magnetization process.

2.2 Wiegand Wire

2.2.1 Magnetic Wires and Large Barkhausen Jump

A magnetic wire possesses low longitudinal demagnetization, high working frequency, and high radial spatial resolution. It is widely used in microelectronics, magnetic sensors, intelligent composite materials, security, and other fields. In the beginning, iron wires, cobalt wires, and nickel wires were the main research objects, and their applications were developed.[45-47] Subsequently, researchers observed that magnetic wires made of two or more elements possess better physical and chemical properties and application characteristics than those made of any one of the aforementioned elements. Then, researchers developed the widely used permalloy wire, Wiegand wire, amorphous wire, magnetic nanowires, and other alloy magnetic wires.[48-51]

The Barkhausen effect was first observed in iron by Barkhausen in 1919. It implies that discontinuous magnetization variation occurs in the irreversibly magnetized part of the magnetization curve of ferromagnetic materials, i.e., domain walls are shifted irreversibly. The displacement does not vary continuously. Instead, it shows certain jumps, which can cause discontinuous variations in the magnetic flux of magnetic materials. The discontinuous variations in the magnetic flux can be enhanced using an amplifier, and the voltage pulse can be observed using an oscilloscope (Figure 2.8 (a)).[52]

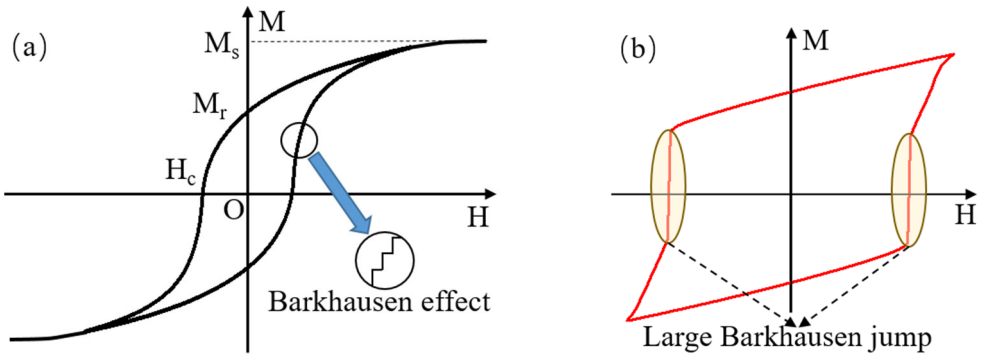

Figure 2.8 (a) Barkhausen effect. (b) Large Barkhausen jump.

The large Barkhausen discontinuities were first observed by Forrer in the hysteresis loop of a nickel wire.[53] Moreover, Preisach identified large Barkhausen discontinuities in an iron–nickel alloy wire.[54] These large Barkhausen discontinuities correspond to the reversal of multiple magnetic elements in magnetic materials. Subsequently, Sixtus

and Tonks renamed the large Barkhausen discontinuities as large Barkhausen jump (Figure 2.8 (b)).[55-58] The large Barkhausen jump can be observed in Wiegand and amorphous wires.

2.2.2 Wiegand Wire

A magnetic wire with the Wiegand effect (described in Section 2.2.3) is known as a Wiegand wire. It was first developed by John R. Wiegand using a $Ni_{0.48}Fe_{0.52}$ magnetic wire in 1974.[23] Then, in 1981, he observed that a vicalloy wire (chemical composition: $Fe_{0.4}Co_{0.5}V_{0.1}$) exhibited a better Wiegand effect. Therefore, Wiegand wires are now made of vicalloy.[24]

Wiegand wires are made of vicalloy wire with a diameter of ~0.25 mm using a cold-working process. This refers to the repeated torsional strain of a vicalloy wire under applied tension. After cold-working, it is age-hardened to retain the tension formed in the cold-working process. This process alters the coercivity of the vicalloy wire along the radial direction. This results in a shell with low coercivity and a core with high coercivity, i.e., low coercivity in the outer layer and high coercivity in the inner layer.[59-60] When an alternating magnetic field is applied to the Wiegand wire along the longitudinal direction, the outer layer would reverse owing to the low coercivity. This is accompanied by a large Barkhausen jump,[61] i.e., the cold-working process imparts the Wiegand wires with a permanent capability to exhibit a large Barkhausen jump.

2.2.3 Wiegand Effect and Wiegand Pulse

When an alternating magnetic field is applied along the longitudinal direction of a Wiegand wire and the magnetic field strength becomes higher than the switching field of the wire, the soft layer of the wire undergoes fast magnetization reversal, accompanied by a large Barkhausen jump.[62-63] When the magnetic field strength continues to increase, the hard layer undergoes magnetization reversal, and the direction of the magnetization of the soft and hard layers becomes consistent with that of the applied magnetic field. At this time, the magnitude of the magnetic field is reduced to zero. Then, the direction of the magnetic field is reversed. When the strength of the reversed magnetic field is larger than the switching field, the soft layer of the Wiegand wire undergoes reversed magnetization along the direction of the reversed magnetic field, accompanied by a large Barkhausen jump. When the reversed magnetic field intensity continuously increases, the hard layer undergoes reversed magnetization toward the direction of the reversed magnetic field. The magnetization direction of the soft and hard layers is consistent with the direction of the reversed magnetic field. At this point, the Wiegand wire completes a periodic magnetization reversal. In the process of the magnetization reversal of one cycle, the Wiegand wire generates two large Barkhausen jumps in opposite directions. If the magnetic field periodically varies, the Wiegand wire periodically generates the large Barkhausen jump.[64] This phenomenon of Wiegand wires is known as the Wiegand effect.[65-66]

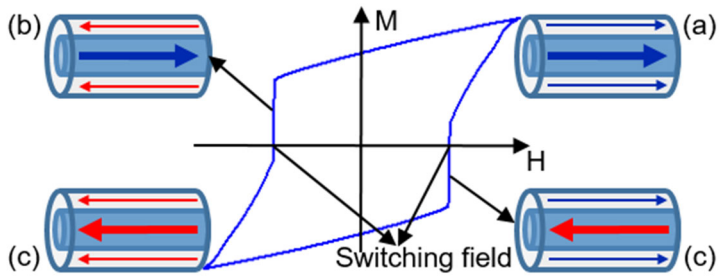

Figure 2.9 Wiegand effect: (a) parallel state; (b) antiparallel state; (c) parallel state; (d) antiparallel state.

The magnetization reversal of a Wiegand wire is shown in Figure 2.9. As shown in Figures 2.9 (a) and (c), the magnetization directions of the soft and hard layers are identical. This is known as a parallel state. As shown in Figures 2.9 (b) and (d), the soft and hard layers are in the opposite direction. This is known as an antiparallel state. A

large Barkhausen jump is generated when the magnetization state of the Wiegand wire becomes antiparallel. This causes an abrupt variation in magnetic flux.[67] Therefore, a pulse voltage would be induced in a pickup coil if it is wound around the Wiegand wire. This is known as the Wiegand pulse.[68] As shown in Figure 2.10, the Wiegand pulse is obtained by a Wiegand wire with a length and diameter of 13 and 0.23 mm, respectively, using a pickup coil with a length of 5 mm and 3000 turns. The amplitude of the pulse voltage achieves ~10 V, and the pulse width achieves ~10 us. The rate of the generation of the Wiegand pulse is independent of the frequency of the applied magnetic field. The Wiegand pulse can be generated even when the frequency of the applied magnetic field is close to zero. This characteristic makes Wiegand wires more effective than other magnetic materials.

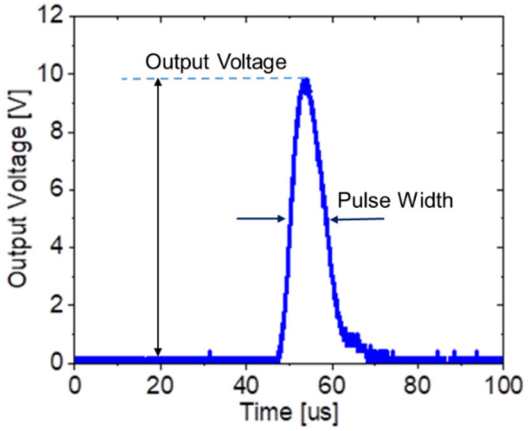

Figure 2.10 Wiegand pulse of the Wiegand wire.

2.2.4 Magnetic Structure of Wiegand Wire

This study focuses on the magnetic structure of Wiegand wires. Initially, the Wiegand wire made of permalloy by Wiegand possessed a magnetic structure comprising a hard outer layer with a high coercive force and a soft inner layer with a low coercive force. Then, he developed a Wiegand wire using vicalloy to enhance its performance. He considered the magnetic structure of this wire to be identical to that of a Wiegand wire made of permalloy. However, there was no direct evidence to demonstrate this. A few researchers considered that the magnetic structure comprises a soft outer layer and hard inner layer. Most current research is based on this magnetic structure. Its typical form is shown in Figure 2.11.

The magnetic structure is two-layered. The outer layer is soft and possesses a coercivity of ~2 mT, and the inner layer is hard and possesses a coercivity of ~8 mT. The diameter is ~0.25 mm.[69] There is no clear boundary between the soft and hard layers along the radial direction. The distribution of the coercivity in the radial direction gradually varies from the outer layer to the inner one. The magnetic structure of Wiegand wires is investigated and analyzed further in this study based on this structure.

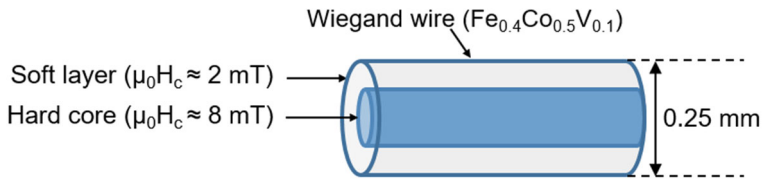

Figure 2.11 Typical magnetic structure of the Wiegand wire.

2.3 Methods for Evaluating the Magnetic Structure of Wiegand Wires

2.3.1 Magnetic Hysteresis Loops

The response characteristic of the magnetization (M) of magnetic materials under the action of an external magnetic field (H) is considered to be the basis of their application. This response characteristic can be demonstrated using a magnetic hysteresis loop, which is one of the important characteristics of magnetic materials.[70-71] In the case of the complete demagnetization of a magnetic material, it is imposed by H. When H increases from zero, M increases abruptly and gradually reaches a definite value (M_s). At this time, M remains constant even when H continues to increase. This indicates that the magnetic material has attained the saturation magnetization state. Accordingly, M_s is also known as saturation magnetization. The curve formed by M and H is also known as the initial magnetization curve (the curve OA in Figure 2.12).

The magnitude of the external magnetic field gradually decreases when the magnetic material achieves the saturation magnetization state. However, the direction remains steady. At this time, the diversion of M is affected by various types of interaction inside the magnetic material. Therefore, M cannot decrease along the direction of the initial magnetization curve. M is non-zero when the magnitude of the applied magnetic field decreases to zero. Then, magnetization is known as residual magnetization. It is referred to as remanence and is represented by M_r. Then, the magnetic field intensity increases along the opposite direction. Magnetization continues to decrease. The magnetic field intensity when it decreases to zero is known as the coercivity of the magnetic material. It is expressed by H_c. If the amplitude of the reversed magnetic field continues to increase, the direction of M reverses and finally achieves a saturation state in the opposite direction. Then, the aforementioned process is repeated, and the magnetization curve is symmetric to the aforementioned process around the origin of coordinates O. M and H form a closed curve when H decreases from a positive maximum value to a negative maximum value and then increases to the positive maximum value again. It is known as a hysteresis loop or major hysteresis loop (Figure 2.12). A small hysteresis loop (also known as a minor hysteresis loop) can be obtained if the strength of the external magnetic field applied to the magnetic material is less than saturation magnetization. Multiple minor hysteresis loops can be obtained if more than one round of magnetization occurs (Figure 2.12).

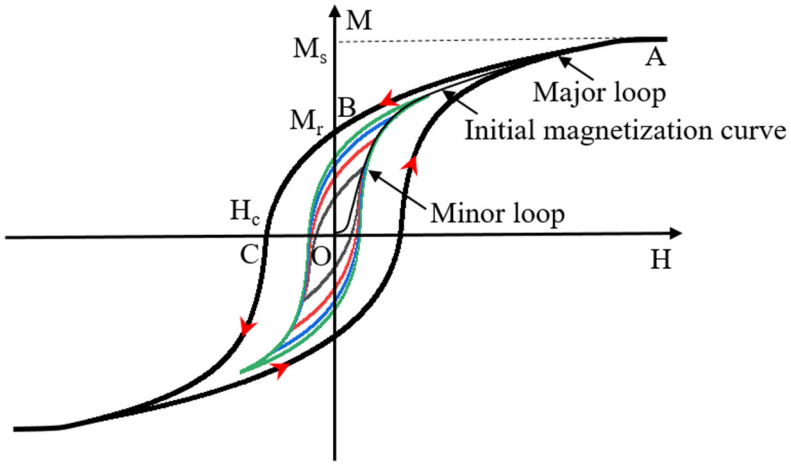

Figure 2.12 Major and minor hysteresis loops of a magnetic material.

The aforementioned major and minor hysteresis loops exhibit various magnetic characteristics of the magnetic materials, i.e., coercivity (H_c), remanence (M_r), and saturation magnetization (M_s).[72-73] With regard to the physical perspective, coercivity represents the capability of a magnetized magnetic material to maintain its magnetization state. It helps distinguish soft and hard magnetic materials. Remanence represents magnetization retained in a magnetized magnetic material without the influence of an applied magnetic field. Saturation magnetization defines the maximum magnetization of a magnetized magnetic material. Therefore, specific magnetic properties of a magnetic material can be comprehended by analyzing their hysteresis loops.

2.3.2 First-Order Reversal Curves (FORCs)

The FORC diagram method was first proposed by Mayergoyz in 1985 to optimize the application of the Preisach model to hysteresis phenomena.[74-75] It can be used to analyze the coercivity and interaction between magnetic particles. The FORC diagram method was first used in the study of geological samples in 1999.[76] Moreover, it helps distinguish the types, sizes, and magnetic domain states of the magnetic particles of various magnetic materials and intuitively calculate the distribution of the coercivity and interaction between magnetic particles.[77-80] These advantages are not comparable with those of the hysteresis loop. Although the major hysteresis loops of magnetic materials differ negligibly in shape, significant differences can be observed in their FORC diagrams. Hence, additional information can be obtained using FORC diagrams compared to the major hysteresis loops.[81-83]

An FORC diagram is obtained based on the second derivative of the external ($\mu_0 H_b$) and reversal ($\mu_0 H_a$) magnetic fields considering the magnetization of any point in the FORC group. Figure 2.13 shows the measurement of the FORC group. First, a saturated positive magnetic field ($\mu_0 H_{sat}$) is applied to magnetize the magnetic material to saturation. Then, the external magnetic field reduces to $\mu_0 H_a$. Hereafter, the external magnetic field increases from $\mu_0 H_a$ to $\mu_0 H_{sat}$. The magnetization curve of the external magnetic field from $\mu_0 H_a$ to $\mu_0 H_{sat}$ is known as the FORC. The magnetization intensity corresponding to $\mu_0 H_b$ on the FORC can be expressed as M ($\mu_0 H_a$, $\mu_0 H_b$). It is determined based on the external and reversal magnetic fields. Here, $\mu_0 H_b \geq \mu_0 H_a$. $\mu_0 H_a$ is selected to vary from $\mu_0 H_{sat}$ to $-\mu_0 H_{sat}$, and the process to obtain a set of FORCs is repeated. The second derivative of M ($\mu_0 H_a$, $\mu_0 H_b$) on the FORC group with respect to $\mu_0 H_a$ and $\mu_0 H_b$ is calculated (Equation (2.3)). The distribution function ρ ($\mu_0 H_a$, $\mu_0 H_b$) of M ($\mu_0 H_a$, $\mu_0 H_b$) on the ($\mu_0 H_a$, $\mu_0 H_b$) plane can be obtained. The graph formed by the contour lines represents the FORC diagram.[84-85] The influence of reversible magnetization in the process of reversal magnetization can be eliminated using the FORC diagram method. In the reversible magnetization process, the magnetization intensity of magnetic materials does not vary with the variation in $\mu_0 H_a$. Hence, its derivative is zero. This results in the absence of distribution on the FORC diagram.[86]

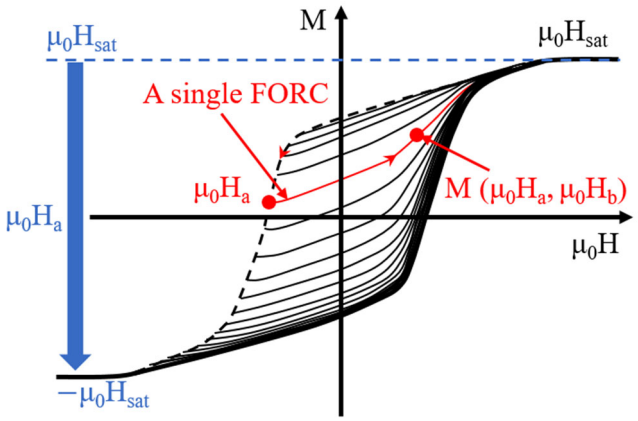

Figure 2.13 Individual FORC and a group of FORCs.

$$\rho(\mu_0H_a, \mu_0H_b) = -\frac{\partial^2 M(\mu_0H_a, \mu_0H_b)}{\partial\mu_0H_a\,\partial\mu_0H_b} \tag{2.3}$$

The coordinate system (μ_0H_a, μ_0H_b) is converted to (μ_0H_c, μ_0H_u) to directly observe the distribution of the coercive and interaction fields in magnetic materials. Here, μ_0H_c denotes the coercive field, and μ_0H_u denotes the interaction field. The converted equations are expressed in (2.4) and (2.5).

$$\mu_0H_c = (\mu_0H_b - \mu_0H_a)/2 \tag{2.4}$$

$$\mu_0H_u = (\mu_0H_b + \mu_0H_a)/2 \tag{2.5}$$

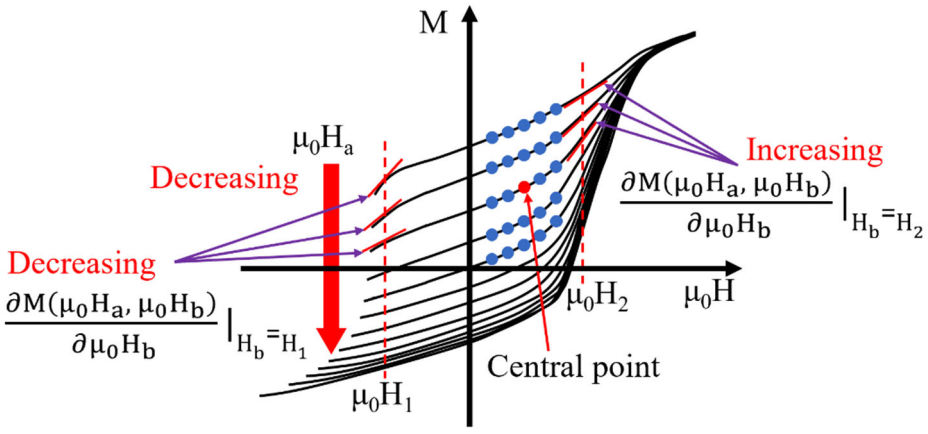

Figure 2.14 The slope of FORC and local square grid of FORC density distribution.

To estimate the FORC density distribution of the red point shown in Figure 2.14, a group of data points is selected in the FORC group considering the red point as the

center. This is shown by the red and blue points in Figure 2.14. This group of data points constitutes a local square grid. Then, a quadratic polynomial is used to fit the data in the local square grid (Equation (2.6)):

$$a_1 + a_2H_a + a_3H_a^2 + a_4H_b + a_5H_b^2 + a_6H_aH_b \quad (2.6)$$

The coefficients of the quadratic polynomial can be obtained using the linear least square method. By substituting Equation (2.6) into Equation (2.3), the value of ρ (μ_0H_a, μ_0H_b) at the central point of the local square grid is calculated as $-a_6$ after the quadratic derivative of the quadratic polynomial is obtained.[87-88]

Equation 2.3 can be redefined as follows:

$$\rho(\mu_0H_a, \mu_0H_b) = -\frac{\partial M}{\partial \mu_0H_a}\left(\frac{\partial M(\mu_0H_a, \mu_0H_b)}{\partial \mu_0H_b}\right) \quad (2.7)$$

In Equation (2.7), $\partial M/(\partial \mu_0H_a)$ represents the variation in μ_0H_a, and $\{\partial M (\mu_0H_a, \mu_0H_b)\}/(\partial \mu_0H_b)$ represents the slope at μ_0H_b on the FORC. At μ_0H_1 shown in Figure 2.14, μ_0H_a gradually decreases with the slope of the FORC. This causes the distribution function (ρ) to be negative. At μ_0H_2, the slope of the FORC increases with a decrease in μ_0H_a. This causes ρ to be positive.

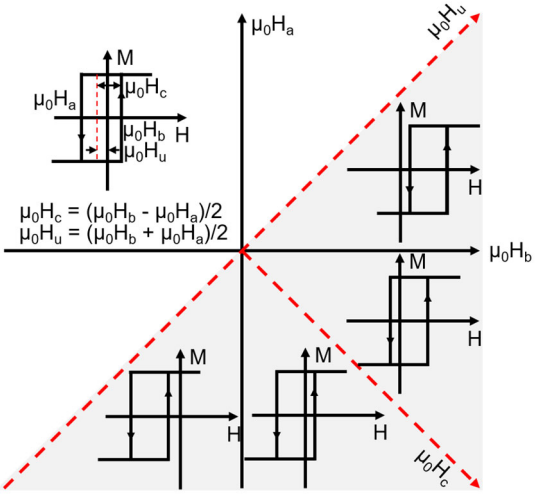

Figure 2.15 μ_0H_a and μ_0H_b, or μ_0H_c and μ_0H_u, coordinates.

The geometric significance of ρ (μ_0H_a, μ_0H_b) in the coordinate system with μ_0H_b as the horizontal axis and μ_0H_a as the vertical axis can be explained by the FORC density contour map projected in the gray triangle area (bounded by $\pm\mu_0H_{sat}$) shown in Figure

2.15. The FORC density contour map in the coordinate system with $\mu_0 H_c$ as the horizontal axis and $\mu_0 H_u$ as the vertical axis is shown by the red dashed line (Figure 2.15).[89-90]

Chapter 3: Analysis of the Magnetic Structure of a Wiegand Wire Using FORCs

In this chapter, the magnetic structures of five Wiegand wires with different diameters are studied using FORCs. It is verified based on the FORC analysis of a Wiegand wire with the minimum diameter, considering that the inner and outer layers of the wire are hard and soft, respectively. The FORC analysis of the other four Wiegand wires with different diameters confirms the similarity between their magnetic structures and the following layers: a soft outer layer, a hard inner layer, and the middle layer generated owing to the interaction between the soft outer and hard inner layers. The reason for the existence of negative regions in the FORC diagram is determined by analyzing the magnetization states of the Wiegand wires at the C, D, and E regions of the diagram.

3.1 Preparation of Wiegand Wires with Different Diameters

Wiegand wires with a length and diameter of 13 and 0.23 mm, respectively, are considered in this study. These wires have been supplied by SWFE, Co. Ltd., Meishan, China. The wire can be made in four steps. First, sufficient tension is applied to it along its length without stretching it. The tension is maintained at 64 counterclockwise and 48 clockwise turn twists. Second, it is twisted counterclockwise and clockwise for eight and a half turns (a cycle). After 17 cycles of twisting, it is twisted counterclockwise for eight and a half turns (which lasts for 10–15 s). Then, the wire is gradually stretched by 1%–2%. Third, the counterclockwise and clockwise twists in the second step are repeated for 60 cycles, while the tension is maintained without stretching the wire. Fourth, the wire is heated by a current of 5.6 A for 120 ms. This completes the fabrication of a Wiegand wire.[25]

In general, the magnetic structure of a Wiegand wire comprises two layers, as depicted in Figure 3.1. The outer layer is soft and has a coercivity of ~2 mT/μ_0. The inner layer is hard and has a coercivity of ~8 mT/μ_0. μ_0 denotes the permeability of vacuum. The coercivity gradually varies along the radial direction. This indicates the absence of a clear boundary between the soft layer and hard core.[91] The $FeCl_3$ solution is used to etch the outer surface of the Wiegand wire to further characterize its radial magnetic structure.[27] The domain structure varies when the outer layer is etched. We assume that the Wiegand effect is maintained in the wires. However, the performance of the Wiegand effect varies. Four Wiegand wires with a length and diameter of 13 and 0.23

mm, respectively, are placed horizontally in a glass beaker. An adequate amount of $FeCl_3$ solution is added to immerse the Wiegand wires. After ~30 min, one of the Wiegand wires is removed, and its diameter is measured by a micrometer. If the diameter has not reduced to 0.18 mm, the wire is placed back into the $FeCl_3$ solution to continue etching for a certain period. Then, the Wiegand wire is removed again, and its diameter is measured. This process is repeated until the diameter is 0.18 mm. After ~20 min, another Wiegand wire is removed, and a 0.14-mm-diameter Wiegand wire is fabricated using the aforementioned process described above. Then, a 0.10-mm-diameter Wiegand wire is obtained. The final one is a 0.06-mm-diameter Wiegand wire. These are etched in the same manner as done for the 0.14-mm-diameter Wiegand wire. Thus, the Wiegand wires with different diameters (0.06, 0.10, 0.14, 0.18, and 0.23 mm) are fabricated.

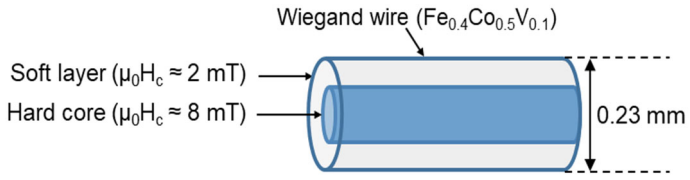

Figure 3.1 Conventional magnetic structure of a Wiegand wire.

3.2 Measurements of FORCs and Hysteresis Loops

In this study, the major and minor hysteresis loops and FORCs of the Wiegand wires are measured using vibrating sample magnetometer (VSM) (Model 8600 series, Lake Shore Cryotronics, Westerville, OH, USA) at room temperature.[91] In addition, the FORC diagrams are obtained using FORCinel and its auxiliary software (Igor Pro®, WaveMetrics Inc., Portland, OR, USA).[92-93] The measurement process of the FORC employed in this study is as follows. First, a saturated applied magnetic field ($\mu_0 H_{sat}$) is used to impart the Wiegand wire with positively saturated polarization. Thereafter, the applied magnetic field is reduced to a reversal magnetic field, i.e., $\mu_0 H_a$. Consequently, the applied magnetic field increases to $\mu_0 H_{sat}$ from $\mu_0 H_a$. The magnetization curve of the Wiegand wire in the aforementioned process is known as the FORC. The FORC depends on the applied magnetic field and can be determined using $\mu_0 H_a$. By adjusting $\mu_0 H_a$ and repeating the process, various FORCs are obtained as $\mu_0 H_a$ varies from $\mu_0 H_{sat}$ to $-\mu_0 H_{sat}$.[94-96]

The maximum field of the major hysteresis loops is 1000 mT, and each step of the applied magnetic field is 1 mT. The applied magnetic field of the minor hysteresis loops ranges from 2 to 15 mT, and each step of the applied magnetic field is 0.025 mT. The average measurement time of the major and minor hysteresis loops is 0.1 s. A magnetic field of $\mu_0 H_a = -500$ mT to $\mu_0 H_{sat} = 500$ mT is applied to measure the reversal curves of Wiegand wires with varying diameters. The step value of the reversal magnetic field $\mu_0 H_a$ of each FORC is 0.5 mT.[91] The average measurement time of the FORCs is 0.1 s, and the number of FORCs is 121. The extreme value of the coercive field is 30 mT, and the interaction field is ±15 mT. The pause time in the calibration and reverse fields is 1 s, and that in the saturation field is 0.1 s.

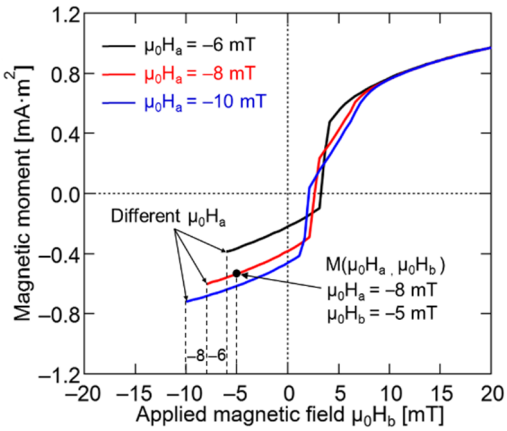

Figure 3.2 FORCs of the Wiegand wire considering various values of $\mu_0 H_a$.

Magnetization corresponding to $\mu_0 H_b$ on an FORC can be expressed by M ($\mu_0 H_a$, $\mu_0 H_b$). Here, $\mu_0 H_b \geq \mu_0 H_a$ (Figure 3.2). In the figure, the $\mu_0 H_a$ values of the three FORCs are –6, –8, and –10 mT, respectively. The black point of magnetization on the FORC is represented by M ($\mu_0 H_a$ = –8 mT, $\mu_0 H_b$ = –5 mT).

3.2.1 Major Hysteresis Loops of Wiegand Wires

The normal and enlarged images of the major hysteresis loops of five Wiegand wires with different diameters are depicted in Figure 3.3 (a). These loops are normalized. The enlarged image indicates that coercivity varies. This variation trend is portrayed in Figure 3.3 (b). It can be concluded that the coercivity of the Wiegand wire decreases as the diameter increases until stagnation at ~2.47 mT. The major hysteresis loops and coercivity are detailed in Chapter 5.

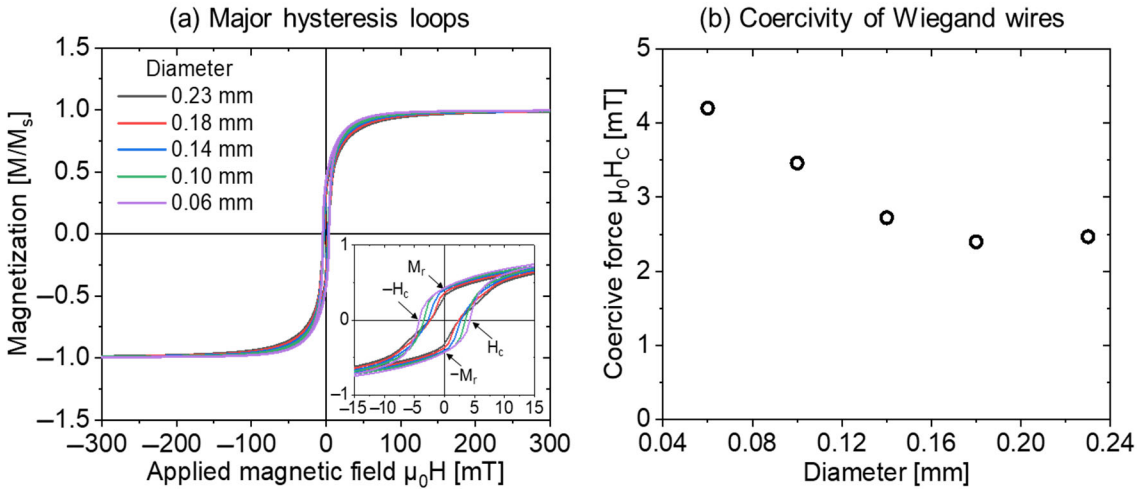

Figure 3.3 (a) Major hysteresis loops of the Wiegand wires and (b) coercivity of the Wiegand wires with varying diameters.

3.2.2 FORCs and FORC Diagrams of Wiegand Wires

The results of the FORCs of the Wiegand wires are illustrated in Figure 3.4. The FORCs between –20 mT and 20 mT are selected. This is because irreversible magnetization, which is considered to be an issue, occurs in this range. The FORC diagrams are calculated using the FORCs of the corresponding diameters. The FORCs illustrated in Figures 3.4 (a), (c), (e), (g), and (i) correspond to the Wiegand wires with diameters of 0.06, 0.10, 0.14, 0.18, and 0.23 mm, respectively. The FORC diagrams of the Wiegand wires with diameters of 0.06, 0.10, 0.14, 0.18, and 0.23 mm are plotted in Figures 3.4 (b), (d), (f), (h), and (j), respectively. Herein, the horizontal and vertical axes of the FORC diagrams denote $\mu_0 H_c$ and $\mu_0 H_u$, respectively.

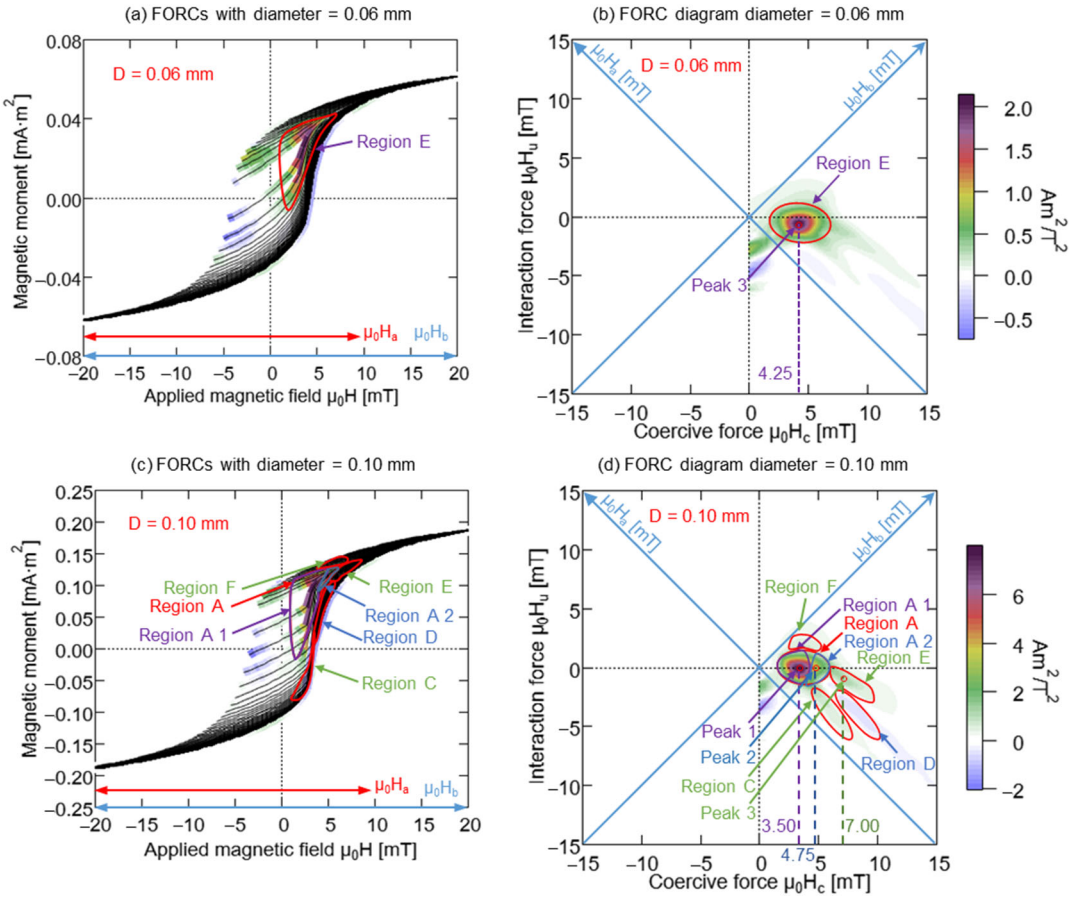

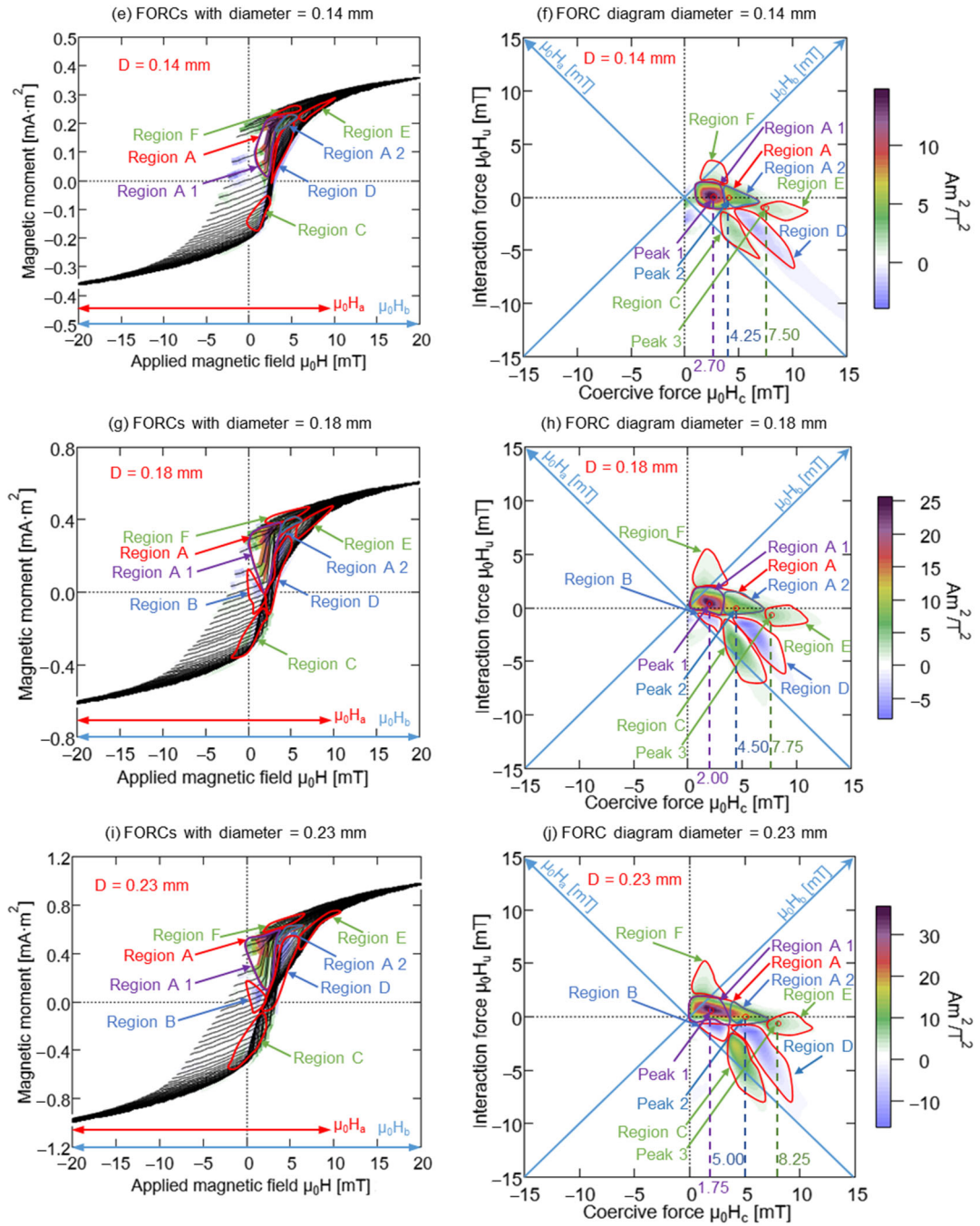

Figure 3.4 FORCs and FORC diagrams of the Wiegand wires with different diameters.

3.3 FORC Analysis of Wiegand Wires of Different Diameters

3.3.1 Relationship Between Coercivity of Major Hysteresis Loop and FORC Distribution

As shown in Figures 3.4 (b), (d), (f), (h), and (j), when $\mu_0 H_u$ = 0 mT, the FORC distribution ρ is plotted along the axis of $\mu_0 H_c$. It is denoted by the blue lines shown in Figure 3.5. The strength ρ increases with the diameter of the Wiegand wire. Meanwhile, $\mu_0 H_c$ corresponding to the maximum strength ρ gradually decreases and finally tends to be constant. The coercive forces of the Wiegand wire shown in Figure 3.3 (b) are marked in Figure 3.5 by the red dotted lines. A comparison reveals that the coercive force of the Wiegand wire with an equal diameter is consistent with the maximum strength ρ.[97]

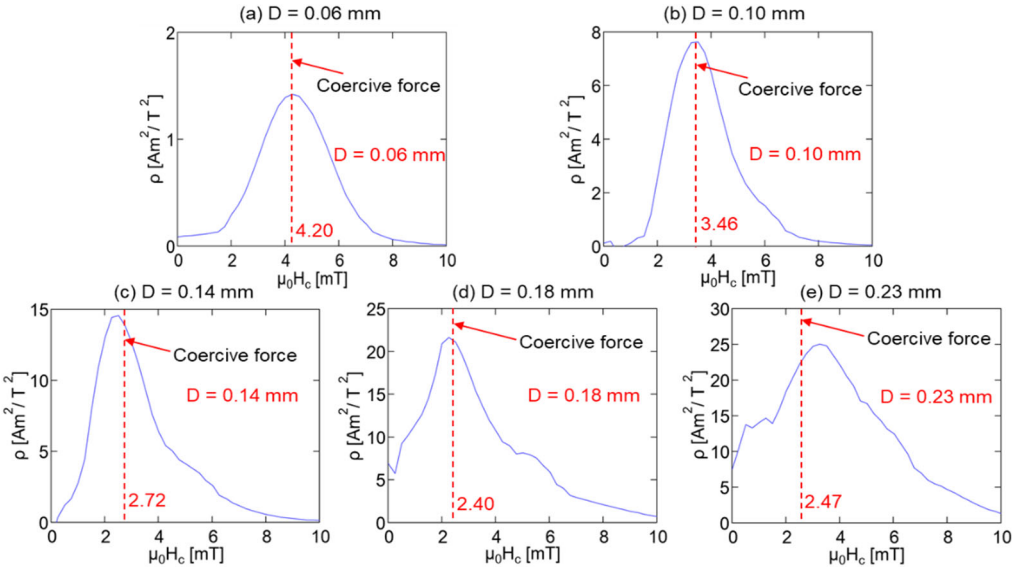

Figure 3.5 Correlation between the maximum of the FORC distribution along the $\mu_0 H_c$ axis and coercivity of the major hysteresis loop. (a) D = 0.06 mm; (b) D = 0.10 mm; (c) D = 0.14 mm; (d) D = 0.18 mm; (e) D = 0.23 mm.

3.3.2 Single and Uniform Magnetic Structure

The FORC diagram provides information with regard to the magnetization process and magnetic interaction inside the Wiegand wire. As shown in Figure 3.4 (a), the FORC of the 0.06-mm-diameter Wiegand wire does not exhibit a large Barkhausen jump. This indicates that the etched outer layer causes the fast magnetization reversal.[27] The various coercivity components of the same magnetic material can be analyzed based on the FORC diagram. Moreover, the FORC diagram illustrated in Figure 3.4 (b) portrays one region and a single peak. This indicates that only one component of coercivity exists. Its interaction field is distributed near $\mu_0 H_u = 0$ mT. This can be considered as a single and uniform magnetic structure. As shown in Figure 3.3 (b), the coercivity of the Wiegand wire with a diameter of 0.06 mm is ~4.20 mT (> 2 mT). It signifies that the single area is the hard core. This further verifies that the inner layer is hard and the outer layer is soft. Peak 3 exhibits the maximum value of the FORC distribution (Figure 3.4 (b)). It is located at the position where the coercivity is ~4.25 mT. This is consistent with the coercivity of the Wiegand wire with a diameter of 0.06 mm. The single magnetic structure is shown in Figure 3.6.

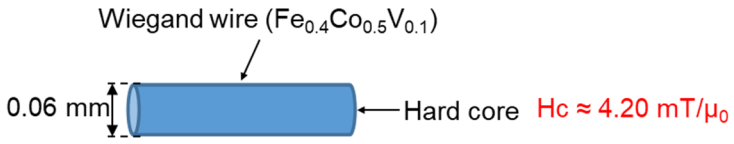

Figure 3.6 Single magnetic structure.

3.3.3 Three Layers of the Magnetic Structure

According to the magnetic structure of the 0.06-mm-diameter Wiegand wire, the inner layer is hard, and the outer layer is soft. An analysis of the FORC diagrams of the Wiegand wires with diameters of 0.10, 0.14, 0.18, and 0.23 mm reveals that their FORC diagrams are segmented into six or seven small regions with similar distributions. This implies the existence of multiple coercivity components.[97] The distribution intensity of each small region of the FORC diagram increases with an increase in diameter. This is similar to the concluded result described in Section 3.3.1. These small regions cease to be distributed around the interactive force $\mu_0 H_u = 0$, which is similar to the distribution in the 0.06-mm-diameter Wiegand wire. However, these expanded along the $\mu_0 H_u$ axis. The interactions between the components of the soft and hard layers within the Wiegand wire may cause these components to deviate from the zero-offset axis and thereby forming ridges.[98] This indicates an interaction between the soft and hard layers of the Wiegand wire, i.e., the existence of an interaction or middle layer.

Owing to the similar distribution of the FORC diagram, this study considers the FORC distribution diagram of the 0.23-mm-diameter Wiegand wire. As shown in Figure 3.4 (j), region A is distributed along the $\mu_0 H_c$ axis and exhibits a wide distribution range. Region A is divided into subregions, i.e., A1 and A2, as shown in Figure 3.4 (i). The large Barkhausen jump is evident, and the slope of the FORC is relatively high in subregion A1. However, the large Barkhausen jump does not exist in subregion A2, and the FORC is relatively flat. In Figure 3.4 (j), subregions A1 and A2 corresponding to Figure 3.4 (i) are segmented further. In particular, the distribution range of the coercive force in subregion A1 is 0–3.5 mT, and that of the interactive force is –0.5 to 1.5 mT. Therefore, subregion A1 can be considered as a soft layer with relatively small interaction. In subregion A2, the coercive force distribution ranges from 3.5 to 6.5 mT, and the interactive force distribution ranges from –0.5 to 1.25 mT. Thus, this subregion can be considered as a middle layer with relatively small interaction.

As indicated in Figure 3.4 (i), region B is distributed prior to the large Barkhausen jump. In Figure 3.4 (j), the distribution value of this region is negative, and the distribution ranges of the coercive and interactive forces are 0.75–3.25 mT and –2 to –0.75 mT, respectively. Therefore, region B can be considered as a soft layer with negligible interaction. When the applied magnetic field is 0–2.5 mT, owing to the presence of the magnetostatic coupling and demagnetizing field, the magnetization direction of a portion of the soft layer becomes opposite to that of the hard layer before the large Barkhausen jump. This indicates the existence of a negative region, i.e., region

B. Region B in the soft layer gradually etches away as the diameter decreases. Thereby, this region is absent in Figures 3.4 (c) and (e).

As observed in Figures 3.4 (i) and (j), region C is primarily distributed before the large Barkhausen jump, the coercive force distribution ranges from 3.25–6.5 mT, and the interactive force distribution ranges from –7.5 to –1.5 mT. Thus, region C is formed because of the interaction between the soft and hard layers of the Wiegand wire.

We can infer from Figures 3.4 (i) and (j) that region D is fundamentally distributed after the large Barkhausen jump, and the distribution value of this region is negative; the distribution range of the coercive force is 4–9 mT, and that of the interactive force is –7.5 to 1 mT. Furthermore, we can consider that region D is formed by the interaction between the soft and hard layers of the Wiegand wire.

In the FORC, region E is primarily distributed in the reversible magnetization area and situated farther from the large Barkhausen jump. In addition, the coercive force distribution ranges from 6.5 to 11.25 mT, and the interactive force distribution ranges from –2 to 0.5 mT. Therefore, region E can be considered as a hard core with marginal interaction.

In the FORC diagram, region F can be assumed as an extension of subregion A1, the coercive force distribution ranges from 0.25 to 2.5 mT, and the interactive force distribution ranges from 1.25 to 5 mT. In the FORCs, region F is predominantly distributed in the reversible magnetization area. Thus, region F constitutes the interaction between the soft and hard layers of the Wiegand wire, which does not contribute to the Wiegand effect.

In Figure 3.4 (j), peak 1 located at $\mu_0 H_c$ = 1.75 mT considers the maximum FORC distribution in the soft layer subregion A1. In comparison, peak 2 located at $\mu_0 H_c$ = 5.00 mT is situated at the middle maximum FORC distribution in the middle layer subregion A2. Peak 3 is located at $\mu_0 H_c$ = 8.25 mT. It contributes to the maximum FORC distribution in the hard layer region E. According to the analysis conducted in Section 3.3.1, the coercive force of the Wiegand wire is consistent with the maximum value of the FORC distribution ρ. Thus, the coercivity of the soft, middle, and hard layers are 1.75, 5.00, and 8.25 mT, respectively. This is consistent with the results of previous studies.[91] Its magnetic structure is illustrated in Figure 3.7.

This analysis method can be used to obtain the distribution of the coercive and interactive fields in each region of the FORC and FORC diagram of the Wiegand wires with diameters of 0.18, 0.14, and 0.10 mm. The data are listed in Table 3.1. In addition, the corresponding magnetic structure diagram can be derived (Figures 3.8, 3.9, and 3.10).

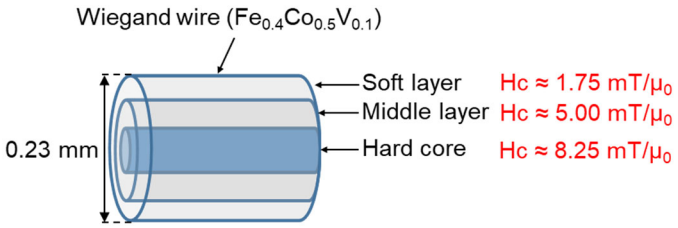

Figure 3.7 Magnetic structure of the 0.23-mm-diameter Wiegand wire.

Table 3.1 Distribution of coercive and interactive fields in various regions of Wiegand wires with varying diameters.

Region or peak	D = 0.06 mm		D = 0.10 mm		D = 0.14 mm		D = 0.18 mm		D = 0.23 mm		Attribute
	μ_0H_c (mT)	μ_0H_u (mT)	μ_0H_c (mT)	μ_0H_u (mT)	μ_0H_c (mT)	μ_0H_u (mT)	μ_0H_c (mT)	μ_0H_u (mT)	μ_0H_c (mT)	μ_0H_u (mT)	
Region A1	/	/	1.75–4.25	–1.5 to 1.25	1.25–3.5	–1 to 1.25	0.25–3.25	–0.75 to 1.5	0–3.5	–0.5 to 1.5	Soft layer
Region A2	/	/	4.25–5.5	–0.75 to 0.75	3.5–6.5	–0.75 to 0	3.25–6.5	–0.75 to 1.25	3.5–6.5	–0.5 to 1.25	Middle layer
Region B	/	/	/	/	/	/	0.75–3	–2.25 to –0.75	0.75–3.25	–2 to –0.75	Soft layer
Region C	/	/	4.5–7.5	–5.5 to –1.5	3.5–6.5	–5.5 to –1.5	3.25–6.5	–6.5 to –1.25	3.25–6.5	–7.5 to –1.5	Interaction
Region D	/	/	6.5–10	–5.5 to –2	4.5–9.75	–6.75 to –1	4–8.25	–5.75 to –1	4–9	–7.5 to –1	Interaction
Region E	2.25–6.5	–2 to 1.25	5.75–9.75	–2.75 to 0.25	6.25–11.25	–2.25 to –0.25	6.5–10.5	–2 to 0.25	6.5–11.25	–2 to 0.5	Hard core
Region F	/	/	2–5.5	1–3	1–3.75	1–3	0.25–3.5	1.5–4.75	0.25–2.5	1.25–5	Interaction
Peak 1	/	/	3.5	0	2.75	0.25	2	0.5	1.75	0.75	Soft layer
Peak 2	/	/	4.5	0	3.75	–0.25	3.5	0	4.25	0.25	Middle layer
Peak 3	4.25	–0.75	7	–1	7.5	–1	7.75	–0.75	8.25	–0.75	Hard core

Figure 3.8 shows the magnetic structure of the 0.18-mm-diameter Wiegand wire with the coercivities of the soft, middle, and hard layers as 2.00, 4.50, and 7.75 mT, respectively.

Figure 3.9 shows the magnetic structure of the 0.14-mm-diameter Wiegand wire with the coercivities of the soft, middle, and hard layers as 2.70, 4.25, and 7.50 mT, respectively.

As shown in Figure 3.10, the magnetic structure of the 0.10-mm-diameter Wiegand wire can be obtained with the coercivities of the soft, middle, and hard layers as 3.50, 4.75, and 7.00 mT, respectively.

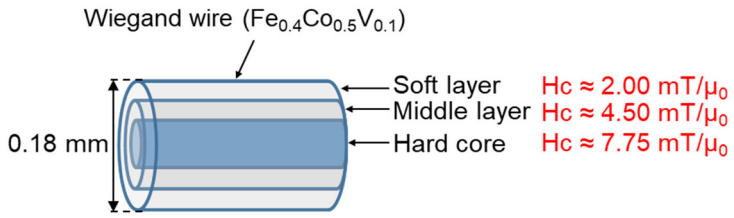

Figure 3.8 Magnetic structure of the 0.18-mm-diameter Wiegand wire.

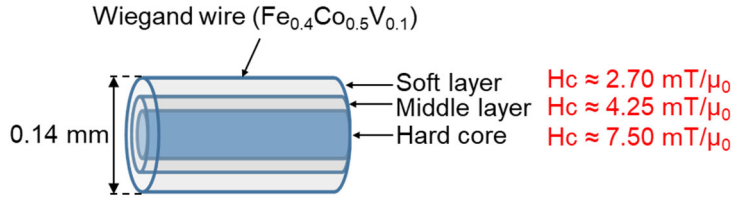

Figure 3.9 Magnetic structure of the 0.14-mm-diameter Wiegand wire.

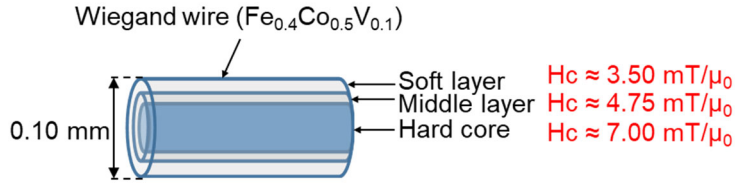

Figure 3.10 Magnetic structure of the 0.10-mm-diameter Wiegand wire.

The comparison of the magnetic structures of the five Wiegand wires with different diameters confirms that the coercivity of the hard core increases with the volume of the soft layer. This further establishes the interaction between the soft and hard layers, which is consistent with prior reports.[91]

3.3.4 Relationship Between Magnetization Reversal Direction of Wiegand Wire and Partial Region of FORC Distribution Diagram

According to the analysis conducted in Section 3.3.2, the 0.06-mm-diameter Wiegand wire displays a single and uniform magnetic structure. It corresponds to the hard core of the Wiegand wire. Its FORC distribution with μ_0H_b as the horizontal axis and μ_0H_a as the vertical axis is illustrated in Figure 3.11 (a). As observed, magnetization reversal and applied magnetic fields at each point of the FORC distribution can be analyzed. For example, the maximum point of the FORC distribution peak 3 corresponds to the magnetization reverse field $\mu_0H_a = -5$ mT and applied magnetic field $\mu_0H_b = 3.5$ mT. In the figure, only region E exhibits a remarkable distribution intensity. The other regions do not exhibit any distribution intensity. Figure 3.11 (b) shows a smooth minor hysteresis loop for the 0.06-mm-diameter Wiegand wire. No prominent large Barkhausen jump is observed during the magnetization of the Wiegand wire. Only two magnetization directions are detected: one is indicated by the blue arrow on the right-hand side, and the other is indicated by the red arrow on the left-hand side.

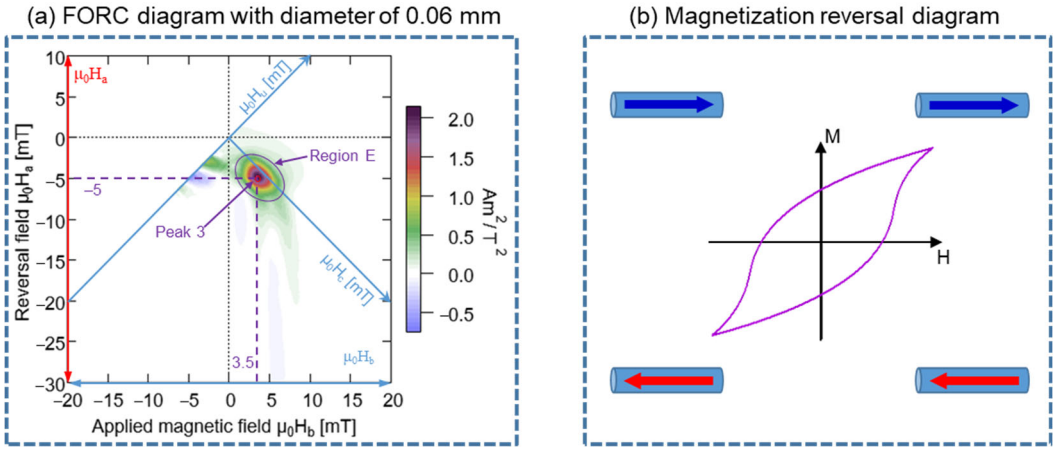

Figure 3.11 (a) FORC diagram of the 0.06-mm-diameter Wiegand wire. (b) Magnetization reversal diagram of the minor loop.

The analysis of the FORC and FORC diagram of the 0.10-mm-diameter Wiegand wire is considered.[97] In Figure 3.12 (a), μ_0H_b denotes the horizontal axis, and μ_0H_a represents the vertical axis. Based on the previous analysis, region C is distributed in the area before the large Barkhausen jump, region D is distributed in the area after the large Barkhausen jump, and region E is distributed predominantly in the area situated at a distance from the large Barkhausen jump. In particular, three FORCs are selected with $\mu_0H_a = -9$, -10, and -12 mT, namely, FORC1, FORC2, and FORC3.

The three FORCs pass through regions C, D, and E. Herein, nine points are considered from the three FORCs with coordinates 1 (–9, 3), 2 (–9, 5), 3 (–9, 6), 4 (–10, 2.5), 5 (–10, 4.5), 6 (–10, 6.5), 7 (–12, 2), 8 (–12, 4), and 9 (–12, 7). Points 1, 4, and 7 are distributed in region C; points 2, 5, and 8 are distributed in region D; points 3, 6, and 9 are distributed in region E.

These nine points and the three regions, i.e., C, D, and E, are indicated in the FORCs, which are displayed in Figure 3.12 (c). Comparing Figures 3.12 (c) and (d), we determine that certain regions of the minor hysteresis loop in Figure 3.12 (d) correspond to regions C, D, and E in Figure 3.12 (c). Region C is distributed before the large Barkhausen jump, and an identical magnetization direction prevails in the soft and hard layers of the Wiegand wire (i.e., toward the left-hand side). In contrast, region D is distributed after the large Barkhausen jump, and an opposite magnetization direction is observed for the soft and hard layers of the Wiegand wire, i.e., the soft layer is directed toward the right-hand side, and the hard layer is oriented toward the left-hand side. Although region E is distributed after the large Barkhausen jump, an identical magnetization direction prevails for the soft and hard layers (i.e., toward the right-hand side).

The three magnetization states in Figure 3.12 (b) correspond to the three regions in Figure 3.12 (a), respectively. Thus, the FORC diagram is positive for identical magnetization directions of the soft and hard layers, whereas it is negative for opposite magnetization directions of these layers. The negative region appearing in the FORC diagram of the Wiegand wire results from the interaction between the soft and hard layers.[91]

The analysis method employed for the Wiegand wire with a diameter of 0.10 mm is applied for those with diameters of 0.14, 0.18, and 0.23 mm. In particular, three FORCs with $\mu_0 H_a$ = –8, –10, and –12 mT are selected. The results are shown in Figures 3.13, 3.14, and 3.15. A conclusion similar to that inferred for the Wiegand wire with a diameter of 0.10 mm can be obtained for the Wiegand wires with diameters of 0.14, 0.18, and 0.23 mm, i.e., the FORC diagram is positive and negative for identical and opposite magnetization directions of the soft and hard layers, respectively.

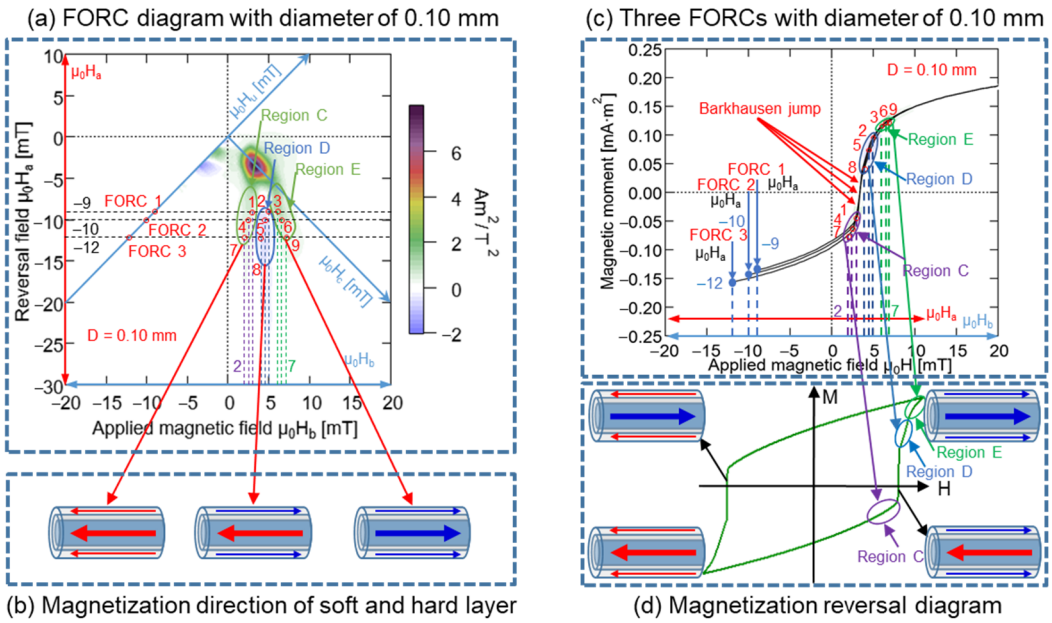

Figure 3.12 Wiegand wire with a diameter of 0.10 mm. (a) FORC diagram and three FORCs with varying reversal fields (μ_0H_a) of –9, –10, and –12 mT. (b) Magnetization reversal directions of the soft and hard layers. (c) Three FORCs under reversal fields of –9, –10, and –12 mT. (d) Magnetization reversal diagram of the minor loop.

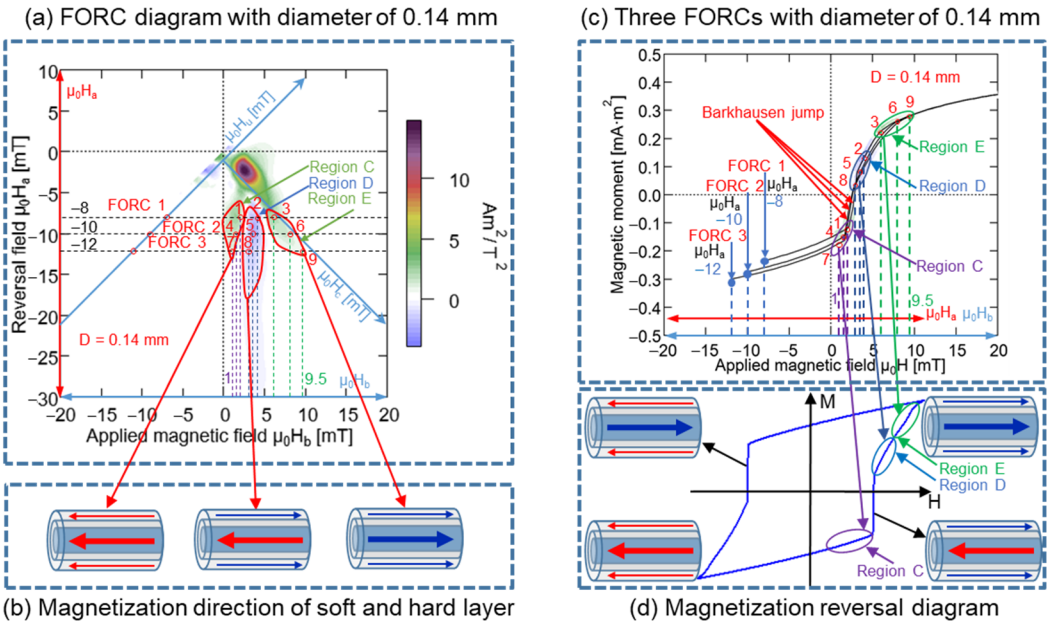

Figure 3.13 Wiegand wire with a diameter of 0.14 mm. (a) FORC diagram and three FORCs with varying reversal fields (μ_0H_a) of –8, –10, and –12 mT. (b) Magnetization reversal directions of the soft and hard layers. (c) Three FORCs under reversal fields of –8, –10, and –12 mT. (d) Magnetization reversal diagram of the minor loop.

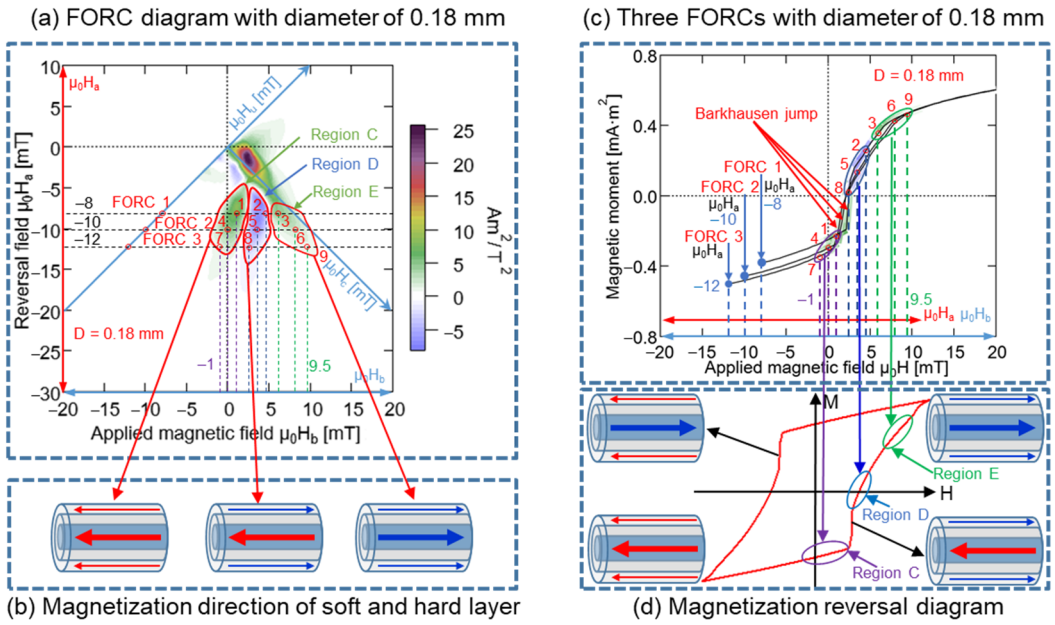

Figure 3.14 Wiegand wire with a diameter of 0.18 mm. (a) FORC diagram and three FORCs with varying reversal fields (μ_0H_a) of –8, –10, and –12 mT. (b) Magnetization reversal directions of the soft and hard layers. (c) Three FORCs under reversal fields of –8, –10, and –12 mT. (d) Magnetization reversal diagram of the minor loop.

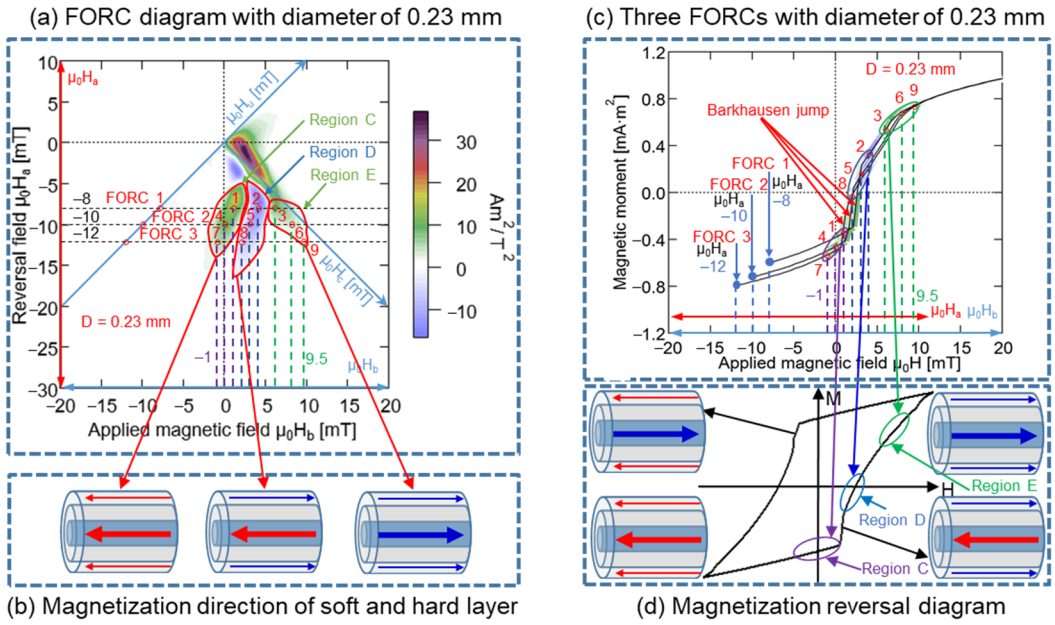

Figure 3.15 Wiegand wire with a diameter of 0.23 mm. (a) FORC diagram and three FORCs with varying reversal fields (μ_0H_a) of –8, –10, and –12 mT. (b) Magnetization reversal directions of the soft and hard layers. (c) Three FORCs under reversal fields of –8, –10, and –12 mT. (d) Magnetization reversal diagram of the minor loop.

3.4 Summary

In this chapter, the measurement data of five Wiegand wires were analyzed. A single uniform magnetic structure with a coercivity of 4.20 mT existed, which is the most significant result, when an adequate volume was etched away from the outer layer of the Wiegand wire. Thus, the central core is the hard magnetic component. In other words, the inner layer of the Wiegand wire is the hard layer, and its outer layer is the soft layer. The analysis of the coercive and interactive force fields of the FORC diagram of Wiegand wires with varying diameters confirmed no evident boundary between the soft and hard layers of these wires. However, interaction existed between the soft and hard layers in conjunction with a corresponding middle layer, i.e., the magnetic structure of the Wiegand wire comprised three layers. The interaction between the hard core with a coercivity of 4.20 mT and soft layer increased the coercivity of the hard core. The coercivity of the hard core increased when the volume of the soft layer increased, i.e., the coercivity of the hard core increased as its interaction with the soft layer increased. The comprehensive coercivity of a magnetic material was produced based on the combined action of all the coercivity components. Therefore, the overall coercivity of the Wiegand wire decreased when the volume of the soft layer with small coercivity increased. Thus, the coercive force distribution of the soft, middle, and hard layers can be determined. This supports the study of the magnetization reversal characteristics of Wiegand wires with varying diameters. These specific features provide evidence for further improving the output voltage and energy derived from Wiegand wires for self-powered devices and sensors.

Chapter 4: Analysis of the Magnetization Process of Wiegand Wires with Different Diameters Based on the Hysteresis Loop

In this chapter, the thickness of each layer of the Wiegand wire is inferred based on the correspondence between the volume of the soft layer and the height of the large Barkhausen jump, combined with the diameter of the hard layer. A theoretical calculation model is proposed for the first time based on the magnetization magnitude of any point on the minor hysteresis loop. The model can be used to deduce the volume of the region of magnetization and reversed magnetization of the Wiegand wire under the applied magnetic field. According to this model, in the magnetization process, we can understand the magnetization state of a Wiegand wire under the applied magnetic field. Then, the entire magnetization process of the Wiegand wire can be accurately comprehended. For example, we can accurately calculate the volume of the soft layer of a Wiegand wire whose direction reverses before and after the large Barkhausen jump. This provides a strong theoretical basis for us to study the application of Wiegand wires.

4.1 Thickness of Each Magnetic Layer of Wiegand Wires with Different Diameters

The minor hysteresis loops (Figure 4.1) of the five Wiegand wires are normalized by the 0.23-mm-diameter Wiegand wire to evaluate the simple magnetic structure of Wiegand wires with varying diameters. The thickness of each magnetic layer can be calculated. The alternating applied magnetic field of $\mu_0 H$ ranges from 2 to 15 mT, and the step value is 1 mT.

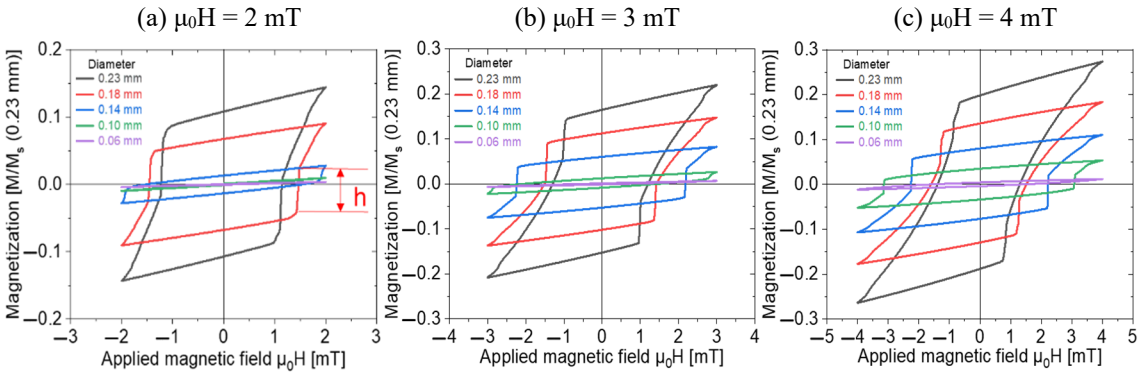

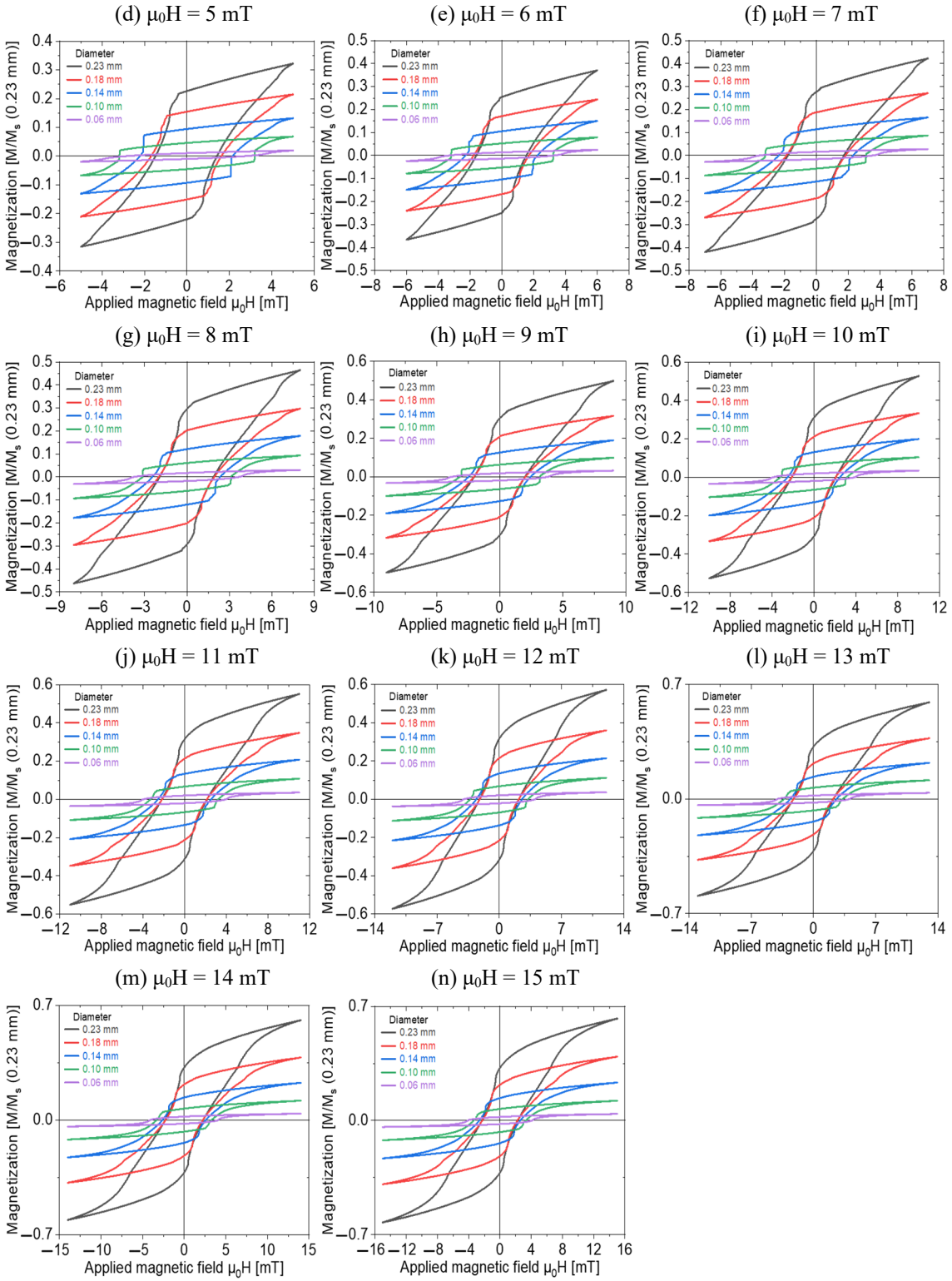

Figure 4.1 Minor hysteresis loops of the Wiegand wires normalized by the 0.23-mm-diameter Wiegand wire.

The FORC analysis reveals that the 0.06-mm-diameter Wiegand wire is a hard core, i.e., the thickness of the hard layer is 0.06 mm. Other Wiegand wires possess a three-layered structure: soft, middle, and hard layers.[99] A large Barkhausen jump is generated by the magnetization reversal of the soft layer. The height of the large Barkhausen jump is proportional to the volume of the soft layer. Hence, the thickness of the soft layer can be calculated using Equations (4.1) and (4.2).

$$\Delta d = (D - d)/2 \tag{4.1}$$

$$\frac{(\pi d^2 L)/4}{(\pi D^2 L)/4} = \frac{1 - h}{1} \tag{4.2}$$

Here, Δd denotes the thickness of the soft layer, d denotes the thicknesses of the middle and hard layers, D denotes the diameter of the Wiegand wire, and L denotes the length of the wire (Figure 4.2). The maximum height of a large Barkhausen jump is expressed as h. Thus, we can obtain the simple magnetic structure of the five Wiegand wires (Figure 4.3). As the magnetic structure of a Wiegand wire displays cylindrical symmetry, we describe the semi-cross-sectional structure along the axial direction.

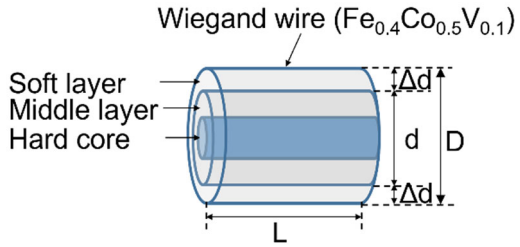

Figure 4.2 Calculation model of the simple magnetic structure.

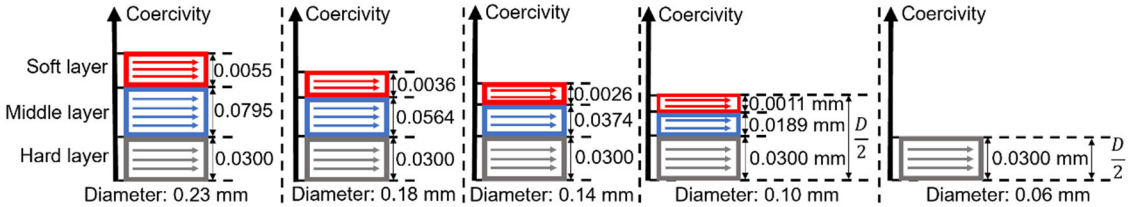

Figure 4.3 Magnetic structures of Wiegand wires with varying diameters.

As shown in Figure 4.3, as the diameter of the Wiegand wire decreases, the thicknesses of the soft and middle layers decrease until the hard core remains. In other words, as the outer layer of the Wiegand wire gradually etched away, the diameter of the Wiegand wire decreased. Consequently, the thicknesses of the external soft and

middle layers decreased. To simplify the analysis and obtain the magnetic structure model shown in Figure 4.3, we assume that the thickness of the hard core of the Wiegand wire does not change during the etching process, as the hard core of the Wiegand wire is in the innermost part. The diameter of the Wiegand wire was etched from 0.23 to 0.18 mm, and it was reduced by 0.05 mm. For the semi-cross-sectional structure, the thickness of the outer layer was reduced by 0.025 mm; it was greater than 0.0055 mm (the thickness of the soft layer of the 0.23-mm-diameter Wiegand wire). At this instant, it can be considered that the soft layer has been etched away, leaving the middle layer and hard core. However, as shown in Figure 4.1, there are still large Barkhausen jumps in the minor hysteresis loops of the 0.18-mm-diameter Wiegand wire. Although the applied magnetic field is 2 mT, a large Barkhausen jump exists. This indicates that there is a soft layer that can generate a large Barkhausen jump in the 0.18-mm-diameter Wiegand wire. The coercivity of the soft layer is less than or equal to 2 mT (which is consistent with the result illustrated in Figure 3.8). This is because while the external soft layer is etched away, the remaining middle layer forms a soft layer on the surface, and a new middle layer is formed. After the soft layer is etched away, the portions of the hard and soft layers in the Wiegand wire change, and the dipole interaction between them changes; therefore, the coercivity of the new soft layer, middle layer, and hard core changes. The diameter of the Wiegand wire etching from 0.18 to 0.14 mm and then to 0.10 mm is similar to the aforementioned analysis and will not be considered again.

4.2 Theoretical Calculation of the Volume of the Region of Magnetization

The magnetic structure of the Wiegand wires with varying diameters in the magnetization process is shown in Figure 4.4. Δd denotes the thickness of the region of magnetization in an applied magnetic field. Δd1 denotes the thickness of the region of magnetization, which reverses before and after the large Barkhausen jump. Δd2 denotes the thickness of the region of magnetization, which does not reverse before and after the large Barkhausen jump. Thus, Δd = Δd1 + Δd2 (Equation (4.3)). d denotes the thickness of the closed domain. D and L denote the diameter and length, respectively, of the Wiegand wire. V_1, V_2, V_d, and V_D represent the volumes of Δd1, Δd2, d, and D, respectively.

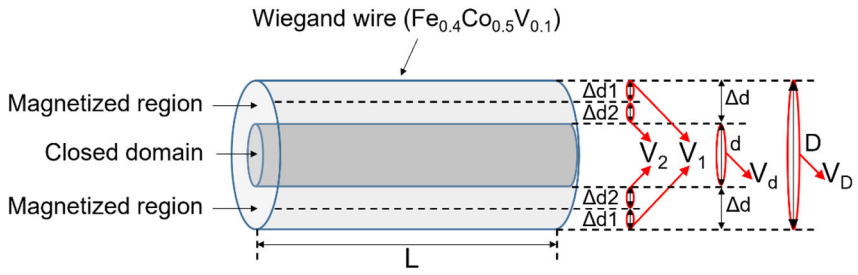

Figure 4.4 Magnetic structure of the Wiegand wires with varying diameters in the magnetization process.

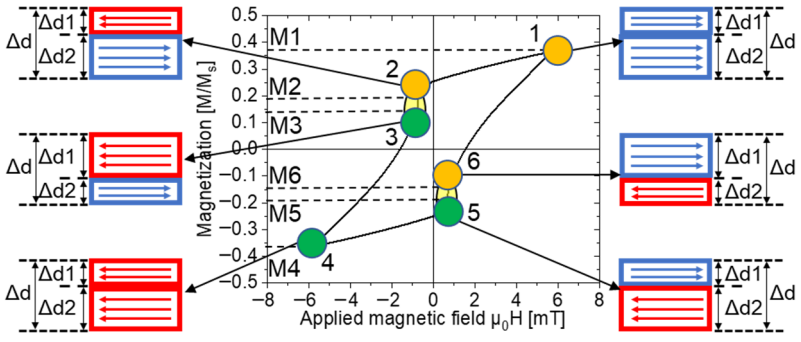

Figure 4.5 Magnetization process under an applied magnetic field.

The magnetization process under an applied magnetic field is depicted in Figure 4.5. M1 and M4 are the maximum and minimum values, respectively, of the magnetization in an applied magnetic field. M2 and M5 are the magnetization values before a large

Barkhausen jump occurs. M3 and M6 are the magnetization values after a large Barkhausen jump occurs. M1 and M4, M2 and M5, and M3 and M6 are individually symmetric to the origin point. Δd, Δd1, and Δd2 in Figure 4.5 are identical to those illustrated in Figure 4.4.

MX (X = 1, 2, 3, 4, 5, and 6) is the normalized value of magnetization. When the Wiegand wire is fully magnetized, the value of M1 or M4 is 1 or –1. M1 or M4 is proportional to the volume of Δd. Thus, we can calculate the thickness of Δd using Equations (4.3) and (4.4).

$$\Delta d = (D - d)/2 = \Delta d1 + \Delta d2 \tag{4.3}$$

$$\frac{V_D - V_d}{V_D} = \frac{|MX|}{1} \tag{4.4}$$

As shown in Figure 4.5, to simplify the model, we assume that there are two magnetization directions, one is to the left and the other is to the right. M1 is positive, and we assume that its magnetization direction is toward the right side. M4 is negative, and we assume that its magnetization direction is toward the left side. In M2 and M3, the magnetization of Δd1 is directed toward the left side, and that of Δd2 is directed toward the right side. Thus, M2 or M3 is proportional to the volume of ($V_2 - V_1$). In M5 and M6, the magnetization of Δd1 is directed toward the right side, and that of Δd2 is directed toward the left side. Thus, M5 or M6 is proportional to the volume of ($V_1 - V_2$). Therefore, the thicknesses of Δd1 and Δd2 in M2 or M3 can be calculated using Equations (4.3) and (4.5). The thicknesses of Δd1 and Δd2 in M5 or M6 can be calculated using Equations (4.3) and (4.6).

$$\frac{V_2 - V_1}{V_D} = \frac{MX}{1} \tag{4.5}$$

$$\frac{V_1 - V_2}{V_D} = \frac{MX}{1} \tag{4.6}$$

In Equations (4.4), (4.5), and (4.6), V_D or V_d can be calculated using $(\pi D^2 L)/4$ or $(\pi d^2 L)/4$, V_1 can be calculated using $\pi(D/2)^2 L - \pi(d/2 + \Delta d2)^2 L$, and V_2 can be calculated using $\pi(d/2 + \Delta d2)^2 L - \pi(d/2)^2 L$.

Consequently, d can be calculated using Equation (4.7).

$$d = \sqrt{1 - |MX|} \tag{4.7}$$

Δd2 in M2 or M3 can be calculated using Equation (4.8).

$$\Delta d2 = (\sqrt{[D^2(1 + MX) + d^2]/2} - d)/2 \quad (4.8)$$

Δd2 in M5 or M6 can be calculated using Equation (4.9).

$$\Delta d2 = (\sqrt{[D^2(1 - MX) + d^2]/2} - d)/2 \quad (4.9)$$

According to the aforementioned analysis, we can calculate the volume of the region of magnetization under an applied magnetic field and thicknesses of the reversed and unreversed volumes in the magnetization process under the applied magnetic field. We consider the semi-cross-sectional structure along the axial direction (as mentioned in Section 4.1) to analyze the magnetization process and complex magnetic structure of Wiegand wires with varying diameters. The applied magnetic field ranges from 2 to 15 mT. The calculated data are listed in Table 4.1. A part of the magnetization process and complex magnetic structure is similar. Therefore, we select a specific magnetization process and complex magnetic structure for analysis.

Table 4.1 The thicknesses of Δd, Δd1, and Δd2 of Wiegand wires with varying diameters under different applied magnetic field.

Magnetic field (mT)	Points	D = 0.23 mm			D = 0.18 mm			D = 0.14 mm			D = 0.10 mm		
		Δd (mm)	Δd1 (mm)	Δd2 (mm)	Δd (mm)	Δd1 (mm)	Δd2 (mm)	Δd (mm)	Δd1 (mm)	Δd2 (mm)	Δd (mm)	Δd1 (mm)	Δd2 (mm)
2	1	0.0086	0.0000	0.0086	0.0070	0.0000	0.0070	0.0029	0.0000	0.0029	/	/	/
	2	0.0086	0.0022	0.0064	0.0070	0.0020	0.0050	0.0029	0.0019	0.0010	/	/	/
	3	0.0086	0.0047	0.0039	0.0070	0.0044	0.0026	0.0029	0.0024	0.0005	/	/	/
	4	0.0085	0.0000	0.0085	0.0070	0.0000	0.0070	0.0029	0.0000	0.0029	/	/	/
	5	0.0085	0.0022	0.0063	0.0070	0.0019	0.0051	0.0029	0.0019	0.0010	/	/	/
	6	0.0085	0.0045	0.0041	0.0070	0.0044	0.0026	0.0029	0.0024	0.0005	/	/	/
3	1	0.0134	0.0000	0.0134	0.0118	0.0000	0.0118	0.0090	0.0000	0.0090	/	/	/
	2	0.0134	0.0023	0.0111	0.0118	0.0022	0.0096	0.0090	0.0024	0.0066	/	/	/
	3	0.0134	0.0048	0.0086	0.0118	0.0055	0.0063	0.0090	0.0058	0.0032	/	/	/
	4	0.0126	0.0000	0.0126	0.0109	0.0000	0.0109	0.0080	0.0000	0.0080	/	/	/
	5	0.0126	0.0022	0.0104	0.0109	0.0022	0.0087	0.0080	0.0024	0.0057	/	/	/
	6	0.0126	0.0050	0.0076	0.0109	0.0052	0.0057	0.0080	0.0058	0.0023	/	/	/
4	1	0.0170	0.0000	0.0170	0.0149	0.0000	0.0149	0.0123	0.0000	0.0123	0.0083	0.0000	0.0083
	2	0.0170	0.0028	0.0142	0.0149	0.0025	0.0124	0.0123	0.0028	0.0095	0.0083	0.0032	0.0051
	3	0.0170	0.0050	0.0120	0.0149	0.0053	0.0096	0.0123	0.0066	0.0057	0.0083	0.0056	0.0027
	4	0.0163	0.0000	0.0163	0.0143	0.0000	0.0143	0.0118	0.0000	0.0118	0.0081	0.0000	0.0081
	5	0.0163	0.0027	0.0136	0.0143	0.0025	0.0118	0.0118	0.0028	0.0090	0.0081	0.0032	0.0049
	6	0.0163	0.0050	0.0114	0.0143	0.0054	0.0089	0.0118	0.0067	0.0051	0.0081	0.0056	0.0025
5	1	0.0203	0.0000	0.0203	0.0178	0.0000	0.0178	0.0150	0.0000	0.0150	0.0109	0.0000	0.0109
	2	0.0203	0.0049	0.0155	0.0178	0.0045	0.0133	0.0150	0.0031	0.0119	0.0109	0.0036	0.0073
	3	0.0203	0.0060	0.0143	0.0178	0.0056	0.0121	0.0150	0.0062	0.0088	0.0109	0.0063	0.0046
	4	0.0199	0.0000	0.0199	0.0174	0.0000	0.0174	0.0148	0.0000	0.0148	0.0108	0.0000	0.0108
	5	0.0199	0.0046	0.0152	0.0174	0.0042	0.0132	0.0148	0.0031	0.0117	0.0108	0.0037	0.0071
	6	0.0199	0.0060	0.0139	0.0174	0.0056	0.0118	0.0148	0.0068	0.0080	0.0108	0.0067	0.0041
6	1	0.0238	0.0000	0.0238	0.0205	0.0000	0.0205	0.0174	0.0000	0.0174	0.0129	0.0000	0.0129
	2	0.0238	0.0054	0.0184	0.0205	0.0050	0.0155	0.0174	0.0034	0.0140	0.0129	0.0040	0.0089
	3	0.0238	0.0066	0.0172	0.0205	0.0064	0.0142	0.0174	0.0070	0.0104	0.0129	0.0069	0.0060
	4	0.0234	0.0000	0.0234	0.0202	0.0000	0.0202	0.0172	0.0000	0.0172	0.0128	0.0000	0.0128
	5	0.0234	0.0054	0.0180	0.0202	0.0050	0.0152	0.0172	0.0035	0.0137	0.0128	0.0041	0.0087

	6	0.0234	0.0065	0.0169	0.0202	0.0062	0.0140	0.0172	0.0068	0.0104	0.0128	0.0074	0.0054
	1	0.0277	0.0000	0.0277	0.0233	0.0000	0.0233	0.0195	0.0000	0.0195	0.0145	0.0000	0.0145
	2	0.0277	0.0060	0.0217	0.0233	0.0055	0.0177	0.0195	0.0051	0.0144	0.0145	0.0043	0.0103
7	3	0.0277	0.0072	0.0205	0.0233	0.0068	0.0164	0.0195	0.0075	0.0120	0.0145	0.0074	0.0071
	4	0.0274	0.0000	0.0274	0.0231	0.0000	0.0231	0.0194	0.0000	0.0194	0.0144	0.0000	0.0144
	5	0.0274	0.0058	0.0216	0.0231	0.0055	0.0175	0.0194	0.0052	0.0141	0.0144	0.0042	0.0102
	6	0.0274	0.0071	0.0204	0.0231	0.0069	0.0161	0.0194	0.0078	0.0115	0.0144	0.0072	0.0072
	1	0.0309	0.0000	0.0309	0.0259	0.0000	0.0259	0.0214	0.0000	0.0214	0.0158	0.0000	0.0158
	2	0.0309	0.0068	0.0241	0.0259	0.0061	0.0198	0.0214	0.0053	0.0161	0.0158	0.0049	0.0110
8	3	0.0309	0.0076	0.0233	0.0259	0.0073	0.0186	0.0214	0.0071	0.0143	0.0158	0.0072	0.0086
	4	0.0307	0.0000	0.0307	0.0257	0.0000	0.0257	0.0213	0.0000	0.0213	0.0158	0.0000	0.0158
	5	0.0307	0.0066	0.0241	0.0257	0.0061	0.0197	0.0213	0.0056	0.0157	0.0158	0.0049	0.0109
	6	0.0307	0.0077	0.0230	0.0257	0.0074	0.0184	0.0213	0.0082	0.0130	0.0158	0.0074	0.0083
	1	0.0337	0.0000	0.0337	0.0280	0.0000	0.0280	0.0231	0.0000	0.0231	0.0171	0.0000	0.0171
	2	0.0337	0.0075	0.0261	0.0280	0.0067	0.0213	0.0231	0.0058	0.0173	0.0171	0.0046	0.0125
9	3	0.0337	0.0086	0.0251	0.0280	0.0079	0.0201	0.0231	0.0074	0.0157	0.0171	0.0072	0.0099
	4	0.0335	0.0000	0.0335	0.0279	0.0000	0.0279	0.0230	0.0000	0.0230	0.0170	0.0000	0.0170
	5	0.0335	0.0074	0.0261	0.0279	0.0068	0.0211	0.0230	0.0057	0.0173	0.0170	0.0046	0.0125
	6	0.0335	0.0084	0.0251	0.0279	0.0080	0.0200	0.0230	0.0073	0.0157	0.0170	0.0081	0.0089
	1	0.0360	0.0000	0.0360	0.0298	0.0000	0.0298	0.0245	0.0000	0.0245	0.0181	0.0000	0.0181
	2	0.0360	0.0081	0.0279	0.0298	0.0073	0.0225	0.0245	0.0064	0.0181	0.0181	0.0051	0.0130
10	3	0.0360	0.0091	0.0269	0.0298	0.0082	0.0216	0.0245	0.0078	0.0167	0.0181	0.0074	0.0107
	4	0.0359	0.0000	0.0359	0.0298	0.0000	0.0298	0.0245	0.0000	0.0245	0.0180	0.0000	0.0180
	5	0.0359	0.0080	0.0279	0.0298	0.0072	0.0226	0.0245	0.0065	0.0180	0.0180	0.0051	0.0129
	6	0.0359	0.0090	0.0269	0.0298	0.0084	0.0214	0.0245	0.0078	0.0166	0.0180	0.0075	0.0105
	1	0.0381	0.0000	0.0381	0.0315	0.0000	0.0315	0.0258	0.0000	0.0258	0.0190	0.0000	0.0190
	2	0.0381	0.0088	0.0293	0.0315	0.0078	0.0237	0.0258	0.0068	0.0191	0.0190	0.0048	0.0142
11	3	0.0381	0.0098	0.0283	0.0315	0.0088	0.0227	0.0258	0.0082	0.0176	0.0190	0.0075	0.0115
	4	0.0380	0.0000	0.0380	0.0314	0.0000	0.0314	0.0258	0.0000	0.0258	0.0190	0.0000	0.0190
	5	0.0380	0.0086	0.0293	0.0314	0.0077	0.0237	0.0258	0.0067	0.0191	0.0190	0.0049	0.0141
	6	0.0380	0.0096	0.0283	0.0314	0.0089	0.0225	0.0258	0.0081	0.0177	0.0190	0.0076	0.0114
	1	0.0399	0.0000	0.0399	0.0329	0.0000	0.0329	0.0270	0.0000	0.0270	0.0199	0.0000	0.0199
	2	0.0399	0.0094	0.0305	0.0329	0.0081	0.0248	0.0270	0.0071	0.0199	0.0199	0.0051	0.0148
12	3	0.0399	0.0100	0.0299	0.0329	0.0093	0.0237	0.0270	0.0085	0.0185	0.0199	0.0079	0.0121
	4	0.0398	0.0000	0.0398	0.0329	0.0000	0.0329	0.0269	0.0000	0.0269	0.0199	0.0000	0.0199
	5	0.0398	0.0093	0.0306	0.0329	0.0081	0.0247	0.0269	0.0070	0.0200	0.0199	0.0051	0.0148
	6	0.0398	0.0102	0.0296	0.0329	0.0093	0.0236	0.0269	0.0084	0.0186	0.0199	0.0079	0.0120
	1	0.0416	0.0000	0.0416	0.0343	0.0000	0.0343	0.0281	0.0000	0.0281	0.0207	0.0000	0.0207
	2	0.0416	0.0099	0.0317	0.0343	0.0085	0.0257	0.0281	0.0074	0.0207	0.0207	0.0050	0.0157
13	3	0.0416	0.0107	0.0310	0.0343	0.0097	0.0246	0.0281	0.0088	0.0192	0.0207	0.0080	0.0127
	4	0.0415	0.0000	0.0415	0.0342	0.0000	0.0342	0.0280	0.0000	0.0280	0.0207	0.0000	0.0207
	5	0.0415	0.0098	0.0317	0.0342	0.0086	0.0256	0.0280	0.0073	0.0207	0.0207	0.0050	0.0157
	6	0.0415	0.0108	0.0307	0.0342	0.0096	0.0246	0.0280	0.0087	0.0193	0.0207	0.0080	0.0127
	1	0.0432	0.0000	0.0432	0.0355	0.0000	0.0355	0.0291	0.0000	0.0291	0.0214	0.0000	0.0214
	2	0.0432	0.0102	0.0329	0.0355	0.0089	0.0266	0.0291	0.0075	0.0216	0.0214	0.0052	0.0163
14	3	0.0432	0.0112	0.0320	0.0355	0.0101	0.0254	0.0291	0.0090	0.0201	0.0214	0.0081	0.0134
	4	0.0431	0.0000	0.0431	0.0354	0.0000	0.0354	0.0290	0.0000	0.0290	0.0215	0.0000	0.0215
	5	0.0431	0.0102	0.0329	0.0354	0.0089	0.0265	0.0290	0.0075	0.0216	0.0215	0.0051	0.0163
	6	0.0431	0.0112	0.0318	0.0354	0.0101	0.0254	0.0290	0.0088	0.0202	0.0215	0.0081	0.0134
	1	0.0446	0.0000	0.0446	0.0366	0.0000	0.0366	0.0300	0.0000	0.0300	0.0222	0.0000	0.0222
	2	0.0446	0.0107	0.0339	0.0366	0.0091	0.0275	0.0300	0.0078	0.0222	0.0222	0.0052	0.0169
15	3	0.0446	0.0117	0.0329	0.0366	0.0104	0.0262	0.0300	0.0092	0.0208	0.0222	0.0084	0.0137
	4	0.0446	0.0000	0.0446	0.0366	0.0000	0.0366	0.0300	0.0000	0.0300	0.0221	0.0000	0.0221
	5	0.0446	0.0107	0.0338	0.0366	0.0091	0.0275	0.0300	0.0078	0.0221	0.0221	0.0052	0.0169
	6	0.0446	0.0118	0.0328	0.0366	0.0105	0.0261	0.0300	0.0094	0.0205	0.0221	0.0085	0.0136

4.3 Magnetization Process and Magnetic Structure of Wiegand Wires

4.3.1 Wiegand Wire with a Diameter of 0.23 mm

The magnetization process and complex magnetic structure of the 0.23-mm-diameter Wiegand wire under the applied magnetic field of 2 mT are shown in Figure 4.6. The magnetized region of the Wiegand wire is indicated by a magnetic moment directed toward left or right, and the closed domain is indicated by a set of oblique lines.

At point 1, the thickness of the magnetized region of the Wiegand wire is 0.0086 mm, and magnetization is directed toward the right side. Point 4 is symmetric to point 1. Hence, the thickness of the magnetized region of point 4 is 0.0086 mm. However, the magnetization direction is to the left. At point 2, which is before the large Barkhausen jump, the surface of the Wiegand wire, whose coercivity is low, reverses during demagnetization. The thickness of the reversed volume is 0.0022 mm, and that of the unreversed volume is 0.0064 mm. At point 3, which is after the large Barkhausen jump, it generates a large Barkhausen jump because of the Wiegand effect. Therefore, the thickness of the reversed volume increases to 0.0047 mm, and that of the unreversed volume is 0.0039 mm. Point 5 or 6 is symmetric to point 2 or 3. Thus, the magnetization process is similar, whereas the magnetization direction is opposite.

The thickness of the soft layer is 0.0055 mm (Figure 4.3). Therefore, a part of the volume of the soft layer reverses before and after the large Barkhausen jump at an applied magnetic field of 2 mT. In the entire magnetization process, a part of the region of the middle layer magnetizes and reverses. However, the hard layer is not magnetized. The magnetization process of points 1–6 exhibits the dynamic transformation of the complex magnetic structure.

The magnetization process of the 0.23-mm-diameter Wiegand wire at 2 mT is analyzed based on the semi-cross-sectional structure shown in Figure 4.6. In the initial state, the magnetic moments are distributed in arbitrary directions, which is similar to the state of point O in Figure 2.7, and the Wiegand wire does not show magnetism macroscopically. When the positive magnetic field of 2 mT is applied to the Wiegand wire, the thickness of the magnetized region of the Wiegand wire is 0.0086 mm, and magnetization is directed toward the right side, i.e., the magnetic moments are directed toward the right side (point 1 in Figure 4.6). The applied magnetic field gradually diminishes to zero. At this instant, magnetization induced by reversible magnetization can be reverted to its initial state, whereas magnetization induced by irreversible

magnetization cannot be reverted to its initial state. The total magnetic moment of the Wiegand wire is not zero; thus, magnetization is not zero. In other words, when the applied magnetic field decreases to zero, residual magnetization exists in the Wiegand wire.

Then, the applied magnetic field increases along the opposite direction. The soft layer with low coercivity on the surface of the Wiegand wire undergoes magnetization reversal. Consequently, the magnetization of the Wiegand wire continues to decrease. When the reversal magnetic field increases toward point 2, the soft layer with a thickness of 0.0022 mm on the surface of the Wiegand wire has been reversed. At this instant, the reversed magnetic field intensity reaches the critical value of the switching field of the Wiegand wire; thus, the Wiegand effect occurs. Consequently, the Wiegand wire can generate a large Barkhausen jump, and the magnetization state of the Wiegand wire varies from points 2 to 3. The soft layer with a thickness of 0.0025 mm undergoes magnetization reversal.

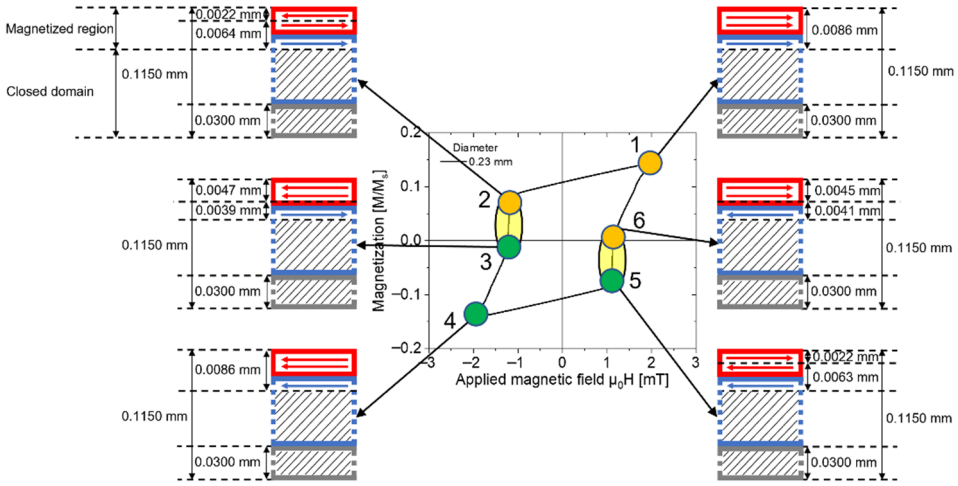

Figure 4.6 Magnetization process of the 0.23-mm-diameter Wiegand wire under the applied magnetic field of 2 mT.

When the reversal magnetic field increases to –2 mT, that is, at point 4, the region of the Wiegand wire with a thickness of 0.0086 mm is reversely magnetized, which is symmetrical to the state of point 1 with respect to the origin. The reversal magnetic field gradually reduces to zero and a positive magnetic field of 2 mT is applied. The magnetization state of the Wiegand wire undergoes through points 4–5–6–1, which is symmetrical to points 1–2–3–4 with respect to the origin. At this instant, a periodic magnetization process of the Wiegand wire is completed under the applied magnetic field of 2 mT. The magnetization process of Wiegand wires with different diameters

under different applied magnetic fields is similar to the aforementioned process. Only the volumes of the regions of magnetization of the soft, middle, and hard layers vary in different magnetization states. Consequently, the magnetization process is not repeated later, and only the change in the volume of the region of magnetization in each layer is analyzed.

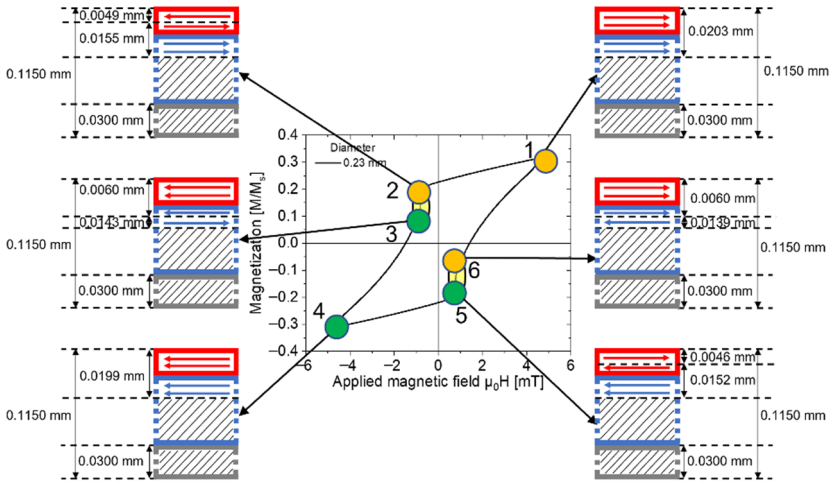

Figure 4.7 Magnetization process of the 0.23-mm-diameter Wiegand wire under the applied magnetic field of 5 mT.

The magnetization process and complex magnetic structure of the 0.23-mm-diameter Wiegand wire at 5 mT are shown in Figure 4.7. At point 1, the thickness of the magnetized region of the Wiegand wire is 0.0203 mm, and the magnetization direction indicates toward the right side. Point 4 is symmetric to point 1. Therefore, the thickness of the magnetized region of point 4 is 0.0203 mm. The calculated value is 0.0199 mm, which is significantly close to 0.0203 mm. However, the magnetization direction indicates toward the left side. At point 2, which is before the large Barkhausen jump, the surface of the Wiegand wire, whose coercivity is low, reverses during demagnetization. The thicknesses of the reversed and unreversed volumes are 0.0049 and 0.0155 mm, respectively. At point 3, which is after the large Barkhausen jump, it generates a large Barkhausen jump because of the Wiegand effect. Therefore, the thicknesses of the reversed and unreversed volumes increase to 0.0060 and 0.0143 mm, respectively. Point 5 or 6 is symmetric to point 2 or 3. Thus, the magnetization process is similar, although the magnetization direction is opposite. The thickness of the soft layer is 0.0055 mm (Figure 4.3). Thus, at 3 mT, a part of the volume of the soft layer reverses before the large Barkhausen jump. The volume of the soft layer and a part of the volume of the middle layer reverses after the large Barkhausen jump. In the entire

magnetization process, a part of the region of the middle layer magnetizes and reverses. However, the hard layer is not magnetized. The magnetization process of points 1–6 also shows the dynamic transformation process of the complex magnetic structure.

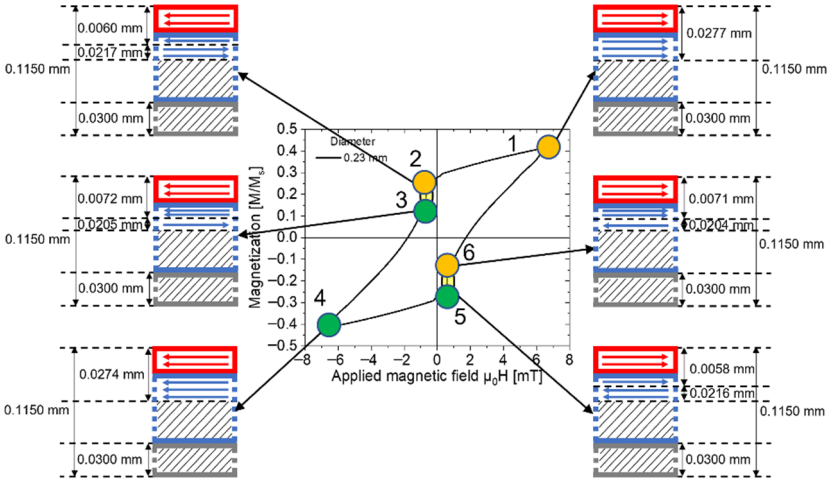

Figure 4.8 Magnetization process of the 0.23-mm-diameter Wiegand wire under the applied magnetic field of 7 mT.

The magnetization process and complex magnetic structure of the 0.23-mm-diameter Wiegand wire at 7 mT are shown in Figure 4.8. At point 1, the thickness of the magnetized region of the Wiegand wire is 0.0277 mm, and the magnetization direction indicates toward the right side. Point 4 is symmetric to point 1. Therefore, the thickness of the magnetized region of point 4 is 0.0277 mm. The calculated value is 0.0274 mm, which is significantly close to 0.0277 mm. However, the magnetization direction is toward the left side. At point 2, which is before the large Barkhausen jump, the surface of the Wiegand wire, whose coercivity is low, reverses during demagnetization. The thicknesses of the reversed and unreversed volumes are 0.0060 and 0.0217 mm, respectively. At point 3, which is after the large Barkhausen jump, it generates a large Barkhausen jump because of the Wiegand effect. Thereby, the thicknesses of the reversed and unreversed volumes increase to 0.0072 and 0.0205 mm, respectively. Point 5 or 6 is symmetric to point 2 or 3. Thus, the magnetization process is similar, whereas the magnetization direction is opposite. The thickness of the soft layer is 0.0055 mm (Figure 4.3). Therefore, under the applied magnetic field of 7 mT, the entire volume of the soft layer and a part of the middle layer reverses before the large Barkhausen jump. The reversed volume of the middle layer increases after the large Barkhausen jump. In the entire magnetization process, a part of the region of the middle layer magnetizes and reverses. However, the hard layer is not magnetized. The magnetization process of

points 1–6 also shows the dynamic transformation process of the complex magnetic structure.

The magnetization process and complex magnetic structure of the 0.23-mm-diameter Wiegand wire at 15 mT are shown in Figure 4.9. At point 1, the thickness of the magnetized region of the Wiegand wire is 0.0446 mm, and the magnetization direction indicates toward the right side. Point 4 is symmetric to point 1. Therefore, the thickness of the magnetized region of point 4 is 0.0446 mm. However, the magnetization direction is toward the left side. At point 2, which is before the large Barkhausen jump, the surface of the Wiegand wire, whose coercivity is low, reverses during demagnetization. The thicknesses of the reversed and unreversed volumes are 0.0107 and 0.0339 mm, respectively. At point 3, which is after the large Barkhausen jump, it generates a large Barkhausen jump because of the Wiegand effect. Therefore, the thicknesses of the reversed and unreversed volumes increase to 0.0117 and 0.0329 mm, respectively. Point 5 or 6 is symmetric to point 2 or 3. Thus, the magnetization process is similar, although the magnetization direction is opposite. The magnetization process is similar to that under the applied magnetic field of 7 mT. The magnetization process of points 1–6 also shows the dynamic transformation process of the complex magnetic structure.

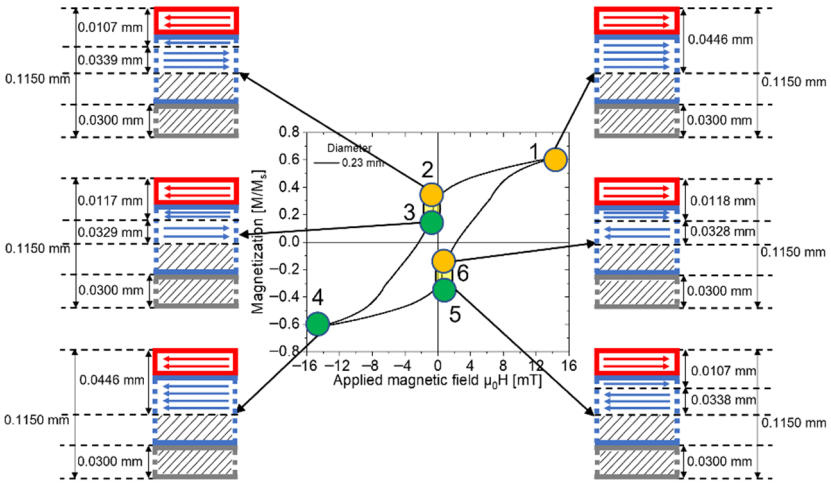

Figure 4.9 Magnetization process of the 0.23-mm-diameter Wiegand wire under the applied magnetic field of 15 mT.

4.3.2 Wiegand Wire with a Diameter of 0.18 mm

The thickness of the soft layer of the 0.18-mm-diameter Wiegand wire is 0.0036 mm (Figure 4.3). The magnetization process and complex magnetic structure of the 0.18-mm-diameter Wiegand wire when the applied magnetic field is 2 mT are similar to those of the 0.23-mm-diameter Wiegand wire when the applied magnetic field is 2 mT (Figure 4.10). At points 1 and 4, the thickness of the magnetized region of the Wiegand wire is 0.0070 mm. At points 2 and 5, the thicknesses of the reversed and unreversed volumes are 0.0020 and 0.0050 mm, respectively. At points 3 and 6, the thickness of the reversed volume increases to 0.0044 mm, and the thickness of the unreversed volume becomes 0.0026 mm.

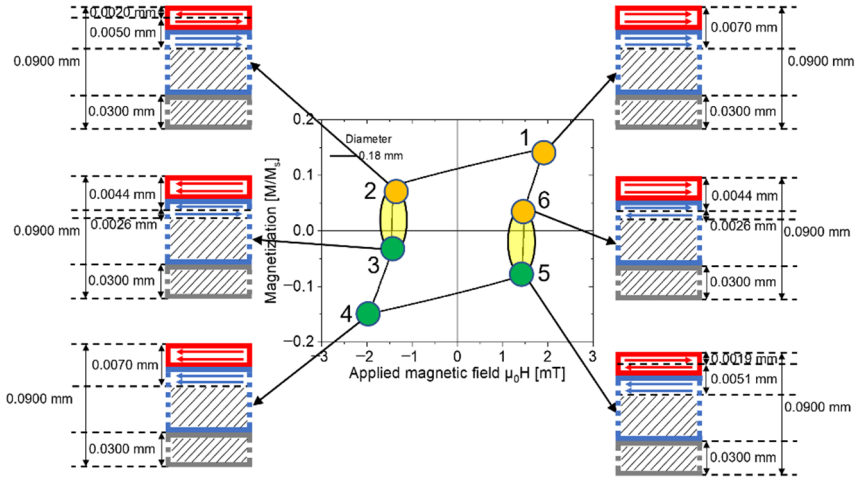

Figure 4.10 Magnetization process of the 0.18-mm-diameter Wiegand wire under the applied magnetic field of 2 mT.

The magnetization process and complex magnetic structure of the 0.18-mm-diameter Wiegand wire when the applied magnetic field is 5 mT are similar to those of the 0.23-mm-diameter Wiegand wire when the applied magnetic field is 7 mT (Figure 4.11). At points 1 and 4, the thickness of the magnetized region of the Wiegand wire is 0.0178 mm. At points 2 and 5, the thicknesses of the reversed and unreversed volumes are 0.0045 and 0.0133 mm, respectively. At points 3 and 6, the thickness of the reversed volume increases to 0.0056 mm, and the thickness of the unreversed volume becomes 0.0121 mm.

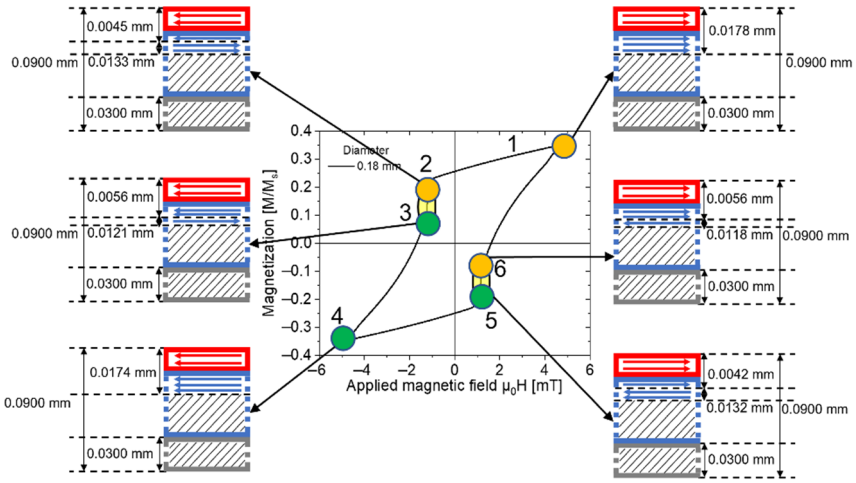

Figure 4.11 Magnetization process of the 0.18-mm-diameter Wiegand wire under the applied magnetic field of 5 mT.

The magnetization process and complex magnetic structure of the 0.18-mm-diameter Wiegand wire when the applied magnetic field is 15 mT are similar to those of the 0.23-mm-diameter Wiegand wire when the applied magnetic field is 15 mT (Figure 4.12). At points 1 and 4, the thickness of the magnetized region of the Wiegand wire is 0.0366 mm. At points 2 and 5, the thicknesses of the reversed and unreversed volumes are 0.0091 and 0.0275 mm, respectively. At points 3 and 6, the thickness of the reversed volume increases to 0.0104 mm, and the thickness of the unreversed volume becomes 0.0262 mm.

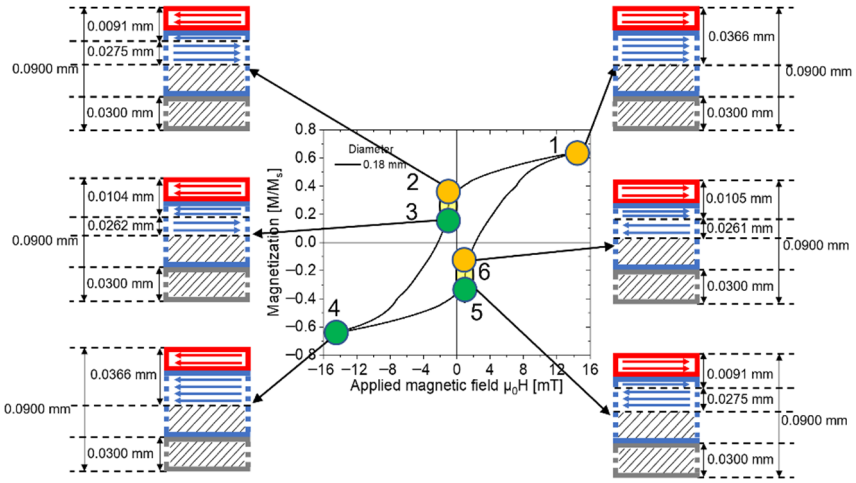

Figure 4.12 Magnetization process of the 0.18-mm-diameter Wiegand wire under the applied magnetic field of 15 mT.

4.3.3 Wiegand Wire with a Diameter of 0.14 mm

The thickness of the soft layer of the 0.14-mm-diameter Wiegand wire is 0.0026 mm (Figure 4.3). The magnetization process and complex magnetic structure of the Wiegand wire at an applied magnetic field of 2 mT are similar to those of the 0.23-mm-diameter Wiegand wire at 2 mT (Figure 4.13). At points 1 and 4, the thickness of the magnetized region of the Wiegand wire is 0.0029 mm. At points 2 and 5, the thicknesses of the reversed and unreversed volumes are 0.0019 and 0.0010 mm respectively. At points 3 and 6, the thicknesses of the reversed and unreversed volumes increase to 0.0024 and 0.0005 mm, respectively.

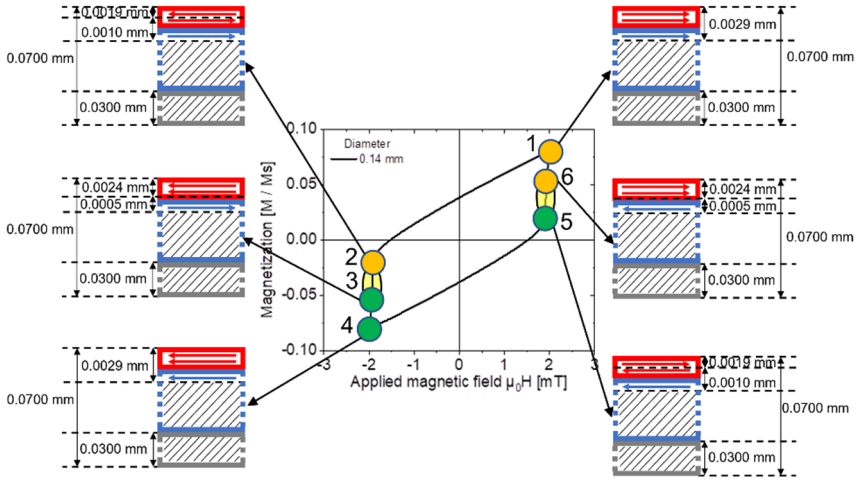

Figure 4.13 Magnetization process of the 0.14-mm-diameter Wiegand wire under the applied magnetic field of 2 mT.

The magnetization process and complex magnetic structure of the 0.14-mm-diameter Wiegand wire under the applied magnetic field of 4 mT are similar to those of the 0.23-mm-diameter Wiegand wire at 7 mT (Figure 4.14). At points 1 and 4, the thickness of the magnetized region of the Wiegand wire is 0.0123 mm. At points 2 and 5, the thicknesses of the reversed and unreversed volumes are 0.0028 and 0.0095 mm, respectively. At points 3 and 6, the thickness of the reversed volume increases to 0.0066 mm, and the thickness of the unreversed volume becomes 0.0057 mm.

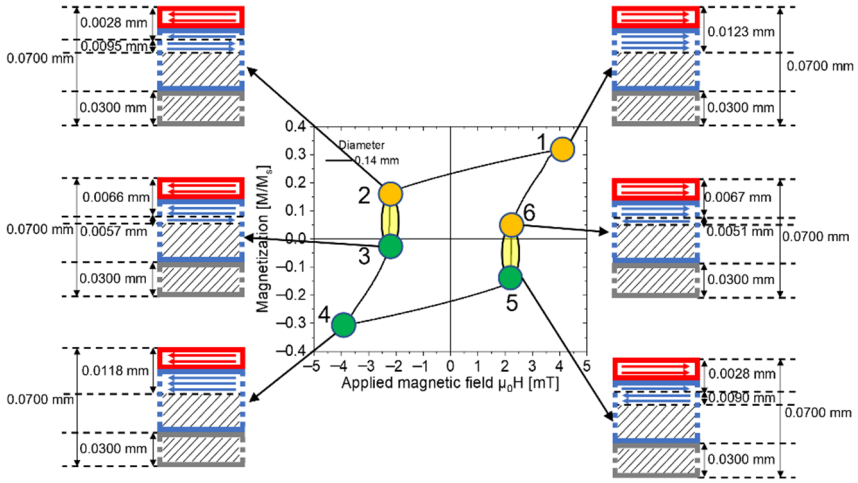

Figure 4.14 Magnetization process of the 0.14-mm-diameter Wiegand wire at an applied magnetic field of 4 mT.

The magnetization process and complex magnetic structure of the 0.14-mm-diameter Wiegand wire at an applied magnetic field of 15 mT are similar to those of the 0.23-mm-diameter Wiegand wire at 15 mT (Figure 4.15). At points 1 and 4, the thickness of the magnetized region of the Wiegand wire is 0.0300 mm. At points 2 and 5, the thicknesses of the reversed and unreversed volumes are 0.0078 and 0.0222 mm, respectively. At points 3 and 6, the thickness of the reversed volume increases to 0.0092 mm, and the thickness of the unreversed volume becomes 0.0208 mm.

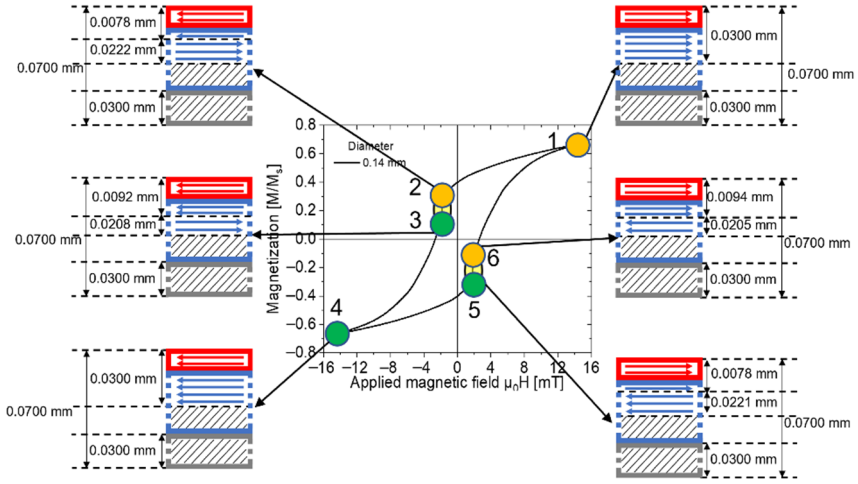

Figure 4.15 Magnetization process of the 0.14-mm-diameter Wiegand wire at an applied magnetic field of 15 mT.

4.3.4 Wiegand Wire with a Diameter of 0.10 mm

The thickness of the soft layer of the 0.10-mm-diameter Wiegand wire is 0.0011 mm (Figure 4.3). The magnetization process and complex magnetic structure of the 0.10-mm-diameter Wiegand wire at an applied magnetic field of 4 mT are similar to those of the 0.23-mm-diameter Wiegand wire at 7 mT (Figure 4.16). At points 1 and 4, the thickness of the magnetized region of the Wiegand wire is 0.0083 mm. At points 2 and 5, the thickness of the reversed volume is 0.0032 mm. The thickness of the unreversed volume is 0.0051 mm. At points 3 and 6, the thickness of the reversed volume increases to 0.0056 mm. The thickness of the unreversed volume is 0.0027 mm.

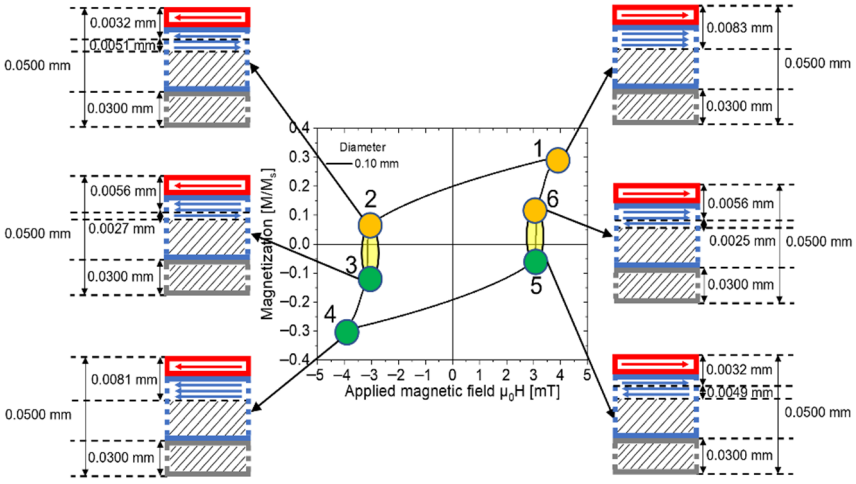

Figure 4.16 Magnetization process of the 0.10-mm-diameter Wiegand wire at an applied magnetic field of 4 mT.

The magnetization process and complex magnetic structure of the 0.10-mm-diameter Wiegand wire at 13 mT are shown in Figure 4.17. At point 1, the thickness of the magnetized region of the Wiegand wire is 0.0207 mm, and the magnetization direction indicates toward the right side. Point 4 is symmetric to point 1. Therefore, the thickness of the magnetized region of point 4 is also 0.0207 mm. However, the magnetization direction indicates toward the left side. At point 2, which is before the large Barkhausen jump, the surface of the Wiegand wire whose coercivity is low reverses during demagnetization. The thicknesses of the reversed and unreversed volumes are 0.0050 and 0.0157 mm, respectively. At point 3, which is after the large Barkhausen jump, it generates a large Barkhausen jump owing to the Wiegand effect. Therefore, the thickness of the reversed volume increases to 0.0080 mm. The thickness of the unreversed volume is 0.0127 mm. Point 5 or 6 is symmetric to point 2 or 3. Thus, the

magnetization process is similar, although the magnetization direction is opposite. The thicknesses of the soft and middle layers are 0.0011 and 0.0189 mm, respectively (Figure 4.3). Therefore, the volume of the soft layer and a part of the middle layer reverses before the large Barkhausen jump at an applied magnetic field of 13 mT. The reversed volume of the middle layer increases after the large Barkhausen jump. In the entire magnetization process, the region of the soft and middle layers magnetizes and reverses, and a part of the region of the hard layer magnetizes and reverses. This is different from the other Wiegand wires (i.e., with different diameters). The magnetization process of points 1–6 also shows the dynamic transformation process of the complex magnetic structure.

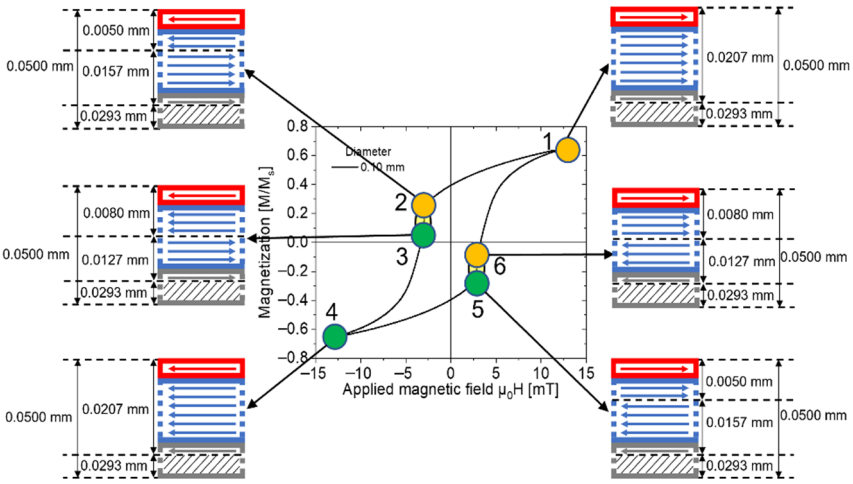

Figure 4.17 Magnetization process of the 0.10-mm-diameter Wiegand wire at an applied magnetic field of 13 mT.

The magnetization process and complex magnetic structure of the 0.10-mm-diameter Wiegand wire at 15 mT are shown in Figure 4.18. At point 1, the thickness of the magnetized region of the Wiegand wire is 0.0222 mm, and the magnetization direction indicates toward the right side. Point 4 is symmetric to point 1. Thus, the thickness of the magnetized region of point 4 is 0.0222 mm. However, the magnetization direction indicates toward the left. At point 2, which is before the large Barkhausen jump, the surface of the Wiegand wire, whose coercivity is low, reverses during demagnetization. The thicknesses of the reversed and unreversed volumes are 0.0052 and 0.0169 mm, respectively. At point 3, which is after the large Barkhausen jump, it generates a large Barkhausen jump owing to the Wiegand effect. Therefore, the thicknesses of the reversed and unreversed volumes increase to 0.0084 and 0.0137 mm, respectively. Point 5 or 6 is symmetric to point 2 or 3. Thus, the magnetization process is similar. However,

the magnetization direction is opposite. The magnetization process is similar to that at 13 mT. The magnetization process of points 1–6 also shows the dynamic transformation process of the complex magnetic structure.

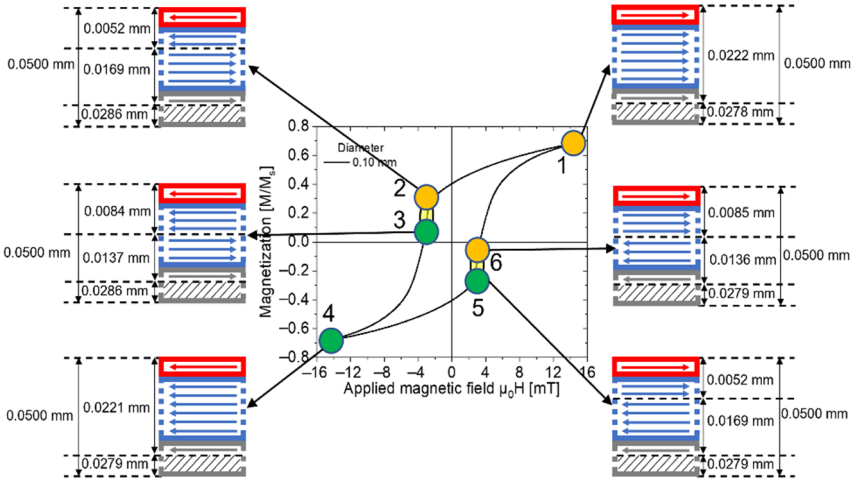

Figure 4.18 Magnetization process of the 0.10-mm-diameter Wiegand wire at an applied magnetic field of 15 mT.

4.4 Summary

In this chapter, the thickness of the region of magnetization was theoretically calculated for the first time. This is a novel observation of this study. Previous studies only performed qualitative analyses. The thickness of the region of magnetization under an alternating magnetic field ranged from 2 to 15 mT, and the thicknesses of the regions of magnetization with and without reversal of the magnetization states in the magnetization process can be calculated. The dynamic complex magnetic structure of each state in the magnetization process can be obtained based on the theoretical results. This provides a theoretical basis for the study of the magnetization process of a Wiegand wire.

Chapter 5: Analysis of the Magnetic Characteristics of Wiegand Wires with Different Diameters Using Hysteresis Loops

In this chapter, the magnetic characteristics of Wiegand wires with different diameters are analyzed. The variation tendency of the major hysteresis loops of Wiegand wires under different normalization conditions is analyzed. Moreover, the variation trends of coercivity and remanence in major and minor hysteresis loops are analyzed in detail. The change rule of the large Barkhausen jump in the minor hysteresis loops is analyzed and compared with the amplitude of the pulse voltage in the pickup coil. Finally, variation in the switching field of Wiegand wires under different external magnetic fields is discussed.

5.1 Major Hysteresis Loops

The normal and magnified perspectives of major hysteresis loops are measured to compare the comprehensive magnetic characteristics of Wiegand wires with varying diameters under saturation magnetization (Figures 3.3 (a) and 5.2). As shown in Figure 3.3 (a), the major hysteresis loops are normalized by themselves. As shown in Figure 5.2, the major hysteresis loops are normalized using the 0.23-mm-diameter Wiegand wire.

5.1.1 Normalized Major Hysteresis Loops

Figure 3.3 (b) shows that the coercivity of the major hysteresis loop increases with the diameter of the Wiegand wire decreases. This is because the coercivity of the hard magnetic material is larger than that of the soft magnetic material.[100] Thus, it indicates that the portion of the hard layer in the Wiegand wire with a small diameter is higher than that in the Wiegand wire with a large diameter. This further verifies that the outer layer etched is a soft layer. With the continuous etching of the soft outer layer, the portion of the hard layer in the Wiegand wire expands and finally transforms into a single hard layer. Figure 5.1 shows that the remanence increases with a decrease in the diameter of the Wiegand wire. This is because the Wiegand wire with a smaller

diameter exhibits larger coercivity; its magnetic moment is hard to reverse. In the demagnetizing process, when the applied field is zero, the reversed volume of the soft layer of the Wiegand wire with a larger diameter is higher than that of the Wiegand wire with a smaller diameter. Thus, the remanence of the Wiegand wire with a smaller diameter is higher than that of the Wiegand wire with a larger diameter.

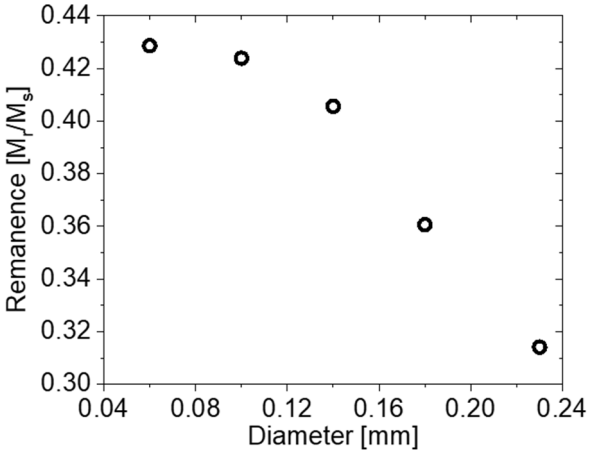

Figure 5.1 Remanence of the Wiegand wires with varying diameters.

5.1.2 Major Hysteresis Loops Normalized Using the Wiegand Wire with a Diameter of 0.23 mm

As shown in Figure 5.2, the data in the first quadrant are selected to analyze the saturation magnetization of Wiegand wires with varying diameters. The relationship between saturation magnetization and the cross-sectional area is shown in Figure 5.3. The remanence of the Wiegand wires normalized using a 0.23-mm-diameter Wiegand wire is shown in Figure 5.4.

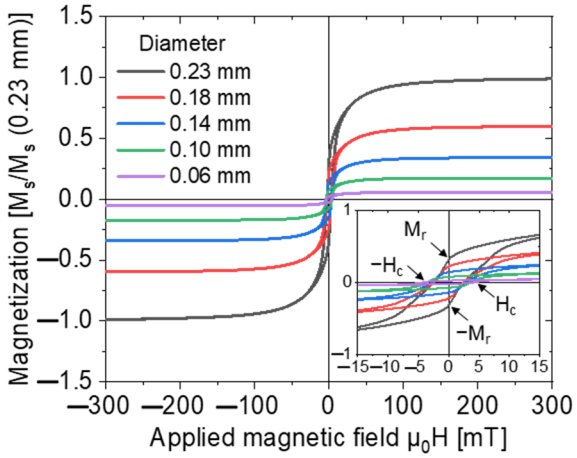

Figure 5.2 Major hysteresis loops of the Wiegand wires with varying diameters normalized using the 0.23-mm-diameter Wiegand wire.

Figure 5.3 shows that the saturation magnetization of Wiegand wires with different diameters is proportional to the cross-sectional area. This is because the magnetic moment is the same for the Wiegand wires of the same material. When the Wiegand wires with different diameters attain saturation magnetization, the total magnetic moment of the Wiegand wires with different diameters is proportional to the volume of the Wiegand wire, as the lengths of the Wiegand wires with different diameters are identical. Thus, the saturation magnetization of a Wiegand wire is proportional to the cross-sectional area. When the outer layer of the Wiegand wire is etched, the portions of the soft and hard layers in the Wiegand wire vary. This causes variation in the coercivity of the Wiegand wire and magnetic domain structure of the Wiegand wire. According to the measurement of the saturation magnetization of Wiegand wires with different diameters, it can be inferred that the influence of the variation on saturation magnetization in the magnetic domain structure is negligibly compared with that in the cross-sectional area.

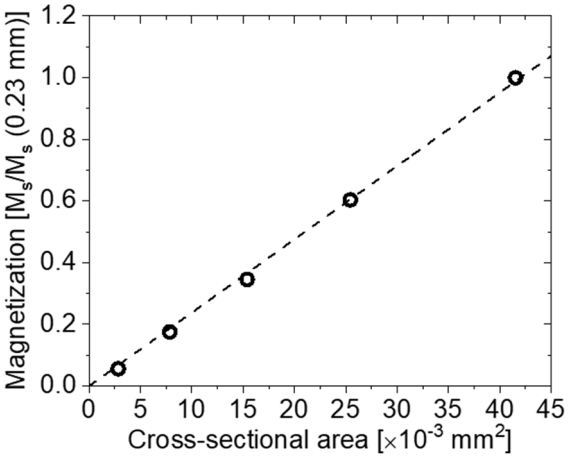

Figure 5.3 Relationship between magnetization and the cross-sectional area.

Figure 5.4 shows the remanence variations of Wiegand wires with different diameters after being normalized using the 0.23-mm-diameter Wiegand wire. The remanence decreases with the cross-sectional area decreases; however, the relationship is not linear.

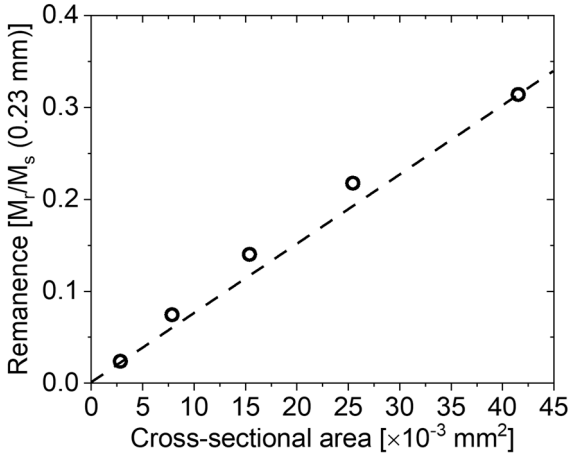

Figure 5.4 Remanence of the Wiegand wires normalized using the 0.23-mm-diameter Wiegand wire.

The portion of the hard layer of Wiegand wires with a smaller diameter (also known as thin wire) is higher than that of the Wiegand wires with a larger diameter (also known as thick wire). Consequently, the coercivity of the thin wire is larger. When the Wiegand wires with different diameters achieve saturation magnetization, the direction of magnetic moments in the Wiegand wires becomes consistent with the applied magnetic field.

In the demagnetizing process, owing to the larger coercivity of the thin wire, it

becomes more difficult to reverse its magnetic moment compared with that of the thick wire. Therefore, when the applied magnetic field decreases to zero, the reversed magnetic moment per unit volume of the thin wire will be less than that of the thick wire. Thus, the vector sum of the magnetic moment per unit volume of the thin wire is higher than that of the thick wire. The area above the dotted line shown in Figure 5.4 indicates that the remanence of the Wiegand wire with a smaller cross-sectional area.

5.2 Minor Hysteresis Loops

Minor hysteresis loops are measured to analyze the magnetic characteristics of Wiegand wires with different diameters under alternating magnetic fields (Figure 5.5). The amplitude of the alternating magnetic field ranges from 2 to 15 mT, and the step size is 1 mT. All the minor hysteresis loops are themselves normalized. The variation in the coercivity of the Wiegand wires with different diameters under the alternating magnetic field can be analyzed using the minor hysteresis loops. Moreover, the variation in the remanence of Wiegand wires with different diameters under the alternating magnetic field can be observed intuitively. The variation trend of the switching fields of Wiegand wires with different diameters under the alternating magnetic field can be obtained based on minor hysteresis loops.

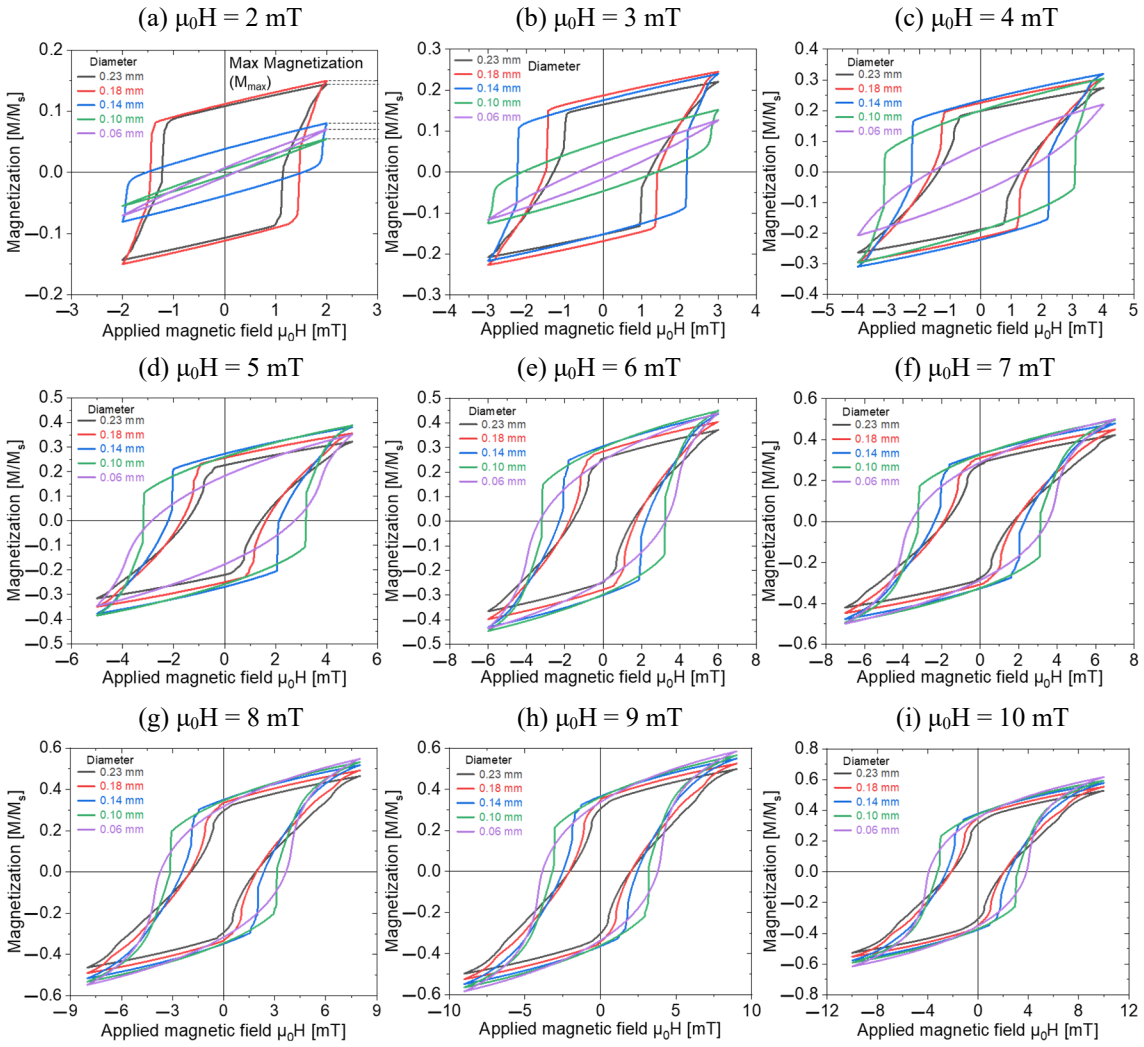

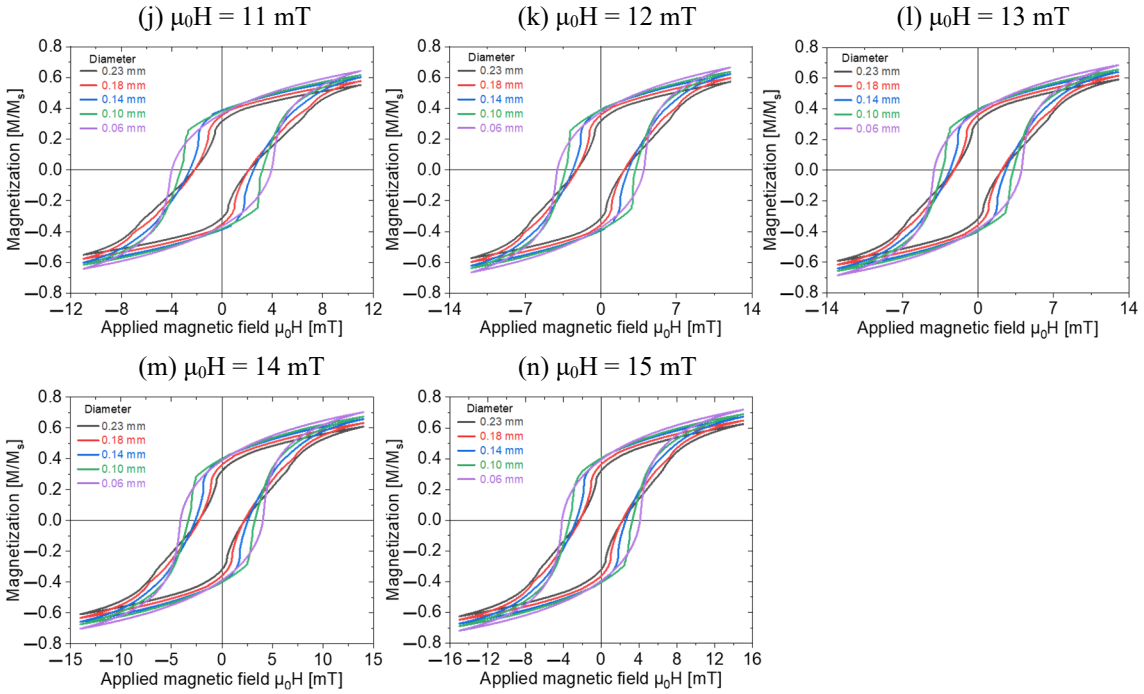

Figure 5.5 Minor hysteresis loops of the Wiegand wires normalized by themselves.

5.2.1 Coercive Force of Minor Hysteresis Loops

The coercive force (also known as coercivity) of the minor loops of Wiegand wires with different diameters under the alternating external magnetic field can be obtained from Figure 5.5 (Figure 5.6). The coercivity of the major loop of the solid point is higher than the applied magnetic field. The hollow points represent the coercivity of the major loop that is less than the applied magnetic field. For the Wiegand wire with an equal diameter, when the applied magnetic field is less than the coercivity of the major loop, it becomes difficult to reverse the magnetic moment in the Wiegand wire. Consequently, the Wiegand wire is not magnetized conveniently. Thus, the applied magnetic field required to make the magnetization zero in the process of reversal magnetization is marginal, whereby the coercivity of the minor loop reflected by the Wiegand wire is marginal.

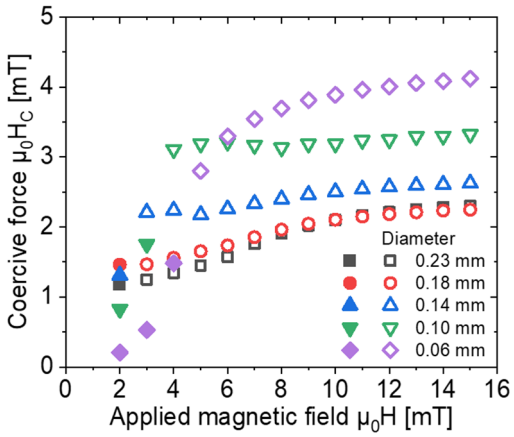

Figure 5.6 Coercivity of Wiegand wires with varying diameters during minor hysteresis loops.

When the applied magnetic field is higher than the coercivity of the major loop, the magnetic moment in the Wiegand wire becomes easier to reverse. An increasing region of the Wiegand wire would be magnetized by increasing the applied magnetic field intensity. At this time, the Wiegand wire is magnetized conveniently, and the magnetization of the Wiegand wire increases with an increase in the applied magnetic field. In addition, the applied magnetic field required to eliminate magnetization in the process of reversal magnetization gradually increases. Thus, the coercivity of the minor loop reflected by the Wiegand wire increases gradually. At this point, the coercivity of the minor loop would approach the coercivity of saturation magnetization as the applied magnetic field increases.

For the Wiegand wires with different diameters, the smaller the diameter of the Wiegand wires, the greater the portion of the hard layer is. Therefore, the coercivity of the major loop would be larger. When the applied magnetic field is small (e.g., 2 mT), the thin wire is less magnetized than that of the thick wire. Therefore, the reversal magnetic field required to eliminate magnetization is smaller, i.e., the coercivity of the minor loop of the thin wire is smaller than that of the thick wire. When the applied magnetic field is large (e.g., 6 mT), the thin wire is more magnetized than that of the thick wire. It becomes more difficult to reverse the magnetic moment of the thin wire compared with that of the thick wire. In the process of reversal magnetization, a large reversal magnetic field is required to eliminate the magnetization of the thin wire. This implies that the coercivity of the minor loop of the thin wire is higher than that of the thick wire.

5.2.2 Remanence of the Minor Hysteresis Loops

The variations in the remanence of the Wiegand wires with different diameters with regard to minor hysteresis loops are shown in Figure 5.7. When the amplitude of the magnetic field is small (e.g., 3 mT), it is larger than the coercivity of Wiegand wires with diameters of 0.23 mm, 0.18 mm, and 0.14 mm, and less than that of Wiegand wires with diameters of 0.10 mm and 0.06 mm. At this point, the degree of magnetization in the Wiegand wires with the first three diameters is larger. Therefore, the magnetization is larger. The degree of magnetization of the Wiegand wires with the other two diameters is smaller. Thus, the magnetization is smaller. Consequently, the remanence of the Wiegand wires with the first three diameters is larger than that of the Wiegand wires with the remaining two diameters when the applied magnetic field is zero.

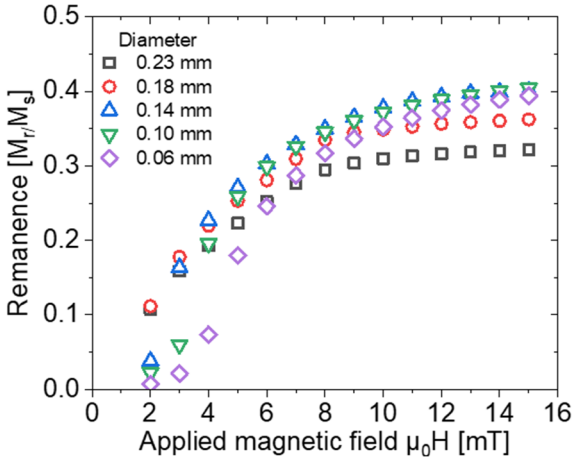

Figure 5.7 Remanence of the Wiegand wires with varying diameters with regard to the minor hysteresis loops.

The degree of magnetization in the Wiegand wires increases with an increase in the applied magnetic field. As the applied magnetic field increases, the degree of magnetization of the thin wire becomes larger than that of the thick wire under a certain applied magnetic field. And because of the coercivity of the thin wire is higher than that of the thick wire. Consequently, in the process of reversal magnetization, the magnetic moment of the thin wire is more difficult to reverse than that of the thick wire. Therefore, when the applied magnetic field decreases to zero, the vector sum of the total magnetic moment per unit volume of the thin wire is larger than that of the thick wire, i.e., the remanence maintained by the thin wire is larger.

The phenomenon illustrated in Figure 5.7 is as follows: the remanence of the thin wire

increases with an increase in the amplitude of the applied magnetic field. Under a certain amplitude of the magnetic field, it would be larger than that of the thick wire. According to the remanence of saturation magnetization shown in Figure 5.1, the smaller the diameter of the Wiegand wire, the higher the remanence. This verifies the aforementioned final result.

5.2.3 Maximum Magnetization of Minor Hysteresis Loops

The variation in the maximum magnetization of Wiegand wires with different diameters under different applied magnetic fields for the minor hysteresis loops is shown in Figure 5.8. When the amplitude of the applied magnetic field is low, the volume of the region of magnetization in a Wiegand wire is small. Therefore, magnetization is low. Magnetization increases with an increase in the amplitude of the applied magnetic field. The phenomenon shown in Figure 5.8 is as follows: for the Wiegand wire of an equal diameter, magnetization increases with an increase in the amplitude of the applied magnetic field. When the applied magnetic field is greater than the coercivity of the Wiegand wires considering all the diameters, the degree of magnetization of the thin wire is larger than that of the thick wire. Therefore, the magnetization of a thin wire is higher than that of a thick wire.

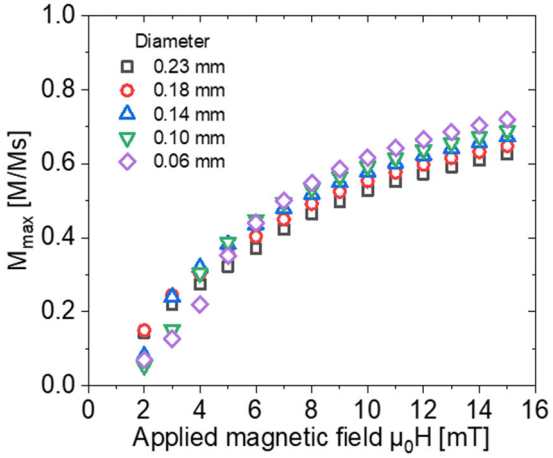

Figure 5.8 Maximum magnetization of the Wiegand wires with varying diameters with regard to the minor hysteresis loops.

5.3 Large Barkhausen Jump and Induced Pulse of the Wiegand Wires

In Figure 4.1, h denotes the height of a large Barkhausen jump. The height of the large Barkhausen jump of the Wiegand wires with varying diameters under the changing applied magnetic field is shown in Figure 5.9. When the applied magnetic field is 2 or 3 mT, the 0.23-, 0.18-, and 0.14-mm-diameter Wiegand wires exhibit the large Barkhausen jump. However, no large Barkhausen jump occurs for the etched Wiegand wires with diameters of 0.10 and 0.06 mm. In the previous study, the coercivity of the soft and hard layers of the unetched Wiegand wire were ~2 and ~8 mT, respectively.[91] When the applied magnetic field is 2 or 3 mT, Wiegand wires with diameters of 0.23, 0.18, and 0.14 mm can generate a large Barkhausen jump, whereas those with diameters of 0.10 and 0.06 mm cannot. When the applied magnetic field is 4 mT, Wiegand wires with diameters of 0.23, 0.18, 0.14, and 0.10 mm can generate a large Barkhausen jump, whereas that with a diameter of 0.06 mm cannot. This phenomenon indicates that the etched outer layer is a soft layer with a decreased diameter, whereas the inner layer is a hard layer. This is consistent with the FORC analysis.[99] If the etched outer layer is a hard layer and the Wiegand wire with a diameter of 0.10 mm can generate a large Barkhausen jump at 4 mT, it should be able to generate a large Barkhausen jump at 2 or 3 mT. This is because the coercivity of the soft layer is ~2 mT. However, it could not generate large Barkhausen jumps based on the measured minor hysteresis loop.

Figure 5.9 shows that when the applied magnetic field increases, the height of the large Barkhausen jump of the Wiegand wires with diameters other than 0.06 mm first increases gradually and then, decreases gradually when it attains an extreme value. Finally, the height of the large Barkhausen jump tends to remain constant. The volume of the soft layer of the Wiegand wire in which the magnetization reversal occurs at the beginning increases. The height of the large Barkhausen jump increases accordingly. When the applied magnetic field increases to a certain value, the volume of the soft layer of magnetization reversal in the Wiegand wire achieves the maximum value. Therefore, the height of the large Barkhausen jump generated becomes maximum. As the applied magnetic field continues to increase, before the large Barkhausen jump is generated, considering that the volume of the soft layer that has undergone magnetization reversal increases during the process of magnetization reversal, the volume of this part of the soft layer cannot generate the large Barkhausen jump. Consequently, the volume of the soft layer that can generate the large Barkhausen jump

decreases. The aforementioned results can be obtained based on the analysis of the magnetization processes of Wiegand wires with different diameters, as explained in Section 4.3. Thus, the height of the large Barkhausen jump gradually decreases. As the applied magnetic field continues to increase, the volume of the soft layer that can generate the large Barkhausen jump continues to decrease until it essentially remains constant. The height of the large Barkhausen jump tends to remain constant.

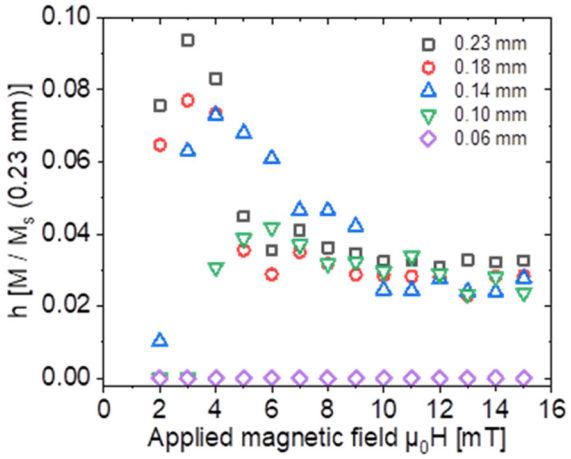

Figure 5.9 Height of the large Barkhausen jump of the Wiegand wires with varying diameters under the changing applied magnetic field.

A pulse voltage measurement system is constructed to verify the relationship between the amplitude of the pulse voltage of a Wiegand wire and the volume of the soft layer. The measuring system includes exciting and pickup coils. The exciting coil includes 320 turns of lacquered wires with a diameter of 0.7 mm. Its length is ~30 mm. The pickup coil includes 100 turns of lacquered wires with a diameter of 0.07 mm. An exciting magnetic field of 1 mT is generated in the Wiegand wire when an alternating current of 100 mA is applied to the exciting coil. A linear relationship is displayed. The exciting magnetic field applied to the Wiegand wire ranges from 2 to 10 mT, and the step size of the increment is 1 mT. The amplitude of the pulse voltage generated in the pickup coil is shown in Figure 5.10. Under an equal applied magnetic field, the variation trend of the pulse voltage generated in the pickup coil is identical to the height of the large Barkhausen jump (which is generated by the soft layer of magnetization reversal in the Wiegand wire). This indicates that the pulse voltage of the Wiegand wire is induced by the soft layer of magnetization reversal.

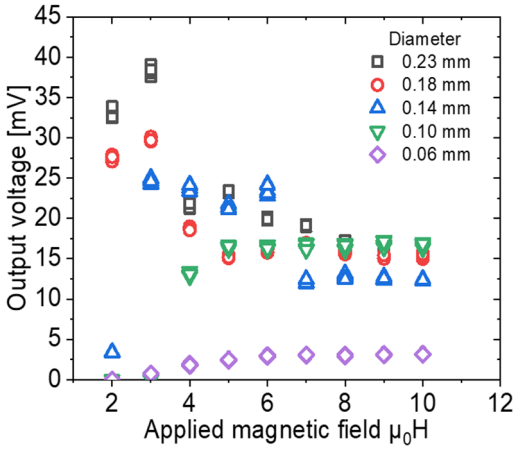

Figure 5.10 Output voltage of the Wiegand wires with varying diameters under the applied magnetic field.

5.4 Switching Field of Wiegand Wires with Different Diameters

The switching field of four Wiegand wires with varying diameters under an applied magnetic field is shown in Figure 5.11. It is evident from Figure 5.9 that when the applied magnetic field is 2 or 3 mT, the 0.10-mm-diameter Wiegand wire does not exhibit a large Barkhausen jump. Therefore, the 0.10-mm-diameter Wiegand wire does not possess switching field under the applied magnetic field of 2 or 3 mT.

The length of four Wiegand wires is 13 mm, and the diameter decreases from 0.23 to 0.10 mm. Therefore, the length-to-diameter ratio of the Wiegand wire (L/D) increases. The increase in L/D would induce a decrease in the demagnetizing field of Wiegand wires.[101] It can be concluded from Figures 3.7–3.10 that the coercivity of the soft layer gradually increases with a decrease in diameter. As the diameter decreases, the increase in the coercivity of the soft layer and decrease in the demagnetizing field hinder the reversal of the soft layer. This causes an increase in the switching field.

It is evident from Figure 5.11 that the switching field of each Wiegand wire decreases when the applied magnetic field increases from 2 to 15 mT. This occurs because the demagnetizing field of Wiegand wires increases as the applied magnetic field increases. It induces a part of the soft layer to reverse automatically during demagnetization, as concluded in Chapter 4. Thus, it is convenient to reverse the soft layer, and the switching field decreases.

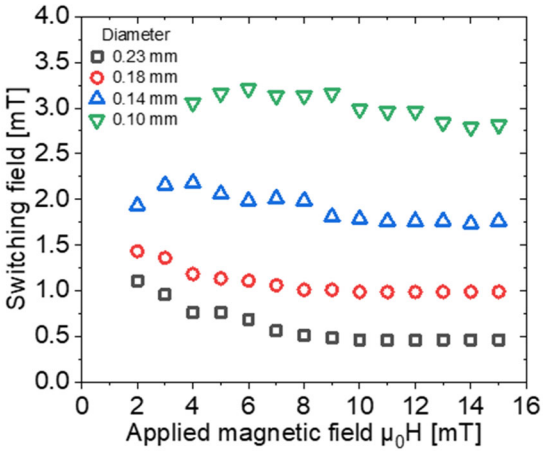

Figure 5.11 Switching fields of the Wiegand wires with varying diameters under the applied magnetic field.

5.5 Summary

In this chapter, the magnetic characteristics of Wiegand wires with different diameters were analyzed. The major and minor hysteresis loops of five types of Wiegand wires with different diameters were normalized by themselves and the 0.23-mm-diameter Wiegand wire. The variation trend of the coercivity and remanence of the major and minor hysteresis loops of the Wiegand wires under the two normalized methods were discussed. Moreover, the mechanism of the variation trend is analyzed. Based on the analysis of the variation trend of the height of the large Barkhausen jump of the Wiegand wires, it was inferred that the inner layer of a Wiegand wire is hard and the outer layer is soft. This is consistent with the result of the FORC diagram method. Then, the variation trends of the pulse voltage and height of the large Barkhausen jump in the pickup coil were compared. We observed that the variation trend of the pulse voltage generated by a Wiegand wire is related to the volume of the soft layer that generates the large Barkhausen jump. Finally, the switching fields of the Wiegand wires under different applied magnetic fields were discussed.

Chapter 6: Conclusion

An increasing number of countries are attaching importance to the development of the IoT; the IoT would play a key role in production and human life. IoT devices are widely used in daily life. With an increase in the number of installations of IoT devices and the complex and dynamic environment, there is an increasing demand for the portability, stability, and endurance of power supply. The self-powered supply comprising a Wiegand sensor does not require an external power supply and exhibits a stable output voltage. Its pulse width and amplitude are unaffected by the exciting frequency. It can generate a pulse voltage even when the exciting frequency is close to zero. Considering the aforementioned advantages of a Wiegand sensor, it is the preferred power supply for IoT devices.

The core components of Wiegand sensors (the Wiegand wire) need to be studied in detail to improve their performance in terms of power generation. In this study, the magnetic structure, magnetization process, coercivity, remanence, height of the large Barkhausen jump, and switching field of Wiegand wires were analyzed using the FORC diagram method and hysteresis loops.

The major and minor hysteresis loops and FORCs of five types of Wiegand wires with different diameters were measured using VSM. The FORC analysis of the Wiegand wire with the smallest diameter confirmed that the wire possessed a uniform magnetic structure. This indicated that the inner layer of the Wiegand wire was hard, and the outer one was soft. This new observation resolved a year of debate over the magnetic structure of Wiegand wires. The distribution of coercive and interaction fields of the Wiegand wires with the remaining diameters in the FORC diagram revealed an interaction between the soft and hard layers of Wiegand wires, i.e., a middle layer existed between the soft and hard layers. Thus, the magnetic structure of the Wiegand wires comprised three layers. Based on the analysis of the negative region in the FORC diagram, it was inferred that the negative region is generated by the opposite magnetization directions of the soft and hard layers during the magnetization process. A simple magnetic structure model of a Wiegand wire was proposed for the first time. Herein, the thicknesses of the soft, middle, and hard layers were determined based on theoretical calculation. The thickness of the hard layer was 0.06 mm. The thicknesses of the soft and middle layers decreased with a decrease in diameter.

A theoretical model for calculating the thicknesses of regions considering each direction of magnetization was proposed for the first time. The previous study only

considered qualitative analysis. The thicknesses of regions considering each direction of magnetization in each magnetization state during the magnetization process when the alternating magnetic field varied from 2 to 15 mT could be calculated. The magnetization process of the Wiegand wires with different diameters was analyzed in detail based on the theoretical results.

By analyzing the variation trend of the height of the large Barkhausen jump of the five kinds of Wiegand wires with different diameters in the minor hysteresis loop, it can be inferred that the outer and inner layers of a Wiegand wire are magnetically soft and hard, respectively. This is consistent with the final results obtained using the FORC method. Moreover, it was observed that the height of the large Barkhausen jump was consistent with the amplitude of the pulse voltage in the picking coil. This indicated that the generation of the pulse voltage of a Wiegand wire is related to the volume of the soft layer. The magnetic characteristics of Wiegand wires, such as coercivity, remanence, and switching field, were analyzed in detail. The switching field that produced a large Barkhausen jump increased with a decrease in the diameter of the Wiegand wire under an equal applied magnetic field. This was caused by a decrease in the demagnetizing field and increase in the coercivity of the soft layer with a decrease in diameter. For the same Wiegand wire, the switching field that produced a large Barkhausen jump decreased with an increase in the applied magnetic field. This is related to the increase in the demagnetizing field. It could induce a part of the soft layer to automatically reverse in the demagnetizing process, thereby facilitating the reversal of the soft layer.

The performance of Wiegand wires can be improved after understanding their magnetic structures, magnetic characteristics, and magnetization process. This helps provide a theoretical basis for improving the reliability and efficiency of power supply and a strong foundation for the application of the Wiegand wires in the IoT.

References

1. K. Ashton, S. Sarma, L.D. Brock, “The networked physical world”, *Auto-ID Center White Paper*, 2000.

2. M.W. Ryu, J. Kim, S.S. Lee, M.H. Song, “Survey on internet of things: toward case study”, *SmartCR*, Vol. 2, pp. 195-202, 2012.

3. H. Duce, “Internet of things in 2020”, *EPOSS Report*, 2008.

4. E. Fleisch, “What is the internet of things? An economic perspective”, *Economics, Management, and Financial Markets*, Vol. 5, pp 125-157, 2010.

5. Y. Chen, Y. Lu, L. Bulysheva, M.Y. Kataev, “Applications of blockchain in industry 4.0: A review”, *Information Systems Frontiers*, pp. 1-15, 2022.

6. S. Balakrishna, M. Thirumaran, V.K. Solanki, “A framework for IoT sensor data acquisition and analysis”, *EAI Endorsed Transactions on Internet of Things*, Vol. 4, pp. 1-13, 2018.

7. A. Hosozawa, J. Sekiguchi, T. Asai, T. Takahashi, “Application of a Hall sensor for pulsed magnetic field measurement in the FAT-CM FRC experiments”, *Review of Scientific Instruments*, Vol. 89, 10J120, 2018.

8. P. Romano, A. Imburgia, G. Ala, “Partial discharge detection using a spherical electromagnetic sensor”, *Sensors*, Vol. 19, 1014, 2019.

9. F. Xie, R. Weiss, R. Weigel, “Hysteresis compensation based on controlled current pulses for magnetoresistive sensors”, *IEEE Transactions on Industrial Electronics*, Vol. 62, pp. 7804-7809, 2015.

10. G. KUERS, H.-J. GEVATTER, “Wiegand-Sensoren für Weg-und Geschwindigkeitsmessungen/Wiegand effect position and speed sensors”, *Technisches Messen*, Vol. 51, pp. 123-129, 1984.

11. A. Matsushita, Y. Takemura, “Power generating device using compound magnetic wire”, *Journal of Applied Physics*, Vol. 87, pp. 6307-6309, 2000.

12. K. Takahashi, T. Yamada, Y. Takemura, “Circuit parameters of a receiver coil using a Wiegand sensor for wireless power transmission”, *Sensors*, Vol. 19, 2710, 2019.

13. K. Takahashi, A. Takebuchi, T. Yamada, Y. Takemura, “Power supply for medical implants by Wiegand pulse generated from a magnetic wire”, *Journal of the Magnetics Society of Japan*, Vol. 42, pp. 49-54, 2018.

14. R. Serizawa, T. Yamada, S. Masuda, S. Abe, S. Kohno, F. Kaneko, Y. Takemura, “Energy harvesting derived from magnetization reversal in FeCoV wire”, *In Proceedings of the IEEE Sensors*, Taipei, Taiwan, 28-31, October 2012.

15. S. Abe, A. Matsushita, K. Negishi, Y. Baba, M. Naoe, “Generation of large Barkhausen jump in bilayered thin film”, *IEEE Transactions on Magnetics*, Vol. 35, pp. 3634-3636, 1999.

16. J. Chotai, M. Thakker, Y. Takemura, “Single-bit, Self-powered digital counter using a Wiegand sensor for rotary applications”, *Sensors*, Vol. 20, 3840, 2020.

17. X. Sun, T. Yamada, Y. Takemura, “Output Characteristics and Circuit Modeling of Wiegand Sensor”, *Sensors*, Vol. 19, 2991, 2019.

18. X. Sun, H. Iijima, S. Saggini, Y. Takemura, “Self-Oscillating Boost Converter of Wiegand Pulse Voltage for Self-Powered Modules”, *Energies*, Vol. 14, 5373, 2021.

19. Y. Takemura, T. Yamada, “Output Properties of Zero-Speed Sensors Using FeCoV Wire and NiFe/CoFe Multilayer Thin Film”, *IEEE Sensors Journal*, Vol. 6, pp. 1186-1190, 2006.

20. G. Rauscher, C. Radeloff, “Wiegand and Pulse-Wire Sensors”, *Sensors*, Vol. 5, pp. 315-319, 1989.

21. T. Kohara, T. Kusunoki, T. Yamada, T. Suzuki, H. Fujimoto, Y. Takemura, S. Abe, S. Kohno, H. Itoi, F. Kaneko, “Fabrication and implementation of a rotation sensor

using a separated structure consisting of magnetic wire and a pick-up coil", *Journal of the Magnetics Society of Japan*, Vol. 34, pp. 347-351, 2010.

22. T. Kohara, T. Yamada, S. Abe, S. Kohno, F. Kaneko, Y. Takemura, "Effective excitation by single magnet in rotation sensor and domain wall displacement of FeCoV wire", *Journal of applied physics*, Vol. 109, 07E531, 2011.

23. J.R. Wiegand, M. Velinsky, "Bistable Magnetic Device", U.S. Patent 3,820,090, 25 June 1974.

24. J.R. Wiegand, M. Velinsky, "Method of manufacturing bistable magnetic device", U.S. Patent 3,892,118, 01 July 1975.

25. J.R. Wiegand, "Switchable Magnetic Device", U.S. Patent 4,247,601, 27 January 1981.

26. S. Abe, A. Matsushita, M. Naoe, "Annealing and torsion stress effect on magnetic anisotropy and magnetostriction of Vicalloy fine wire", *IEEE Transactions on Magnetics*, Vol. 33, pp. 3916-3918, 1997.

27. Y. Takemura, N. Fujiyama, A. Takebuchi, T. Yamada, "Battery-less hall sensor operated by energy harvesting from a single Wiegand pulse", *IEEE Transactions on Magnetics*, Vol. 53, 4002706, 2017.

28. B.D. Cullity, C.D. Graham, "Introduction to magnetic materials", *John Wiley & Sons*, 2011.

29. R.M. Bozorth, "Magnetism", *Reviews of Modern Physics*, Vol. 19, pp. 29-89, 1947.

30. C.A. Dirdal, J. Skaar, "Diamagnetism and the dispersion of the magnetic permeability", *The European Physical Journal B*, Vol. 91, pp. 131, 2018.

31. J. Van Den Handel, "Paramagnetism", *In Advances in Electronics and Electron Physics*, Vol. 6, pp. 463-518, 1954.

32. J.H. Van Vleck, "A Survey of the Theory of Ferromagnetism", *Reviews of Modern*

Physics, Vol. 17, pp. 27-47, 1945.

33. T. Nagamiya, K. Yosida, R. Kubo, “Antiferromagnetism”, *Advances in Physics*, Vol. 4, pp. 1-112, 1955.

34. L. Néel, “Antiferromagnetism and ferrimagnetism”, *Proceedings of the Physical Society. Section A*, Vol. 65, pp. 869-886, 1952.

35. M. Getzlaff, “Fundamentals of magnetism”, *Springer Science & Business Media*, 2007.

36. J.M.D. Coey, “Magnetism and Magnetic Materials”, *Cambridge University Press*, 2010.

37. B. Sai Ram, A.K. Paul, S.V. Kulkarni, “Soft magnetic materials and their applications in transformers”, *Journal of Magnetism and Magnetic Materials*, Vol. 537, pp. 1-13, 2021.

38. E.P. Wohlfarth, “Hard magnetic materials”, *Advances in physics*, Vol. 8, pp. 87-224, 1959.

39. N.A. Spaldin, “Magnetic Materials: Fundamentals and Applications”, *Cambridge University Press*, 2010.

40. Kannan M. Krishnan, “Fundamentals and Applications of Magnetic Materials”, *Oxford University Press*, 2016.

41. H. Kikuchi, S. Kamata, T. Nakai, S. Hashi, K. Ishiyama, “Influence of demagnetizing field on thin-film GMI magnetic sensor elements with uniaxial magnetic anisotropy”, *Sensors and Actuators A-Physical*, Vol. 230, pp. 142-149, 2015.

42. T. Nakamura, H. Tanaka, T. Horiuchi, T. Yamada, Y. Takemura, “Surface Magnetization Reversal of Wiegand wire Measured by the Magneto-Optical Kerr Effect”, *Materials*, Vol. 14, 5417. 2021.

43. Y. Takemura, A. Matsushita, “Frequency dependence of output voltage generated from bundled compound magnetic wires”, *IEEE transactions on magnetics*, Vol. 37, pp. 2862-2864, 2001.

44. H.J. Williams, R.M. Bozorth, W. Shockley, “Magnetic domain patterns on single crystals of silicon iron”, *Physical review*, Vol. 75, pp. 155-178, 1949.

45. R.M. Bozorth, J.F. Dillinger, “Propagation of Magnetic Disturbances along Wires”, *Nature*, Vol. 127, pp. 777, 1931.

46. E. McMILLAN, “A Magnetic Effect on Pirani Gauges using Nickel Wires”, *Nature*, Vol. 133, pp. 831-832, 1934.

47. T.F. Wall, “Abnormal Magnetic Behaviour of Treated Cobalt Wire”, *Nature*, Vol. 136, pp. 397, 1935.

48. C.W. Sandweg, N. Wiese, D. McGrouther, S.J. Hermsdoerfer, H. Schultheiss, B. Leven, S. McVitie, B. Hillebrands, J.N. Chapman, “Direct observation of domain wall structures in curved permalloy wires containing an antinotch”, *Journal of Applied Physics*, Vol. 103, 093906, 2008.

49. N. Normann, “Magnetic field sensor comprising Wiegand wires or similar bistable magnetic elements”, U.S. Patent 4,639,670, 27 January 1987.

50. K. Mohri, F.B. Humphrey, K. Kawashima, K. Kimura, M. Mizutani, “Large Barkhausen and Matteucci effect in FeCoSiB, FeCrSiB, and FeNiSiB amorphous wires”, *IEEE Transactions on Magnetics*, Vol. 26, pp. 1789-1791, 1990.

51. A. Hultgren, M. Tanase, C.S. Chen, G.J. Meyer, D.H. Reich, “Cell manipulation using magnetic nanowires”, *Journal of Applied Physics*, Vol. 93, pp. 7554-7556. 2003.

52. H. Barkhausen, “Two phenomena revealed with the help of new amplifiers”, *Phys. Z.*, Vol. 29, pp. 401-403, 1919.

53. R. Forrer, “Sur les grands phénomènes de discontinuité dans l'aimantation du nickel

et l'acquisition d'un état à cycle particulièrement simple", *Phys. Radium*, Vol. 7, pp. 109-124, 1926.

54. F. Preisach, "Untersuchungen über den Barkhauseneffekt", *Annalen der Physik*, Vol. 395, pp. 737-799, 1929.

55. K.J. Sixtus, L. Tonks, "Propagation of large Barkhausen discontinuities", *Physical Review*, Vol. 37, pp. 930-959, 1931.

56. K.J. Sixtus, L. Tonks, "Propagation of large Barkhausen discontinuities, II", *Physical Review*, Vol. 42, pp. 419-435, 1932.

57. L. Tonks, K.J. Sixtus, "Propagation of large Barkhausen discontinuities, III. Effect of a Circular Field with Torsion", *Physical Review*, Vol. 43, pp. 70-80, 1933.

58. L. Tonks, K.J. Sixtus, "Propagation of large Barkhausen discontinuities, IV. Regions of Reversed Magnetization", *Physical Review*, Vol. 43, pp. 931-940, 1933.

59. S. Abe, A. Matsushita, "Construction of electromagnetic rotation sensor using compound magnetic wire and measurement at extremely low frequency rotations", *IEEE Transactions on Magnetics*, Vol. 30, pp. 4635-4637, 1994.

60. S. Abe, A. Matsushita, "Induced pulse voltage in twisted Vicalloy wire with compound magnetic effect", *IEEE transactions on magnetics*, Vol. 31, pp. 3152-3154, 1995.

61. J.E. Opie, J.W. Bossoli, "A new era of application for the Wiegand effect", *SAE transactions*, Vol. 97, pp. 426-431, 1988.

62. S. Abe, A. Matsushita, M. Naoe, "Dependence of large Barkhausen jump on length of a vicalloy fine wire with torsion stress", *IEEE Transactions on Magnetics*, Vol. 34, pp. 1318-1320, 1998.

63. H. Felix, B. Andreas, "Direct Observation of Large Barkhausen Jump in Thin Vicalloy Wires", *IEEE Magnetics Letters*, Vol. 11, pp. 1-4, 2020.

64. S. Abe, T. Ikenaga, K. Suwa, et al. “Bias magnetic effect using compound magnetic wire sensor in AC magnetic field”, *IEEE Transactions on Magnetics*, Vol. 32, pp. 4971-4973, 1996.

65. D.J. Dlugos, D. Small, D.A. Siefer, “Wiegand effect energy generator”, U.S. Patent 6,191,687, 20 February 2001.

66. D.J. Dlugos, “Wiegand Effect Sensors Theory and Applications”, *Sensors*, Vol. 15, pp. 32-34, 1998.

67. A. Takebuchi, T. Yamada, Y. Takemura, “Reduction of vibration amplitude in vibration-type electricity generator using magnetic wire”, *Journal of the magnetics Society of Japan*, Vol. 41, pp. 34-40, 2017.

68. C.C. Lin, Y.C. Tseng, T.S. Chin, “A Review of the Self-Powered Wiegand Sensor and Its Applications”, *Magnetochemistry*, Vol. 8, 128, 2022.

69. H. Tanaka, T. Yamada, Y. Takemura, S. Abe, S. Kohno, H. Nakamura, “Constant velocity of domain wall propagation independent of applied field strength in vicalloy wire”, *IEEE transactions on magnetics*, Vol. 43, pp. 2397-2399, 2007.

70. P.J. Wasilewski, “Magnetic hysteresis in natural materials”, *Earth and Planetary Science Letters*, Vol. 20, pp. 67-72, 1973.

71. D. Lin, P. Zhou, C. Lu, N. Chen, M. Rosu, “Construction of magnetic hysteresis loops and its applications in parameter identification for hysteresis models”, *In 2014 International Conference on Electrical Machines (ICEM), IEEE*, pp. 1050-1055, 2014.

72. H. David, A.P. Roberts, “A method for unmixing magnetic hysteresis loops”, *Journal of Geophysical Research*, Vol. 117, B03103, 2012.

73. C. Yang, T. Sakai, T. Yamada, Z. Song, Y. Takemura, “Improvement of pulse voltage generated by Wiegand sensor through magnetic-flux guidance”, *Sensors* Vol. 20, 1408, 2020.

74. T. Doong, I. Mayergoyz, “On numerical implementation of hysteresis models”, *IEEE Transactions on Magnetics*, Vol. 21, pp. 1853-1855, 1985.

75. I. Mayergoyz, “Mathematical models of hysteresis”, *IEEE Transactions on magnetics*, Vol. 22, pp. 603-608, 1986.

76. C. Pike, A. Fernandez, “An investigation of magnetic reversal in submicron-scale Co dots using first order reversal curve diagrams”, *Journal of applied physics*, Vol. 85, pp. 6668-6676, 1999.

77. C.R. Pike, A.P. Roberts, K.L. Verosub, “First order reversal curve diagrams and thermal relaxation effects in magnetic particles”, *Geophysical Journal International*, Vol. 145, pp. 721-730, 2001.

78. Y. Pan, N. Petersen, M. Winklhofer, “Rock magnetic properties of uncultured magnetotactic bacteria”, *Earth and Planetary Science Letters*, Vol. 237, pp. 311-325, 2005.

79. V. Franco, T. Gottschall, K. Skokov, O. Gutfleisch, “First-Order Reversal Curve (FORC) Analysis of Magnetocaloric Heusler-Type Alloys”, *IEEE Magnetics Letters*, Vol. 7, pp. 1-4, 2016.

80. C. Carvallo, A.R. Muxworthy, D.J. Dunlop, “First-order reversal curve (FORC) diagrams of magnetic mixtures: Micromagnetic models and measurements”, *Physics of the Earth and Planetary Interiors*, Vol. 154, 308-322, 2006.

81. B. Dodrill, J. Lindemuth, C. Radu, H. Reichard, “White Paper: High-temperature FORC study of single-and multi-phase permanent magnets”, *MRS Bulletin*, Vol. 40, pp. 903–905, 2015.

82. G. Muscas, M. Menniti, R. Brucas, P.E. Jönsson, “Mesoscale magnetic rings: Complex magnetization reversal uncovered by FORC”, *Journal of Magnetism and Magnetic Materials*, Vol. 502, 166559, 2020.

83. R. Tanasa, A. Stancu, “Statistical characterization of the FORC diagram”, *IEEE transactions on magnetics*, Vol. 42, pp. 3246-3248, 2006.

84. C.R. Pike, A.P. Roberts, M.J. Dekkers, K.L. Verosub, “An investigation of multi-domain hysteresis mechanisms using FORC diagrams”, *Physics of the Earth and Planetary Interiors*, Vol. 126, pp. 11-25, 2001.

85. F. Béron, L. Clime, M. Ciureanu, et al. “Magnetostatic interactions and coercivities of ferromagnetic soft nanowires in uniform length arrays”, *Journal of nanoscience and nanotechnology*, Vol. 8, pp. 2944-2954, 2008.

86. C.R. Pike, “First-order reversal-curve diagrams and reversible magnetization”, *Physical Review B*, Vol. 68, 104424, 2003.

87. C.R. Pike, A.P. Roberts, K.L. Verosub, “Characterizing interactions in fine magnetic particle systems using first order reversal curves”, *Journal of Applied Physics*, Vol. 85, pp. 6660-6667, 1999.

88. A.R. Muxworthy, A.P. Roberts, “First-order reversal curve (FORC) diagrams”, *Encyclopedia of geomagnetism and paleomagnetism*, Vol. 1, pp. 266-272. 2007.

89. A.R. Muxworthy, D.J. Dunlop, “First-order reversal curve (FORC) diagrams for pseudo-single-domain magnetites at high temperature”, *Earth and Planetary Science Letters*, Vol. 203, pp. 369-382, 2002.

90. A.P. Roberts, C.R. Pike, K.L. Verosub, “First-order reversal curve diagrams: A new tool for characterizing the magnetic properties of natural samples”, *Journal of Geophysical Research: Solid Earth*, Vol. 105, pp. 28461-28475, 2000.

91. C. Yang, Y. Kita, Z. Song, Y. Takemura, “Magnetic Reversal in Wiegand Wires Evaluated by First-Order Reversal Curves”, *Materials*, Vol. 14, 3868, 2021.

92. R.J. Harrison, J.M. Feinberg, “FORCinel: An improved algorithm for calculating first-order reversal curve distributions using locally weighted regression smoothing”, *Geochemistry, Geophysics, Geosystems*, Vol. 9, pp. 1-11, 2008.

93. R.A. Gallardo, S. Khanal, J.M. Vargas, L. Spinu, C.A. Ross, C. Garcia, “Angular dependent FORC and FMR of exchange-biased NiFe multilayer films”, *Journal of Physics D: Applied Physics*, Vol. 50, 075002, 2017.

94. B. Dodrill, P. Ohodnicki, M. McHenry, A. Leary, “High-Temperature First-Order-Reversal-Curve (FORC) Study of Magnetic Nanoparticle Based Nanocomposite Materials”, *MRS Advances*, Vol. 2, pp. 2669-2674, 2017.

95. D. Heslop, A.R. Muxworthy, “Aspects of calculating first-order reversal curve distributions”, *Journal of magnetism and magnetic materials*, Vol. 288, pp. 155-167, 2005.

96. C.R. Pike, C.A. Ross, R.T. Scalettar, G. Zimanyi, “First-order reversal curve diagram analysis of a perpendicular nickel nanopillar array”, *Physical Review B*, Vol. 71, 134407, 2005.

97. G. Sha, C. Yang, Z. Song, Y. Takemura, “Magnetic interactions in Wiegand wires evaluated by first-order reversal curves”, *Materials*, Vol. 15, 5936, 2022.

98. G. Acton, Q.Z. Yin, K.L. Verosub, L. Jovane, A. Roth, B. Jacobsen, D.S. Ebel, “Micromagnetic coercivity distributions and interactions in condrules with implications for paleointensities of the early solar system”, *Journal of Geophysical Research*, Vol. 112, B03S90, 2007.

99. L. Jiang, C. Yang, Z. Song, Y. Takemura, “Magnetic Structure of Wiegand Wire Analyzed by First-Order Reversal Curves”, *Materials*, Vol. 15, 6951. 2022.

100. A. Zhukov, J. González, J.M. Blanco, M. Vázquez, V. Larin, “Microwires coated by glass: A new family of soft and hard magnetic materials”, *Journal of Materials Research*, Vol. 15, pp. 2107-2113, 2000.

101. Y. Takemura, T. Aoki, H. Tanaka, T. Yamada, S. Abe, S. Kohno, H Nakamura, “Control of demagnetizing field and magneto static coupling in FeCoV wires for zero-speed sensor”, *IEEE transactions on magnetics*, Vol. 42, pp. 3300-3302, 2006.

Publications

[Papers]

[1] Liang Jiang, Chao Yang, Zenglu Song, and Yasushi Takemura
"Magnetic Structure of Wiegand Wire Analyzed by First-Order Reversal Curves"
Materials (Q1, IF=3.748), Vol.15, No.19, 6951, pp. 1-15, 2022.
DOl: 10.3390/ma15196951

[2] Liang Jiang, Chao Yang, Zenglu Song, and Yasushi Takemura
"Magnetization of Wiegand wires with varying diameters and analysis of their magnetic structure via hysteresis loops"
Preparing for submission